

May 18, 2022  
DRAFT

Thesis Proposal

**Joint Analysis and Prediction of  
Human Actions and Paths in Video**

Junwei Liang

May 18, 2022

Language Technologies Institute  
School of Computer Science  
Carnegie Mellon University  
Pittsburgh, PA 15123

**Thesis Committee:**

Alexander Hauptmann (Chair)	Carnegie Mellon University
Alan W. Black	Carnegie Mellon University
Kris Kitani	Carnegie Mellon University
Lu Jiang	Google Research

*Submitted in partial fulfillment of the requirements  
for the degree of Doctor of Philosophy.*

Copyright © 2020 Junwei Liang

May 18, 2022  
DRAFT

**Keywords:** Action Recognition, Trajectory Prediction, Action Prediction, Human Behavioral Analysis, Future Prediction, Machine Perception, Autonomous Driving

## **Abstract**

With the advancement in computer vision deep learning, systems now are able to analyze an unprecedented amount of rich visual information from videos to enable applications such as autonomous driving, socially-aware robot assistant and public safety monitoring. Deciphering human behaviors to predict their future paths/trajectories and what they would do from videos is important in these applications. However, modern vision systems in self-driving applications usually perform the detection (perception) and prediction task in separate components, which leads to error propagation and sub-optimal performance. More importantly, these systems do not provide high-level semantic attributes to reason about pedestrian future. This design hinders prediction performance in video data from diverse domains and unseen scenarios. To enable optimal future human behavioral forecasting, it is crucial for the system to be able to detect and analyze human activities leading up to the prediction period, passing informative features to the subsequent prediction module for context understanding.

In this thesis, with the goal of improving the performance and generalization ability of future trajectory and action prediction models, we conduct human action analysis and jointly optimize models for action detection, prediction and trajectory prediction. This thesis consists of three parts. The first part analyzes human actions. We aim to develop an efficient object detection and tracking system similar to the perception system used in self-driving, and tackle action recognition problem under weakly-supervised learning settings. We propose a method to learn viewpoint invariant representations for video action recognition and detection with better generalization. In the second part, we tackle the problem of trajectory forecasting with semantic context understanding. We study multiple-future trajectory prediction using scene semantics and exploit 3D simulation for robust learning. Finally, in the third part, we explore joint analysis and prediction of human actions and trajectories. Our final goal is to build a robust end-to-end vision system that could jointly detect and forecast future actions and trajectories.





# Contents

<b>1</b>	<b>Introduction</b>	<b>1</b>
1.1	Motivation of Research . . . . .	1
1.2	Applications . . . . .	3
1.3	Terminology . . . . .	4
1.4	Thesis Overview . . . . .	5
1.5	Comparison to Related Work . . . . .	6
1.6	Summary of the Work Progress . . . . .	7
1.7	Proposed Timeline . . . . .	8
<b>I</b>	<b>Human Action Analysis</b>	<b>9</b>
<b>2</b>	<b>Efficient Object Detection and Tracking in Extended Videos</b>	<b>13</b>
2.1	Overview . . . . .	14
2.2	Efficient Object Detection and Tracking . . . . .	15
<b>3</b>	<b>Weakly-supervised Action Event Recognition</b>	<b>21</b>
3.1	Overview . . . . .	21
3.2	Related Work . . . . .	24
3.3	Multi-modal WEbly-Labeled Learning (WELL-MM) . . . . .	26
3.4	Experimental Results . . . . .	30
<b>4</b>	<b>Viewpoint Invariant Representation Learning for Action Recognition and De- tection</b>	<b>39</b>
4.1	Overview . . . . .	39
4.2	Initial Experimental Results . . . . .	41
4.3	Future Plan . . . . .	43

<b>II</b>	<b>Human Trajectory Prediction with Scene Semantics</b>	<b>45</b>
<b>5</b>	<b>Multiple-future Pedestrian Trajectory Prediction</b>	<b>49</b>
5.1	Overview . . . . .	49
5.2	Related Work . . . . .	51
5.3	The <i>Multiverse</i> Model . . . . .	52
5.4	The Forking Paths Dataset . . . . .	56
5.5	Experimental Results . . . . .	59
<b>6</b>	<b>Learning from 3D Simulation</b>	<b>65</b>
6.1	Overview . . . . .	65
6.2	Related Work . . . . .	67
6.3	The <i>SimAug</i> Model . . . . .	69
6.4	Approach . . . . .	69
6.5	Experiments . . . . .	75
<b>III</b>	<b>Joint Analysis and Prediction of Human Actions and Paths</b>	<b>83</b>
<b>7</b>	<b>Joint Pedestrian Trajectory and Action Prediction</b>	<b>87</b>
7.1	Overview . . . . .	87
7.2	Related Work . . . . .	89
7.3	The <i>Next</i> Model . . . . .	90
7.4	Experimental Results . . . . .	97
<b>8</b>	<b>Long-term Joint Trajectory and Action Prediction with Intention Recognition</b>	<b>105</b>
8.1	Overview . . . . .	105
8.2	Related Work . . . . .	107
8.3	Future Plan . . . . .	107
<b>9</b>	<b>Joint Modeling of Action Detection, Action Prediction and Path Prediction</b>	<b>109</b>
9.1	Overview . . . . .	109
9.2	Future Plan . . . . .	110
<b>10</b>	<b>Conclusion</b>	<b>113</b>
	<b>Bibliography</b>	<b>115</b>

# Chapter 1

## Introduction

### 1.1 Motivation of Research

With the advancement in deep learning and computer vision, systems now are able to analyze an unprecedented amount of rich visual information from videos to enable many AI applications. Researchers have achieved great successes in a wide range of computer vision tasks like image classification [52], object detection and instance segmentation [53], object tracking [152, 185] and scene semantic segmentation [23]. Computer vision engineers and scientists are able to put these models into production for applications like image/video content retrieval and in areas like retail and public safety. One of the most exciting applications is autonomous driving, which may revolutionize how people get around places and how freight moves. While many prototypes from companies like Waymo and Baidu Apollo system have been built over the years, many challenges remain. One of the main challenges is collision avoidance, which is crucial for self-driving systems co-mingling with humans. This requires systems to anticipate human motions and actions in the future. This important analysis is called future person trajectory and action prediction. In self-driving systems, the perception system is usually responsible for the object detection and tracking. The outputs of the perception system is then input to the prediction system [9], which may cause an interruption of information flow and model training to be sub-optimal. Moreover, these systems do not provide high-level semantic attribute detection like current human activities and intention recognition to reason about pedestrian future. In this thesis, our goal is to build a robust trajectory and action prediction system with in-depth semantic context understanding. We utilize joint analysis of human actions and enhanced contextual cues from the environment to achieve intent-aware future trajectory

and action prediction. The future trajectory and action prediction task has received a lot of attention in the research community [3, 50, 82, 107, 143] (see also this comprehensive survey paper [149]). It is regarded as an fundamental building block in video understanding because forecasting human behaviors is useful in many applications other than self-driving cars like socially-aware robots [116], advanced surveillance systems, etc.

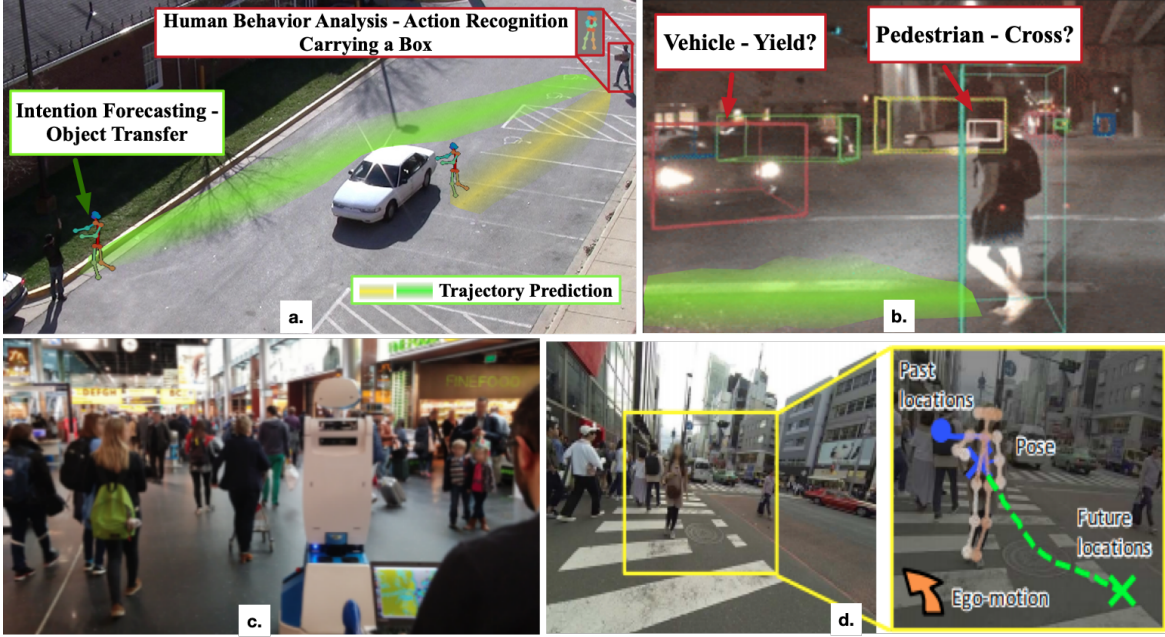


Figure 1.1: Our goal is to jointly analyze human actions and predict their future trajectories and actions. (a.) Joint analysis in stationary 45-degree view cameras. The green and yellow line show two possible future trajectories. By recognizing that the person is carrying a box, the system should be able to forecast the intention based on scene constraints and social interactions (the person at the bottom left is waving at the target person), and predict the correct future trajectory. (b.) Future trajectory prediction in self-driving system. (c.) Socially-aware robots from [149]. (d.) First-person view trajectory prediction [194].

Humans navigate through public spaces often with specific purposes in mind, ranging from simple ones like entering a room to more complicated ones like putting things into a car. Even though their intentions might be determined early, their future trajectories might also be altered by other constraints like social interactions and scene constraints (i.e., external stimuli, as noted in [149]). This poses several challenges for the pedestrian future trajectory and action prediction task as follows:

(1) **The scene constraints are complex and they are changing dynamically.** In urban

environment, the scene can be diverse and unpredictable with multiple actors including vehicles and pedestrians performing different tasks. For self-driving systems, as the cars are moving around, the prediction models have to adapt to the dynamic changes of the scene (as well as taking into account the ego-motions), which makes the forecasting problem even more complex.

**(2) The future is often uncertain.** Given the same historical trajectory, a person may take different paths, depending on their (latent) goals. Consider the example in Fig. 1.1 a., the person (at the top-right corner) might take different paths depending on their intention, e.g., they might take the green path to *transfer object* or the yellow path to *load object into the car*. Thus recent work has started focusing on *multi-future trajectory prediction* [16, 92, 97, 122, 172, 173].

**(3) Training data is limited for rare scenarios.** For self-driving applications, safe operation is a priority. Data from incidents can help us better improve the system but they are often very rare and scene-dependent. Some traffic events are impossible or too dangerous to be acted out by actors for data collection purposes. As large amounts of well-annotated video data for such rare scenarios are hard to get, in this thesis we investigate the usage of 3D simulator and weakly-supervised learning to alleviate this challenge.

With the advancement of Convolutional Neural Networks (CNNs), Recurrent Neural Networks (RNNs) and graphical models [180], we will investigate how to design efficient models suitable for joint action analysis and future predictions for both paths and actions. To tackle the aforementioned challenges, in Part I, we first explore and develop action analysis perception system that is efficient to capture behavioral cues and semantic attributes of pedestrians. In Part III, we explore and develop prediction system that could utilize enhanced contextual cues in the scene. For the second challenge, we develop multi-future trajectory prediction model and a new benchmark in chapter 5. For the third challenge, we utilize recent success of learning from 3D simulation [150] and adversarial learning [175] to train a robust model in chapter 6. We also look into weakly-supervised learning by utilizing vastly available Internet data in chapter 3.

## 1.2 Applications

Forecasting human behaviors in complex urban environment is useful in many applications such as autonomous driving, public/traffic safety monitoring, socially-aware robots, etc.

### 1.2.1 Autonomous Driving

Safe operation is a crucial prerequisite for self-driving cars to become ubiquitous in the future. Forecasting human behavior including pedestrians and cyclists is an essential building block to achieve that [79, 107]. In Fig. 1.1 b., it shows an example camera view from the self-driving cars. The human action analysis and prediction system is key to recognizing the pedestrian and whether they are going to continue to walk across the road, making sure that the driving planning system makes the right action for maximum safety.

### 1.2.2 Advanced Public/Traffic Safety Monitoring

Human action analysis and prediction system can also be applied to stationary cameras for safety monitoring. With trajectory prediction enabled, traffic safety system can issue warnings to pedestrians and vehicles before potential accidents happen. Meanwhile, by looking into the predicted collided trajectories that do not actually happen, traffic safety researchers can study these cases as near-misses to identify risky intersections or roadways. In terms of public safety monitoring, the forecasting system can also be applied to predicting the path a suspect may flee after an robbery or other crime incidents, by using long-term prediction model that takes into account scene constraints and external knowledge (chapter 8).

### 1.2.3 Socially-aware Robots

Socially-aware smart robot assistants (Fig. 1.1 c.) can be utilized in the future to help humans in performing everyday tasks, such as grocery shopping and delivery. They are required to operate in a safe and socially-acceptable manner, since they would move closely among other people. The ability to analyze and predict human behaviors from first-person camera view (Fig. 1.1 d.) is essential for motion planning of the robots.

## 1.3 Terminology

In this paper, we use the term “trajectory” and “path” interchangeably to refer to the ground-level 2D positions of an agent (humans, vehicles, etc.) over a period of time. We refer to short-term and long-term prediction to characterize prediction horizons of 3-5 seconds and up to 20 seconds ahead, respectively. We also use the term “actions” and “activities” interchangeably to refer to a predefined set of human actions of various duration from public datasets (VIRAT [131],

Kinetics [81], etc.). We use “intent”, “intention” and “goal” interchangeably to refer to a person’s latent, near-future (same time horizon as the prediction) objective or purpose that associates with a physical destination and an action.

## 1.4 Thesis Overview

This thesis aims to predict pedestrian future trajectories and activities by jointly analyzing human behaviors and contextual cues from the environment. We first investigate human action analysis, including efficient object detection and human action recognition & detection in videos. This provides important semantic attribute inference that could help aid human intention recognition. We then focus on developing models for future trajectory prediction with semantic scene understanding. Finally, we utilize our findings from the first two parts and jointly optimize for action detection, action prediction and trajectory prediction. A detailed overview of each part is as follows:

**Part I Human Action Analysis** In this part, we study the problem of human action analysis, including efficient object detection and tracking, and action recognition. For object detection and tracking, our goal is to build an efficient perception system that utilizes robust image object detection model and fast traditional tracking method for extended videos (chapter 2). Our focus in this part is on action recognition and detection. As human actions are diverse, it is impossible to collect training data for all action classes. Therefore we first study weakly-supervised learning with massive video data with weak labels from Internet platforms like YouTube (chapter 3). To enable better generalization of video action recognition models to all kinds of camera views, we then investigate viewpoint-invariant representation learning (chapter 4).

**Part II Human Trajectory Prediction with Scene Semantics** In this part, we focus on the human future trajectory prediction problem. We study how trajectory prediction can benefit from semantic context understanding of the scene. Since the future is uncertain, we first introduce the *Multiverse* model to tackle the multiple-future trajectory prediction problem (chapter 5). To alleviate the limited training data challenge as mentioned in previous section, we propose a machine learning algorithm called *SimAug*, to efficiently learn from 3D simulation data for trajectory prediction (chapter 6).

**Part III Joint Analysis and Prediction of Human Actions and Paths** In the final part, we aim to build joint end-to-end systems with multi-task learning and utilizing enhanced contextual cues in the scene. We first study jointly predicting pedestrian trajectories and activities ([chapter 7](#)). Since short-term future prediction is not enough to ensure safe operations in autonomous driving applications, we introduce the long-term trajectory and action prediction benchmark and propose a model that takes into account intention forecasting ([chapter 8](#)). Finally in [chapter 9](#), we propose the work to jointly model action detection, action prediction and trajectory prediction to achieve optimal performance.

### 1.4.1 Priorities of Proposed Works

In this section we prioritize the proposed works and set [chapter 9](#) with the highest priority  $P0$ . [chapter 8](#) is set to be  $P1$  and [chapter 4](#) is set to be  $P2$ .

## 1.5 Comparison to Related Work

In this section, we briefly discuss this thesis’ goal and positioning among related works. As noted before, our goal is to build a robust trajectory and action prediction system with in-depth semantic context understanding. We utilize joint analysis of human actions and enhanced contextual cues from the environment to achieve intent-aware future trajectory and action prediction. In order to achieve that, in [Part I](#), we first focus on machine perception, as it is important for prediction models to get enhanced contextual information from the scene and the target agent [149]. We investigate efficient object detection and tracking models in [chapter 2](#). It is not our intention to achieve state-of-the-art on common benchmarks like MSCOCO [112], but to create an efficient framework for video perception that is easy to swap in new models in the future. In [chapter 3](#), we are one of the early works that study how we could better utilize weakly-supervised video data from the Internet using self-paced curriculum learning [69]. In [chapter 4](#), we explore viewpoint-invariant representation for action recognition and detection, which is crucial to detect and forecast pedestrian intent as shown in [chapter 8](#). In [Part II](#), we study trajectory prediction models with scene semantic understanding. Following the taxonomy proposed in [149], in [chapter 5](#), we study a pattern-based sequential model that considers scene semantics as contextual cues for multi-future trajectory prediction. In this work, we propose the first human-annotated benchmark for multi-future trajectory prediction. We then explore adversarial learning in [chapter 6](#) to build robust trajectory prediction models for dif-



ferent environment and camera views, which is an important under-explored problem in this research field [149]. In [chapter 7](#), we develop the first joint action and trajectory prediction model. It utilizes both static and dynamic environment cues. In this work, we are also among the very early works that look into how **noisy input** of imperfect object detection and tracking would affect trajectory prediction performance. Such robustness experiments have been noted in [149] as very important to understand and measure the effectiveness of the prediction models. In [chapter 8](#) and [chapter 9](#), we propose to work on long-term joint prediction and joint optimization, that study enhanced contextual cues including human actions ([chapter 4](#)) and human intentions. Such direction has been mentioned in [149] to be one of the important future direction of human motion prediction research.

## 1.6 Summary of the Work Progress

The work on efficient object detection and tracking in videos ([chapter 2](#)) has been published at a WACV 2020 workshop [114]. This work is part of the system that won the TRECVID 2019 competition on Activities in Extended Video [7]. We have extensively studied the problem of weakly-supervised learning of action event recognition ([chapter 3](#)), which includes a webly learning method published at IJCAI 2016 [100] and a multimodal learning method published at ICMR 2017 [104] and AAAI 2017 Demo [103]. Notably, we won the TRECVID 2016 competition on Adhoc Video Search [98] with the weakly-supervised method we developed. The viewpoint-invariant representation learning for action recognition and detection work ([chapter 4](#)) is proposed as future work in progress.

In [Part II](#), the multiple-future trajectory prediction work ([chapter 5](#)) is published at CVPR 2020 [109] and *SimAug* model ([chapter 6](#)) is published at ECCV 2020 [108].

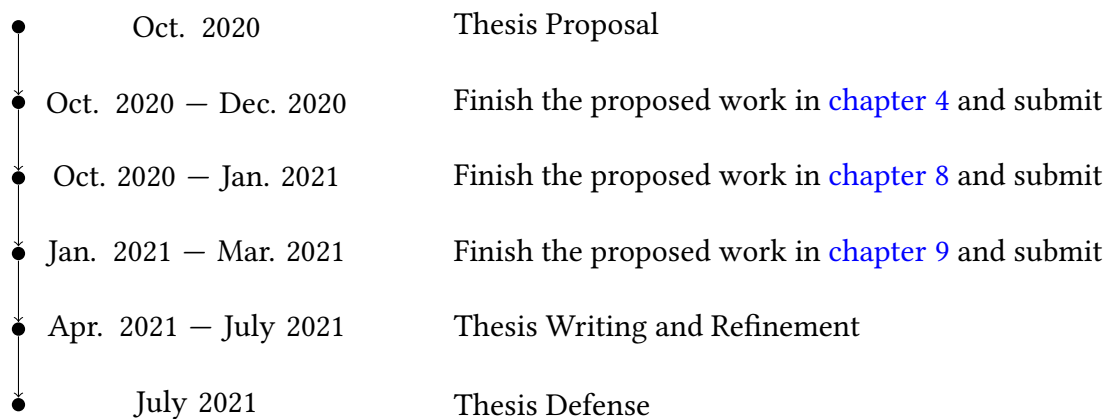
In [Part III](#), the joint trajectory and activity prediction work ([chapter 7](#)) is published at CVPR 2019 [107]. The long-term future prediction work ([chapter 8](#)) is proposed as future work in progress. The final chapter, the joint modeling of action detection and prediction ([chapter 9](#)) is a proposed work.

The work presented here is also related to other relevant research not included in this thesis. The studies related to [Part I](#) include video description generation works published at Interspeech 2016 [75] and ICMR 2016 [74], audio event analysis published at ICASSP 2017 [102], a video retrieval competition at TRECVID 2016 [98], 2017 [21] and 2018 [61]. The studies related to [Part II](#) and [Part III](#) include a focal attention model published at CVPR 2018 [105] and TPAMI 2019 [106], an activity detection competition (in which we won the first-place) at TRECVID

2019 [18].

## 1.7 Proposed Timeline

The timeline for completion of this thesis is as follows:



# **Part I**

## **Human Action Analysis**



In this part, we study the problem of human action analysis, including efficient object detection and tracking, and action recognition. For object detection and tracking, our goal is to build an efficient perception system that utilizes robust image object detection model and fast traditional tracking method for extended videos ([chapter 2](#)). Our focus in this part is on action recognition and detection. As human actions are diverse, it is impossible to collect training data for all action classes. Therefore we first study weakly-supervised learning with massive video data with weak labels from Internet platforms like YouTube ([chapter 3](#)). To enable better generalization of video action recognition models to all kinds of camera views, we then investigate viewpoint-invariant representation learning ([chapter 4](#)).



## Chapter 2

# Efficient Object Detection and Tracking in Extended Videos

In this chapter, we study the problem of building an efficient perception system for extended videos, either from surveillance cameras or onboard cameras from self-driving cars. The perception system, which includes object detection and tracking models, provides the basic inputs, i.e., person and object tracklets, to action recognition and future prediction models in later chapters. We study the object detection and tracking models for videos in the Activities in Extended Videos Prize Challenge (ActEV) [7, 114]. With the availability of large-scale video surveillance dataset such as VIRAT [131], ActEV seeks to encourage the development of real-time robust automatic activity detection algorithms in surveillance scenarios. We aim to develop a robust and efficient object detection and tracking model trained on the MSCOCO dataset [112] as the object annotations in the ActEV dataset are quite small compared to MSCOCO. Many image object detection research works [29, 53] have been done on the MSCOCO dataset [112], which includes 80 object classes. Compared to other object detection datasets including PASCAL VOC dataset [39], MSCOCO has better annotations, with many more bounding boxes and classes (The YouTube-BoundingBox dataset [140] has more boxes than MSCOCO dataset but it is not exhaustively annotated). We also study Tensorflow [1] and TensorRT to build a perception system that reaches faster-than-real-time relative processing speed with certain hardware requirements. It is not our intention to develop State-of-the-Art (SOTA) object detection model but instead to construct a framework for extended videos that we could easily swap the model

---

Code and models are released at [https://github.com/JunweiLiang/Object\\_Detection\\_Tracking](https://github.com/JunweiLiang/Object_Detection_Tracking)

with the latest COCO-trained models (we have implemented Mask-RCNN [53] from 2017 and EfficientDet [170] from 2020.)

## 2.1 Overview



Figure 2.1: Example of the ActEV dataset. The videos are annotated with pedestrian and vehicle tracklets with bounding boxes as well as the pedestrian’s activities. For example, the two persons at the bottom-left are labeled with “talking”.

In recent years, the volume of video data from widely deployed surveillance cameras has grown dramatically. However, camera network operators are overwhelmed with the data to be monitored, and usually cannot afford to view or analyze even a small fraction of their collections. To enable timely response for public safety and traffic safety events, there is thus strong incentive to develop fully-automated methods to identify and localize activities in extended video collections and provide the capability to alert and triage emergent videos. These methods will alleviate the current manual process of monitoring by human operators and scale up with the growth of sensor proliferation in the near future. With the availability of largescale video surveillance dataset such as VIRAT [131], the Activities in Extended Videos Prize Challenge (ActEV) [7] seeks to encourage the development of real-time robust automatic activity detection algorithms in surveillance scenarios. Specifically, an activity is defined to be “one or more people (or vehicle) performing a specified movement or interacting with an object or group of objects”. Fig. 2.1 illustrates the “talking”, “open\_trunk” and “pull” activities. A few recent work applied a two-stage architecture for temporal action localization [30, 191], and demonstrated competitive performance. In particular, R-C3D network [191] closely follows the original Faster R-CNN [142] architecture but in the temporal domain. There are also several



previous works [45, 59] focusing on online action detection or fine-grained action detection untrimmed Internet videos. However, these methods may not generalize to a more challenging spatial-temporal activity detection problem, which is central for extended video analysis in surveillance videos and self-driving cameras. In this chapter, we describe our object detection and tracking models to generate action proposals of our ActEV system.

## 2.2 Efficient Object Detection and Tracking

The activities of concern in ActEV are summarized in Table 2.1. These activities involve either person or vehicle object, we use this prior knowledge to build the event proposal module starting from the object detection step. The output of this step is person and vehicle bounding box for each frame. The immediate natural next step is to associate detected object across frames, which is tracking. The output of this step is person tracklet and vehicle tracklet.

Type	Activities
Person-Only	Transport_HeavyCarry, Riding, Talking, Activity_carrying, Specialized_talking_phone, Specialized_texting_phone, Entering, Exiting, Closing, Opening
Vehicle-Only	Vehicle_turning_left, Vehicle_turning_right, Vehicle_u_turn
Person-Vehicle	Open_Trunk, Loading, Closing_trunk, Unloading

Table 2.1: Activity categorization on the ActEV dataset.

### 2.2.1 Object Detection

We utilize Mask-RCNN [53] with feature pyramid network [113] on ResNet [52] as the backbone for object detection, in which RoIAlign [53] is used to extract features for Region-of-Interest. We also experiment with the latest state-of-the-art EfficientDet [170] model. The object detection models are trained on either MSCOCO [112] object detection training set or the VIRAT [131] training set. We apply object detection on every  $k$  frame (we find 8 to be a good speed-and-accuracy-trade-off number) in the videos. Full resolution images (1920x1080) or HD resolution (1280x720) images are input to the model to generate object bounding boxes.

**Experimental Results.** We first experiment with a number of variations of Mask-RCNN and EfficientDet models on the VIRAT dataset, a representative dataset of extended videos, and the

	COCO-mAP	VIRAT-Person Val-AP	VIRAT-Vehicle Val-AP	VIRAT-Bike Val-AP
MaskRCNN, R50-FPN	0.389	0.374	0.943	0.367
MaskRCNN, R101-FPN	0.407	0.378	0.947	0.399
EfficientDet-d2	0.425	0.371	0.949	0.293
EfficientDet-d6	0.513	0.422	0.947	0.355
MaskRCNN, R101-FPN*	-	0.831	0.982	0.588

Table 2.2: Object detection evaluation on the VIRAT dataset. “\*” is finetuned on the VIRAT training set.

AVA-Kinetics [95] dataset, a recent action detection dataset based on Internet videos. In these experiments, we mainly evaluate the “Person” and/or “Vehicle” object classes, as they are the most dominant and useful classes for action detection and prediction.

Table 2.2 shows the object detection results on the VIRAT dataset. As we see, for MaskRCNN, Resnet-50 backbone and Resnet-101 backbone perform similarly on detection persons and vehicles. Further finetuning helps tremendously on the VIRAT dataset. The EfficientDet models are significantly better than MaskRCNN overall on all 80 classes on the MS-COCO dataset. However, on the three objects we focus on in the VIRAT dataset, the improvement is not efficient: especially for EfficientDet-d6, the computation cost is more than 2x compared to MaskRCNN, R101-FPN.

Since our goal is to develop an efficient object detection and tracking framework for extended videos, we experiment with different infrastructure and different code bases. As shown in Table 2.3, we experiment with 3 machines, with different GPUs, CPUs and I/O condition. In Table 2.4, we show the experiments that we have run. We mainly test different versions of Tensorflow as well as TensorRT acceleration on the VIRAT validation set, with about 206k images. We use full resolution (1920x1080) inputs. The experiments are shown in Table 2.5. All these runs produce the same object detection results. As we see, later version of Tensorflow with later version of CUDA improves speed significantly. The frozen graph method in Tensorflow also helps. The TensorRT acceleration does not show significant improvement with Tensorflow version 1.14. In conclusion, it is enough to use frozen graph of Tensorflow models for object detection inferencing. Other ways to increase speed include using lower resolution input images and smaller backbone like Resnet-50, but these methods will lead to a decrease in detection average precision.

Machine Type	
Machine 1	2 GTX 1080 TI, i7, nvme
Machine 2	3 GTX 1080 TI + 1 TITAN X, E5, nvme
Machine 3	4 RTX 2080 TI , i9-9900X, SSD

Table 2.3: Machine types that we use to test object detection model speed.

Run	
1	tf 1.10 (CUDA 9, cudnn 7.1), Variable Model
2	tf 1.13 (CUDA 10.0 cudnn 7.4), Variable Model
3	tf 1.13 (CUDA 10.0 cudnn 7.4), Frozen Graph (.pb)
4	tf 1.13 (CUDA 10.0 cudnn 7.4), Frozen Graph (.pb) ->TensorRT Optimized
5	tf 1.14.0 (CUDA 10.0 cudnn 7.4), Variable Model
6	tf 1.14.0 (CUDA 10.0 cudnn 7.4), Frozen Graph (.pb)
7	tf 1.14.0 (CUDA 10.0 cudnn 7.4), Frozen Graph (.pb) ->TRT FP32
8	tf 1.14.0 (CUDA 10.0 cudnn 7.4), Frozen Graph (.pb) ->TRT FP16

Table 2.4: Experiments that we run to test the model speed on VIRAT.

Run	Machine	# GPU Used	GPU Average Utilization	Per GPU FPS
1	1	2	65.3%	2.5
2	1	2	62.0%	2.72
2	2	4	33.8%	1.76
3	2	4	23.5%	1.95
3	2	2	38.0%	2.87
2	2	1	41.4%	2.78
3	2	1	54.8%	3.56
2	2	1*4	46.2%	2.94
3	2	1*4	52.3%	3.54
5	2	1*4	53.2%	3.03
6	2	1*4	61.7%	3.84
7	2	1*4	61.0%	3.93
8	2	1*4	52.6%	3.89
2	3	1	61.2%	3.57
3	3	1	61.2%	4.74
2	3	1*4	62.6%	3.65
3	3	1*4	65.2%	4.83

Table 2.5: Speed experiments on VIRAT with the MaskRCNN model. “1\*4” means 4 inference processes are run concurrently, where one process utilizes one GPU.

	COCO-mAP	AVA-Kinetics Train-Person-AP	AVA-Kinetics Val-Person-AP
MaskRCNN, R101-FPN	0.407	0.664	0.682
EfficientDet-d2	0.425	0.650	0.680
EfficientDet-d6	0.513	0.623	0.658
MaskRCNN, R101-FPN*	-	0.735	0.732

Table 2.6: Person detection evaluation on the AVA-Kinetics dataset. “\*” is finetuned on the AVA-Kinetics training set.

Models	Recall (%)	Precision (%)	ID switches	MOTA (%)	MOTAL (%)
KCF	93.5	<b>97.1</b>	2519	91.3	90.5
deep SORT	<b>95.2</b>	96.5	<b>909</b>	<b>91.7</b>	<b>91.8</b>

Table 2.7: Results of multi-object tracking algorithms in the validation set of VIRAT dataset.

Table 2.6 shows the person detection results on the AVA-Kinetics dataset. As we see, even though the EfficientDet models perform better than MaskRCNN on COCO mean average precision over all 80 object classes, MaskRCNN is better on person detection on the AVA-Kinetics dataset. Further finetuning improves further. In later [chapter 4](#), we will utilize the finetuned model for action detection experiments.

### 2.2.2 Object Tracking

We compare the performance of deep SORT [184] and kernelized correlation filter (KCF) [55]. As shown in Table 2.7, deep SORT outperforms KCF for all the metrics except precision. As the tracking module is used to generate tracklets which are proposal candidates, we expect a high recall and low ID switches with a comparable precision. The results are reported in Table 2.7. In the final system, we utilize deep SORT [184] to generate tracklets by associating detected objects across frames. We follow a similar track handling and Kalman filtering framework [55]. We use bounding box center positions, aspect ratio, height and their respective velocities in image coordinates as Kalman states. We compute the Mahalanobis distance between predicted Kalman states and newly arrived measurement to incorporate motion information. For each bounding box detection, we use the feature obtained from object detection module as a appearance descriptor (either from the Resnet backbone or the EfficientNet backbone). We compute the cosine distance between tracks and detections in appearance space. To build the association problem, we combine both metrics using a weighted sum. An association is defined admissible if it is within the gating region of both metrics.

### 2.2.3 Future Plan

Currently, the object detection code implemented in Tensorflow only supports one image per GPU. We plan to improve the code to support multiple images for each GPU to make it more efficient. Also, we will add native python Queue to allow CPUs to continue preprocessing while GPUs are running the inference to further increase the overall efficiency of the system.



## Chapter 3

# Weakly-supervised Action Event Recognition

Learning detectors that can recognize concepts, such as people actions in video content is an interesting but challenging problem for human behavioral analysis. However, as human actions are diverse and combination of atomic actions can lead to an exponential amount of action classes, it is often difficult to have sufficient human-annotated training data for action recognition and detection. In this chapter, we present our work on webly-labeled learning with multimodal video data [100, 103, 104] to tackle the challenge of not enough manual annotations for action recognition. In the next chapter (chapter 4), we propose viewpoint-invariant feature representation learning for action recognition and detection that could be generalized to multiple action datasets.

### 3.1 Overview

Millions of videos are being uploaded to the Internet every day. These videos capture different aspects of multimedia content about our daily lives. Automatically categorizing videos into concepts, such as people actions, events, etc., is an important topic. Recently many studies have been proposed to tackle the problem of concept learning [2, 33, 70, 80, 99, 111].

Many datasets acquire the clean concept labels via annotators. These datasets include ImageNet [33], TRECVID MED [132] and FCVID [73]. Collecting such datasets requires significant human effort, which is particularly expensive for video data. As a result, the labeled video collection is usually much smaller than the image collection. For example, FCVID [73], only contains about 0.09 million labels on 239 concept classes, much less than the 14 million labels

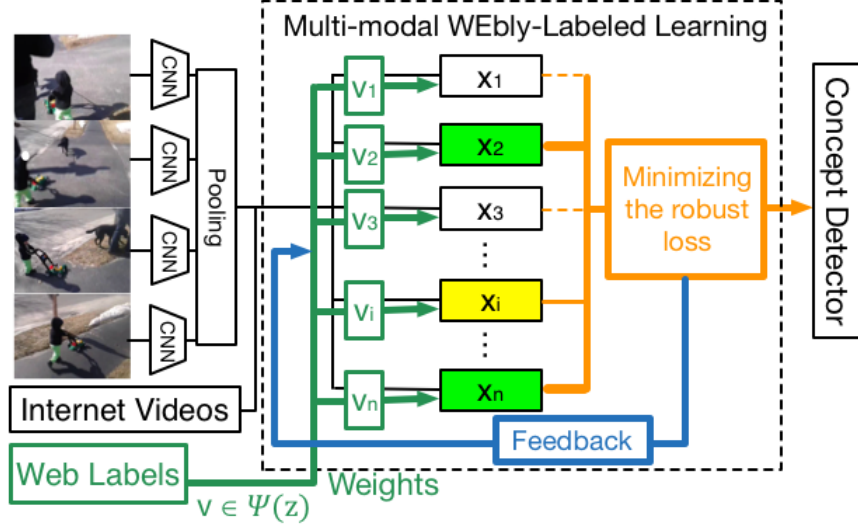


Figure 3.1: Overview of Multi-modal WEbly-Labeled Learning (WELL-MM). The algorithm jointly models the prior knowledge extracted from web labels and the current learned model at each iteration to overcome the noise labels.  $\{x_i\}_{i=1}^n$  are input samples and their current weights are determined by  $\{v_i\}_{i=1}^n$ . Colored samples are the samples with nonzero weights at the current iteration. The blue line indicates the feedback from the previous objective function value.

on over 20,000 classes in the image collection ImageNet [33]. On the other hand, state-of-the-art concept models utilize deep neural networks [80], which need more data to train. However, training only on manually labeled clean data seem insufficient for large-scale concept learning.

Images or videos on the web often contain rich contextual information, such as their titles or descriptions. We can infer the label by the metadata. Fig. 3.2 shows an example of a video with inferred concept label “walking a dog”. In this chapter, we call the samples with inferred labels *weakly labeled* or *webly labeled*. The webly-labeled data are easy to collect and thus usually orders-of-magnitude larger than manually-labeled data. However, the web labels are very noisy and have both low accuracy and low recall.

Concept learning over weakly labeled data becomes popular as it allows for large-scale learning on big data. However, these methods have only focused on utilizing a single text modality to model the noisy labels [24, 100]. For example, in Fig. 3.2, the textual metadata is useful but also contain lots of noises. In fact, the video is of multiple modalities and our intuition is that the inference obtained from multiple modalities is more reliable than that from a single text modality. For example, we can more confident to say this video is about “walk a



dog” if we spot the text in the title, hear the words “good boy” in the speech, and see a dog in some key frames. To this end, we can leverage the prior knowledge in automatically extracted multi-modal features from the video content such as pre-trained still image detectors, automatic speech recognition and optical character recognition. In some cases when videos have little textual metadata, multi-modal knowledge become the only useful clues in concept learning.

Recent studies on weakly labeled concept learning show promising results. However, since existing approaches only focuses on a single modality, two important questions have yet: 1) what are the important multi-modal prior knowledge, except textual metadata, for modeling noisy labels? 2) how to integrate the multiple modalities into concept learning in a theoretically sound manner?

In this chapter, to utilize multi-modal prior knowledge for concept learning, we propose a learning framework called **Multi-modal WEbly-Labeled Learning (WELL-MM)**. The learning framework is motivated by human learning, in which the learner starts from learning easier aspects of a concept, and then gradually take more complex examples into the learning process[11, 69, 87]. Specifically, WELL-MM learns a concept detector iteratively from first using a few samples with more confident labels, then gradually incorporate more samples with noisier labels. Fig. 3.1 shows the overview of the proposed framework. The algorithm integrates multi-modal prior knowledge, which is derived from the multi-modal video and image features, into the dynamic learning procedure. The idea of curriculum and self-paced learning paradigm has been proved to be efficient to deal with noise and outliers [24, 87]. Our proposed method is the first to generalize the learning paradigm to leverage multi-modal prior knowledge into concept learning. Experimental results show that multi-modal prior knowledge is important in concept learning over noisy data. The proposed WELL-MM outperforms other weakly labeled learning methods on three real-world large-scale datasets, and obtains the state-of-the-art results with recent deep learning models.

The contribution of this chapter is threefold. First, we propose a novel solution to address the problem of weakly labeled data learning through a general framework that considers multi-modal prior knowledge. We show that the proposed WELL-MM not only outperforms state-of-the-art learning methods on noisy labels, but also, notably, achieves comparable results with models trained using manual annotation on one of the video dataset. Second, we provide valuable insights by empirically investigating different multi-modal prior knowledge for modeling noisy labels. Experiments validate that by incorporating multi-modal information, our method is robust against certain levels of noisiness. Finally, the efficacy and the scalability have been demonstrated on three public large-scale benchmarks, which include datasets on both Internet



Figure 3.2: Multi-modal prior knowledge from web video.

videos and images. The promising results suggest that detectors trained on sufficient weakly labeled videos may outperform detectors trained on existing manually labeled datasets.

## 3.2 Related Work

**Curriculum and Self-paced Learning:** Recently a learning paradigm called *curriculum learning* (CL) was proposed by Bengio et al., in which a model is learned by gradually incorporating from easy to complex samples in training so as to increase the entropy of training samples [11]. A curriculum determines a sequence of training samples and is often derived by predetermined heuristics in particular problems. For example, Chen et al. designed a curriculum where images with clean backgrounds are learned before the images with noisy backgrounds [24], i.e. their method first builds a feature representation by a Convolutional Neural Network (CNN) on images with clean background and then they fine tune the models on images with noisy background. In [162], the authors approached grammar induction, where the curriculum is derived in terms of the length of a sentence. Because the number of possible solutions grows exponentially with the length of the sentence, and short sentences are easier and thus should be learned earlier.

The heuristic knowledge in a problem often proves to be useful. However, the curriculum

design may lead to inconsistency between the fixed curriculum and the dynamically learned models. That is, the curriculum is predetermined a prior and cannot be adjusted accordingly, taking into account the feedback about the learner. To alleviate the issue of CL, Kumar et al. designed a learning paradigm, called *self-paced learning* (SPL) [87]. SPL embeds curriculum design as a regularizer into the learning objective. Compared with CL, SPL exhibits two advantages: first, it jointly optimizes the learning objective with the curriculum, and thus the curriculum and the learned model are consistent under the same optimization problem; second, the learning is controlled by a regularizer which is independent of the loss function in specific problems. This theory has been successfully applied to various applications, such as action/event detection [68], domain adaption [171], tracking [169] and segmentation [88], reranking [67], etc.

**Learning Detectors in Web Data:** Many recent studies have been proposed to utilize a large amount of noisy data from the Internet. For example, [129] proposed a Never-Ending Language Learning (NELL) paradigm and built adaptive learners that make use of the web data by learning different types of knowledge and beliefs continuously. In the image domain, existing methods try to tackle the problem of constructing qualified training sets based on the search results of text or image search engines [25, 35, 111, 187]. For example, NEIL [25] followed the idea of NELL and learned from web images to form a large collection of concept detectors iteratively via a semi-supervised fashion. By combining the classifiers and the inter-concept relationships it learned, NEIL can be used for scene classification and object detection task. [111] presented a weakly-supervised method called Baby Learning for object detection from a few training images and videos. They first embed the prior knowledge into a pre-trained CNN. When given very few samples for a new concept, a simple detector is constructed to discover much more training instances from the online weakly labeled videos. As more training samples are selected, the concept detector keeps refining until a mature detector is formed. Another recent work in image domain [24] proposed a webly supervised learning of Convolutional Neural Network. They utilized easy images from search engine like Google to bootstrap a first-stage network and then used noisier images from photo-sharing websites like Flickr to train an enhanced model.

In video domain, only a few studies [38, 51, 178] have been proposed for noisy data learning since training robust video concept detectors is more challenging than the problem in the image domain. [38] tackled visual event detection problem by using SVM based domain adaptation method in web video data. [51] described a fast automatic video retrieval method using web images. Given a targeted concept, compact representations of web images obtained from search engines like Google, Flickr are calculated and matched to compact features of videos. Such method can be utilized without any pre-defined concepts. [178] discussed a method that exploits

the YouTube API to train large-scale video concept detectors on YouTube. The method utilized a calibration process and hard negative mining to train a second order mixture of experts model in order to discover correlations within the labels.

### 3.3 Multi-modal WEbly-Labeled Learning (WELL-MM)

#### 3.3.1 Problem Description

In this chapter, following [178], we consider a concept detector as a classifier and our goal is to train concept detectors from webly-labeled video data without any manually annotated labels. Given a collection of training samples with noisy labels, we do not make any assumption over the underlying noise distribution. Formally, we represent the training set as  $\mathcal{D} = \{(\mathbf{x}_i, \mathbf{z}_i, \tilde{\mathbf{y}}_i)\}_{i=1}^n$ , where  $\{\mathbf{x}_1, \dots, \mathbf{x}_n\}$  are the  $d$ -dimensional features of the training set, and  $\{\mathbf{z}_1, \dots, \mathbf{z}_n\}$  represent each sample’s corresponding noisy web labels. We assume that the noisy labels are given. The noisy web labels are often automatically inferred using the sample’s textual metadata provided by its uploader, or from other modalities such as pre-trained convolutional neural network over still images[19], Automatic Speech Recognition [135], or Optical character recognition [161]. For example, for instance, a video might have a noisy label “cat” as its title and speech both contain the word cat. The  $\tilde{\mathbf{y}}_i \subset \mathcal{Y}$  is the inferred concept label set for the  $i^{th}$  observed sample based on its noisy web label, and  $\mathcal{Y}$  denotes the full set of target concepts. In our experiment, to simplify the problem, we employ one-versus-all strategy for multi-class classification, and discuss our method in the context of binary classification over the noisy web labels.

#### 3.3.2 Model

##### Objective Function

In this section, we propose a model called Multi-modal WEbly-Labeled Learning (WELL-MM) to leverage multi-modal prior knowledge for weakly labeled data. Formally, given the training set  $\mathcal{D}$  mentioned previously, Let  $L(\tilde{\mathbf{y}}_i, g(\mathbf{x}_i, \mathbf{w}))$ , denote the loss function which calculates the cost between the inferred label  $\tilde{\mathbf{y}}_i$  and the estimated label given by the decision function  $g(\mathbf{x}_i, \mathbf{w})$ . Here  $\mathbf{w}$  represents the model parameters. Our objective function is to jointly learn the model

parameter  $\mathbf{w}$  and the latent weight variable  $\mathbf{v} = [v_1, \dots, v_n]^T$  by:

$$\min_{\mathbf{w}, \mathbf{v} \in [0,1]^n} \mathbb{E}(\mathbf{w}, \mathbf{v}; \lambda, \Psi) = \sum_{i=1}^n v_i L(\tilde{y}_i, g(\mathbf{x}_i, \mathbf{w})) + f(\mathbf{v}; \lambda), \quad (3.1)$$

subject to  $\mathbf{v} \in \Psi$

where the latent weight variable  $\mathbf{v} = [v_1, \dots, v_n]^T$  represents the inferred labels' confidence, and thus reflects the learning sequence of samples. In order to learn concept detectors in noisy data, we utilize the self-paced regularizer  $f$  [69] to control the learning process, where  $f$  is expect to assign greater weights to samples with confident labels. For simplicity, we consider the linear regularizer Eq. (3.2) proposed in [69]:

$$f(\mathbf{v}; \lambda) = \frac{1}{2} \lambda \sum_{i=1}^n (v_i^2 - 2v_i), \quad (3.2)$$

$\lambda \in (0, 1)$  is a hyper-parameter that controls the pace of model training, which resembles the "age" of the model. We set  $\lambda$  to be small at the beginning and only samples of with small loss will be considered in training. As  $\lambda$  grows, more samples with larger loss will be gradually included. As stated in related studies [100, 127], the self-paced in Eq. (3.2) corresponds to a robust loss function. The robust loss in our problem tends to depress samples with noisy labels or outliers and thus may be instrumental in avoiding bad local minima.

In order to utilize the rich contextual information in the noisy data, we embed the multi-modal prior knowledge derived from the web labels  $\mathbf{z}$  into a convex curriculum region  $\Psi$  for the latent weight variables. The shape of the region weakly implies the learning sequence, where favored samples have larger expected values. Generally,  $\Psi$  can be represented by  $\Psi = \{\mathbf{v} \mid c(\mathbf{v}, \mathbf{a}) \leq b\}$ , where  $\mathbf{a} = [a_1, \dots, a_n]$  is the parameters of the region. In this chapter, we use a linear constraint to form the curriculum region [69]:

$$\Psi = \{\mathbf{v} \mid \sum_{i=1}^n a_i v_i \leq b\} \quad (3.3)$$

The curriculum region is introduced to leverage the prior knowledge about the noisy labels and, as demonstrated in our experiments, is a crucial factor in weakly labeled data learning. We use multi-modal information to derive the probabilities of samples being positive of a class and if the probabilities are below a threshold (in our experiments it is set at zero) the samples will be consider as negatives. We assign value to  $a_i$  in correlated to samples' s probabilities being in the class, and  $b$  is set to 1. We use curriculum as a warm start in training, and set  $\mu$  to zero after

the first iteration. Since we empirically observed that curriculum constraints mostly benefit the first few iterations. We will discuss how to derive the multi-modal curriculum in details in the following section.

Eq. (3.1) is difficult to minimize over big data due to the constraints. In this work, we propose to relax the constraints by introducing a Lagrange multiplier  $\mu$ . The objective function then becomes:

$$\begin{aligned} \min_{\mathbf{w}, \mathbf{v} \in [0,1]^n} \mathbb{E}(\mathbf{w}, \mathbf{v}; \lambda, \mathbf{a}, b, \mu) = \\ \sum_{i=1}^n v_i L(\tilde{y}_i, g(\mathbf{x}_i, \mathbf{w})) + \frac{1}{2} \lambda \sum_{i=1}^n (v_i^2 - 2v_i) + \mu \left( \sum_{i=1}^n a_i v_i - b \right), \end{aligned} \quad (3.4)$$

subject to  $\mu \geq 0$

The proposed Eq. (3.4) has two benefits over Eq. (3.1). First it enables the large-scale training on noisy data. This is important because as our experiments show that training on noisy data can outperform training on manually labeled data only when the noisy data are orders-of-magnitude larger. Second, it may tolerate the noise introduced in the curriculum region.

### Multi-modal Curriculum

In this section we discuss the details on how to construct the curriculum region  $\Psi$ .  $\Psi$  is a feasible region that embeds the multi-modal prior knowledge extracted from the webly-labeled data as shown in Figure. 3.2. It geometrically corresponds to a convex feasible space for the latent weight variable. Given a set of training samples  $\mathbf{X} = \{\mathbf{x}_i\}_{i=1}^n$  with corresponding noisy labels  $\mathbf{Z} = \{\mathbf{z}_i\}_{i=1}^n$ , we want to extract the learning curriculum based on how related the training samples are to the target classes, which is modeled by the probability of the samples being the inferred class label (since we don't have the actual label in webly learning). The training samples with a greater value of probability mean that they are more confident to belong to the true class and should be learned earlier. Similar to Information Retrieval theory [125], here we use random variable  $\mathbf{z}$  to represent the noisy web labels,  $\mathbf{y}$  to represent the label classes, and the curriculum for a sample is then determined by:

$$\mathbf{P}(\mathbf{z} | \mathbf{y}) = \mathbf{P}(\mathbf{y} | \mathbf{z})\mathbf{P}(\mathbf{z})/\mathbf{P}(\mathbf{y}) \quad (3.5)$$

Since  $\mathbf{P}(\mathbf{y})$  is the same for all samples, it can be regarded as a constant. The prior probability of a web video  $\mathbf{P}(\mathbf{z})$  can be implemented with the duration, the view count and comments about the video. In this work we treat the prior as uniform so it can be ignored as well. Therefore,

we calculate the curriculum simply based on  $\mathbf{P}(\mathbf{y} | \mathbf{z})$ , the probability of the sample being class  $\tilde{y}_i$  given the noisy label. Since we want to incorporate the multi-modal prior information, we calculate the curriculum from:

$$\mathbf{P}(\mathbf{y} | \mathbf{z}) \propto \sum_m \theta_m \mathbf{P}(\mathbf{y} | \mathbf{z}_m) \quad (3.6)$$

We use random variable  $z_m$  to represent the  $m$ -th modality of the noisy labels for a sample and  $\theta_m$  is the predetermined weight for modality  $m$ . In this work, other than the textual metadata, we also utilize other modalities such as Automatic Speech Recognition (ASR) [135], Optical Character Recognition (OCR) [161] and basic image detector pre-trained on still images [151] (in this work we use VGG net [160], extract keyframe-level image classification results and average them to get video-level results). Therefore the total number of the modalities is 4. We compare common ways to extract curriculum from web data for concept learning to the proposed novel method that utilizes state-of-the-art topic modeling techniques in natural language processing.

In the following methods (Word Hard Matching and Latent Topic with Word Embedding), we first extract bag-of-words features from different modalities for each video and then match them using specific matching methods to the concept words to get the probabilities in Eq. (3.6).

**Word Hard Matching** We build curriculum directly using exact word matching or stemmed word matching between the textual metadata of the noisy videos to the targeted concept names. This is the same method as stated in Webly Labeled Learning [100]. Noted that this method only utilizes one modality.

**YouTubeTopicAPI** The YouTube topic API is utilized to search for videos that are related to the concept words. The topic API uses textual information of the uploaded videos to obtain related topics of the videos from Freebase. This is the method used in [178].

**SearchEngine** The curriculum is built using the search result from a text-based search engine [126]. It is similar to related web-search based methods.

**Ours** We build the curriculum based on the latent topic we learned from the noisy label. We incorporate Latent Dirichlet Allocation (LDA) [12] to determine how each noisy labeled video is related to each target concept. The intuition is that each web video consists of mixtures of topics (concepts), and each topic is characterized by a distribution of words. We impose asymmetric priors over the word distribution so that each learned topic will be seeded with particular words in our target concept. For example, a topic will be seeded with words "make, phone, cases" for the target concept "MakingPhoneCases". we use the online variational inference algorithm from [57]. We then match noisy labels from each modality  $\mathbf{z}_{im}$  to the latent topic word distribution



using word embedding soft matching [128]. The word embedding is pre-trained using Google News data.

Our method can utilize information from different modalities while common methods like search engine only consider textual information. We compare the performance of different ways of curriculum design by training detectors directly in Section 4.

### 3.3.3 Algorithm

As proven in recent studies [87, 127], Eq. (3.1) is a biconvex optimization problem. We utilize the alternative convex search algorithm (ACS) [10] to optimize Eq. (3.1) following [69, 87]. Algorithm 1 takes the input of the training set, an instantiated self-paced regularizer and the curriculum constraint function; it outputs an optimal model parameter  $\mathbf{w}$ . It derives the curriculum region from multi-modal noisy labels  $\mathbf{Z} \in \mathbb{R}^{m \times n}$  and forms the curriculum constraint function. Then, it initializes the latent weight variables in the feasible region. In the while loop, the algorithm alternates between two steps until it finally converges: In step 4 given the most recent  $\mathbf{v}^*$ , the algorithm learns the optimal model parameters; In step 5, we fix the  $\mathbf{w}^*$  and the algorithm learns the optimal weights  $\mathbf{v}^*$  for each sample. Starting in the beginning, the model grows from learning with easy (less noisy) samples with a small model "age". The model "age" is gradually increased so that the model can incorporate more noisy samples in the training and become more robust over time. Step 4 can be implemented by existing off-the-shelf supervised learning methods such as the Support Vector Machine or back propagation. Gradient-based methods can be used to solve the convex optimization problem in Step 5. According to [48], the alternative search in Algorithm 1 converges as the objective function is monotonically decreasing and is bounded from below.

## 3.4 Experimental Results

In this section, we evaluate our method WELL-MM for learning video detectors on noisy labeled data. We first conduct our method on noisy learning in image domain. The efficacy of our methods are mainly verified on two major public benchmarks: FCVID and YFCC100M, where FCVID is by far one of the biggest manually annotated video dataset [73], and the YFCC100M dataset is the largest multimedia benchmark [174].



---

**Algorithm 1** Multi-modal WEbly-Labeled Learning

---

**input** : Input dataset  $\mathcal{D} = \{\mathbf{X}, \mathbf{Z}, \tilde{\mathbf{Y}}\}$ , self-paced function  $f$  and a curriculum constraint function  $c$

**output**: Model parameter  $\mathbf{w}$

- 1 Derive curriculum region from  $\mathbf{Z} \in \mathbb{R}^{m \times n}$  into  $\mathbf{a}, b$
- 2 Initialize  $\mathbf{v}^*, \lambda$  in the curriculum region
- 3 **while** *not converged* **do**
- 4     Update  $\mathbf{w}^* = \arg \min_{\mathbf{w}} \mathbb{E}(\mathbf{w}, \mathbf{v}^*; \lambda, \mathbf{a}, b)$
- 5     Update  $\mathbf{v}^* = \arg \min_{\mathbf{v}} \mathbb{E}(\mathbf{w}^*, \mathbf{v}; \lambda, \mathbf{a}, b)$
- 6     **if**  $\lambda$  is *small* **then** increase  $\lambda$  by the step size;
- 7 **end**
- 8 **return**  $\mathbf{w}^*$

---

### 3.4.1 Experimental Setup

**Datasets, Features and Evaluation Metrics** Previous studies on noisy learning in image domain have been focusing on noise estimation [166, 187]. We compare our method with them on the synthesized noisy dataset CIFAR-10 generated using code from [187]. We report accuracy on each setting along with the results reported in papers [166, 187] experimented on the same dataset.

Fudan-columbia Video Dataset (FCVID) contains 91,223 YouTube videos (4,232 hours) from 239 categories. It covers a wide range of concepts like activities, objects, scenes, sports, DIY, etc. Detailed descriptions of the benchmark can be found in [73]. Each video is manually labeled to one or more categories. In our experiments, we do not use the manual labels in training, but instead we automatically generate the web labels according to the concept name appearance in the video metadata. The manual labels are used only in testing to evaluate our and the baseline methods. Following [73], the standard train/test split is used. The second set is YFCC100M [174] which contains about 800,000 videos on Yahoo! Flickr with metadata such as the title, tags, the uploader, etc. There are no manual labels on this set and we automatically generate the curriculum from the metadata in a similar way. Since there are no annotations, we train the concept detectors on the most 101 frequent latent topics found in the metadata. There are totally 47,397 webly labeled videos on the 101 concepts for training.

On FCVID, as the manual labels are available, the performance is evaluated in terms of the precision of the top 5 and 10 ranked videos (P@5 and P@10) and mean Average Precision (mAP)

of 239 concepts. On YFCC100M, since there are no manual labels, for evaluation, we apply the detectors to a third public video collection called TRECVID MED which includes 32,000 Internet videos [132]. We apply the detectors trained on YFCC100M to the TRECVID videos and manually annotate the top 10 detected videos returned by each method for 101 concepts.

**Implementation Details** We build our method on top of a pre-trained convolutional neural network as the low-level features (VGG network [160], except in the image experiment we use AlexNet [86] as in [187]). We extract the key-frame level features and create a video feature by the average pooling. The same features are used across different methods on each dataset. The concept detectors are trained based on a hinge loss cost function by SVM. Algorithm 1 is used to train the concept models iteratively and the  $\lambda$  stops increasing after 100 iterations. At each iteration, we apply a dropout of 0.5 when sampling negative samples. We automatically generate curriculum labels based on the video metadata, ASR, OCR and VGG net 1,000 classification results using latent topic modeling with word embedding matching as shown in Section 3.

**Baselines in video domain experiment** The proposed method is compared against the following five baseline methods which cover both the classical and the recent representative learning algorithms on webly-labeled data. *BatchTrain* trains a single SVM model using all samples in the multi-modal curriculum built with our method as described in section 3.2.2. *Self-Paced Learning (SPL)* is a classical method where the curriculum is generated by the learner itself [87]. *BabyLearning* is a recent method that simulates baby learning by starting with few training samples and fine-tuning using more weakly labeled videos crawled from the search engine [111]. *GoogleHNM* is a hard negative mining method proposed by Google [178]. It utilizes hard negative mining to train a second order mixture of experts model according to the video’s YouTube topics. *FastImage* [51] is a video retrieval method that utilizes web images from search engine to match to the video with re-ranking. *WELL-MM* is the proposed method. The hyper-parameters of all methods including the baseline methods are tuned on the same validation set. On FCVID, the set is a standard development set with manual labels randomly selected from 10% of the training set (No training was done using ground truth labels) whereas on YFCC100M it is also a 10% proportion of noisy training set.

### 3.4.2 Experiments on FCVID

**Curriculum Comparison** As discussed in Section 3.2.2, we compare different ways to build curriculum for noisy label learning. Here we also compare their effectiveness by training con-

Table 3.1: Comparison of different curriculum using the BatchTrain learning method.

Method	P@5	P@10	mAP
WordHardMatching	0.782	0.763	0.469
YouTubeTopicAPI	0.587	0.563	0.315
SearchEngine	0.723	0.713	0.413
WordEmbedding	0.790	0.774	0.462
LatentTopic	0.731	0.716	0.409
<b>WELL-MM</b>	<b>0.838</b>	<b>0.820</b>	<b>0.486</b>

cept detectors directly using the curriculum labels. The batch train model is used for all generated curriculum labels. In Table 3.1 we show the batch trained models’ precision at 5, 10 and mean average precision on the test set of FCVID. For WELL-MM, we extract curriculum from different modalities as shown in Section 3.2.2, and combine them using linear weights. The weights are hyper-parameters that are tuned on the validation set, and the optimal weights for textual metadata, ASR, image classification and OCR results are 1.0, 0.5, 0.5 and 0.05, respectively. This attempt to combining curriculum from different modalities serves as a pilot study. However, experiments show that such simple linear weighting is already effective with WELL-MM. Further research in this direction is left for future work. We also compare WELL-MM with using only latent topic modeling and word embedding soft matching. Results show that the curriculum generated by combining latent topic modeling and word embedding using multi-modal prior knowledge is the most accurate, which indicates our claim of exploiting multi-modal information is beneficial.

**Baseline Comparison** Table 3.2 compares the precision and mAP of different methods where the best results are highlighted. As we see, the proposed WELL-MM significantly outperforms all baseline methods, with statistically significant difference at  $p$ -level of 0.05. Comparing SPL with BatchTrain, it shows that the self-paced learning model over-fits to the noise without prior knowledge and performs worse than the simple BatchTrain model. Comparing WELL-MM with SPL and BatchTrain, the effect of incorporating multi-modal curriculum makes a significant difference in terms of performance, which suggests the importance of prior knowledge and preventing over-fitting in webly learning. The promising experimental results substantiate the efficacy of the proposed method.

**Robustness to Noise Comparison** In this comparison we manually control the noise level of the curriculum in order to systematically verify how our methods would perform with re-

Table 3.2: Baseline comparison on FCVID

Method	P@5	P@10	mAP
BatchTrain	0.838	0.820	0.486
FastImage [51]	-	-	0.284
SPL [88]	0.793	0.754	0.414
GoogleHNM [178]	0.781	0.757	0.472
BabyLearning [111]	0.834	0.817	0.496
<b>WELL-MM</b>	<b>0.918</b>	<b>0.906</b>	<b>0.615</b>

spect to the noise level within the web data. To this end, we randomly select video samples with ground truth labels for each concept, so that the noise level of the curriculum labels are set at 20%, 40%, 60%, 80% and we fix the recall of all the labels. We then train WELL-MM using such curriculum and test them on the FCVID testing set. We also compare WELL-MM to three other methods with the same curriculum, among them *GoogleHNM* is a recent method to train video concept detector with large-scale data. We exclude *BabyLearning*, which relies on the returned results by the search engine, since in this experiment the curriculum is fixed. As shown in Table 3.3, as the noise level of the curriculum grows, WELL-MM maintains its performance while other methods drop significantly. Specifically, when the noise level of curriculum increased from 60% to 80%, other methods’ mAP drops 46.5% on average while WELL-MM’s mAP only drops 19.1% relatively. It shows that WELL-MM is robust against different level of noise, which shows great potential in larger scale webly-labeled learning as the dataset gets bigger, the noisier it may become.

Table 3.3: WELL-MM performance with curriculum consisting of multiple artificial noise levels.

Method \ Noise Level	Noise Level			
	20%	40%	60%	80%
BatchTrain	0.592	0.538	0.463	0.232
SPL	0.586	0.515	0.396	0.184
GoogleHNM	0.602	0.552	0.477	0.304
<b>WELL-MM</b>	<b>0.673</b>	<b>0.646</b>	<b>0.613</b>	<b>0.496</b>

**Noisy Dataset Size Comparison** To investigate the potential of concept learning on webly-labeled video data, we apply the methods on different sizes of subsets of the data. Specifically,

we randomly split the FCVID training set into several subsets of 200, 500, 1,000, and 2,000 hours of videos, and train the models on each subset without using manual annotations. The models are then tested on the same test set. Table 3.4 lists the average results of each type of subsets. As we see, the accuracy of WELL-MM on webly-labeled data increases along with the growth of the size of noisy data while other webly learning methods’ performance tend to be saturated.

Comparing to the methods trained using ground truth, In Table 3.4, WELL-MM trained using the whole dataset (2000 hours) outperforms Static CNN (trained using manual labels) using around 1400 hours of data and rDNN-F (trained using manual labels with three features) trained using around 450h of data. And since the incremental performance increase of WELL-MM is close to linear, we conclude that with sufficient webly-labeled videos (which are not hard to obtain) WELL-MM will be able to outperform the rDNN-F trained using 2000h of data, which is currently the largest manual labeled dataset.

Table 3.4: MAP comparison of models trained using web labels and ground-truth labels on different subsets of FCVID. The methods marked by \* are trained using human annotated labels.

Method \ Dataset Size	200h	500h	1000h	2000h
BatchTrain	0.364	0.422	0.452	0.486
SPL [88]	0.327	0.379	0.403	0.414
GoogleHNM [178]	0.361	0.421	0.451	0.472
BabyLearning [111]	0.390	0.447	0.481	0.496
WELL-MM	0.487	0.554	0.595	0.615
Static CNN[73]*	0.485	0.561	0.604	0.638
rDNN-F[73]*	0.550	0.620	0.650	0.754

### 3.4.3 Experiments on CIFAR-10

Following [187], we generate synthesized noisy training data with a noise level of 30%, 40% and 50% on CIFAR-10 dataset. The models are trained on noisy data and tested on clean data. Classification Accuracy is reported. Our method doesn’t assume any kind of noise distribution, while Noisy-CNN [166] assumes the noise distribution depends on classes and Massive-Learning [187] assumes it also depends on the image content. We show the experimental results in Table 3.5. The results show that WELL-MM outperforms the other methods at all noise

Table 3.5: Experimental results on CIFAR-10

Methods \ Noise Level	30%	40%	50%
Noisy-CNN [166]	0.697	0.667	0.634
Massive-Learning [187]	0.698	0.668	0.630
<b>WELL-MM</b>	<b>0.709</b>	<b>0.700</b>	<b>0.682</b>

levels. More interestingly, as the noise level rises from 30% to 50%, the performance of Massive-Learning [187] drops about 9.8%, while WELL-MM only drops 3.8%. It shows that WELL-MM can also effectively learn robust concept detectors in image domain.

#### 3.4.4 Experiments on YFCC100M

In the experiments on YFCC100M, we train 101 concept detectors on YFCC100M and test them on the TRECVID MED dataset which includes 32,000 Internet videos. Since there are no manual labels, to evaluate the performance, we manually annotate the top 10 videos in the test set and report their precisions in Table 3.6. The MED evaluation is done by four annotators and the final results are averaged from all annotations. The Fleiss’ Kappa value for these four annotators is 0.64. A similar pattern can be observed where the comparisons substantiate the rationality of the proposed webly learning framework. Besides, the promising results on the largest multimedia set YFCC100M verify the scalability of the proposed method.

Table 3.6: Baseline comparison on YFCC100M

Method	P@3	P@5	P@10
BatchTrain	0.535	0.513	0.487
SPL [88]	0.485	0.463	0.454
GoogleHNM [178]	0.541	0.525	0.500
BabyLearning [111]	0.548	0.519	0.466
<b>WELL-MM</b>	<b>0.667</b>	<b>0.663</b>	<b>0.649</b>



Figure 3.3: Illustration of representative videos selected by WELL-MM at different iterations

### 3.4.5 Qualitative Analysis

In this section we show training examples of WELL-MM. In Fig. 3.3, we demonstrate the positive samples that WELL select at different stage of training the concept "baseball" and "birthday". For the concept "baseball", at the early stage (1/93, 25/93), WELL-MM selects easier and clearer samples such as the ones with camera directly pointing at the playground, while at the later stage (75/93, 93/93) WELL-MM starts to train with harder samples with different lighting conditions and untypical samples for the concept. For the concept "birthday", as we see, at later stage of the training, complex samples for birthday event like a video with two girl singing birthday song (75/84) and a video of celebrating birthday during hiking (84/84) are included in the training, while at the early stage, only typical "birthday" videos with birthday cake and candles are included.





## Chapter 4

# Viewpoint Invariant Representation Learning for Action Recognition and Detection

In this chapter, we explore viewpoint-invariant feature representations that aim to have better generalization abilities for action recognition and detection.

### 4.1 Overview

Humans can recognize actions from different viewpoints. However, current action recognition and detection models are sensitive to viewpoint changes and susceptible to adversarial attacks [175], which indicates a mismatch between current action models and how humans actually perceive actions. Meanwhile, traditional convolutional neural networks are not designed to be viewpoint-equivariant [85], suggesting the need to develop a new model that could produce consistent feature representations despite viewpoint changes. This quality is especially important for action recognition and detection for moving cameras, as they usually include viewpoint changes and ego-motions.

Inspired by the Spatial Transformer Network [63] and Stacked Capsule Autoencoder [85] for image recognition, we propose Focal Transformer Network (FTN) that aims to learn viewpoint invariant representations for action recognition and action detection. This work is used to research the approach that can be potentially used in training video detectors on in-domain datasets. As shown in Fig. 4.1, we develop a Focal Transformer Network (FTN) Block, which

takes a spatial-temporal feature input tensor, extract viewpoint invariant hints, and outputs a spatial-temporal transformation matrix for feature warping that produces an output tensor of the same shape.

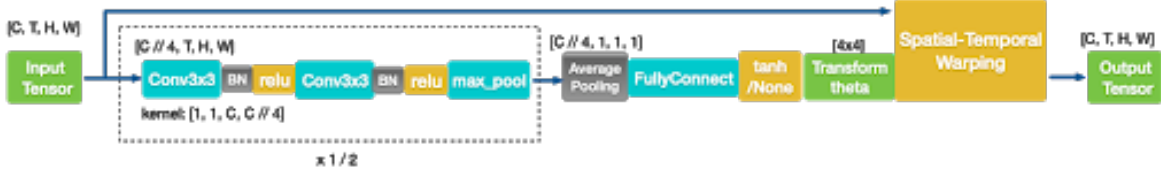


Figure 4.1: Focal transformer network (FTN) block design.

The FTN block is very light-weighted and generic, which could be plugged into existing action recognition models like 3D-Resnet, Non-Local Network [181] and the Slowfast network [41]. In Fig. 4.2, as a preliminary experiment, we put FTN block between Res-1 and Res-2 in 3D ResNet architecture, and the same on the Fast pathway in SlowFast model. For the Slowfast+FTN model, the FLOPS increase is only 1.8% (134.04 gFLOPS vs. 131.67 gFLOPS).

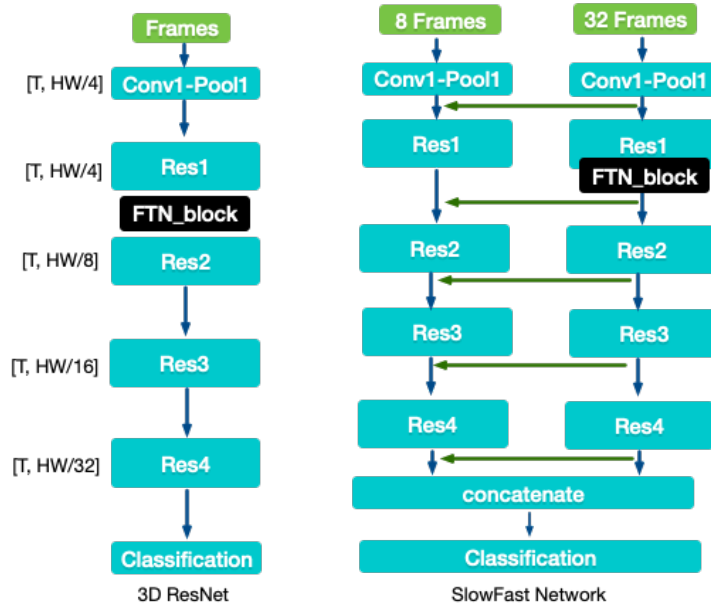


Figure 4.2: Focal transformer network (FTN) block in 3D ResNet and SlowFast Network.

	top-1	top-5
Non-Local Network [181]	0.749	0.916
Resnet3D	0.735	0.908
Resnet3D + FTN (Ours)	<b>0.751</b>	<b>0.916</b>
SLOWFAST [41]	0.759	0.920
SLOWFAST + FTN (Ours)	<b>0.769</b>	<b>0.928</b>

Table 4.1: Experiment results on Kinetics-400 dataset.

Models	256x256 mAP
SLOWFAST [41]	0.386
SLOWFAST + FTN	<b>0.406</b>

Table 4.2: Experiment results on Charades dataset.

## 4.2 Initial Experimental Results

To demonstrate the efficacy of our models, specifically, the viewpoint-invariant design that helps action models to generalize, we experiment on several major action recognition datasets, including Kinetics-400 [81], Charades [158], CharadesEgo [159], and two recent action detection datasets, AVA [49] and AVA-Kinetics [95], where we show significant improvement over baselines while only adding a fraction of computation. The action recognition task is defined to be a multi-class action classification task. The action detection task is similar but the models also have to output action/person bounding boxes, and only predicted boxes with higher IoU (intersection over union) area w.r.t the ground truth boxes are considered true positives.

Table 4.1 shows the experiments on Kinetics-400, where we add FTN to Resnet-3D network and Slowfast network and improve the top-1/5 accuracy. The backbone network is Resnet-50.

Table 4.2 and Table 4.3 show the results on Charades and Charades-Ego datasets, respectively. We measure the mean average precision over 157 action classes and the test spatial crop size is 256x256. On Charades-Ego dataset, the test set is divided into 1st-person videos and 3rd-person videos. Note that the training set of Charades-Ego dataset includes mostly 3rd-person videos, and we can observe from the results that our FTN model achieves more significant improvement on the 1st-person test set, verifying the efficacy of our model’s generalization ability.

Table 4.4 shows the results on AVA dataset [49]. We follow the SLOWFAST [41] paper’s

Models	1st-person	3rd-person
previous SOTA (CVPR’18) [159]	0.282	0.232
Resnet3D	0.298	0.361
Resnet3D + FTN	<b>0.318</b>	<b>0.366</b>
SLOWFAST	0.316	0.391
SLOWFAST + FTN	<b>0.326</b>	<b>0.396</b>

Table 4.3: Experiment results on Charades-Ego dataset.

Models	256x256 mAP
Resnet3D	0.234
Resnet3D + FTN (Ours)	<b>0.241</b>
SLOWFAST [41]	0.252
SLOWFAST + FTN (Ours)	<b>0.263</b>

Table 4.4: Experiment results on AVA dataset.

evaluation protocol and use the same predicted person bounding boxes with ROIAlign to classify actions. We measure the mean average precision over 60 action classes and the test spatial crop size is 256x256.

Table 4.5 shows the results on AVA-Kinetics dataset [95]. We follow the SLOWFAST [41] paper’s evaluation protocol and experiment with ground truth person boxes as well as predicted person boxes using the person detection model (Mask-RCNN) described in chapter 2. We measure the mean average precision over 60 action classes and the test spatial crop size is 256x256.

Models	256x256 GTBox mAP	256x256 PredictedBox mAP
Action Transformer [95]	0.270	0.168
Resnet3D	0.315	0.224
Resnet3D + FTN (Ours)	<b>0.336</b>	<b>0.238</b>
SLOWFAST [41]	0.341	0.242
SLOWFAST + FTN (Ours)	<b>0.358</b>	<b>0.253</b>

Table 4.5: Experiment results on AVA-Kinetics dataset.

### **4.3 Future Plan**

We have completed most of the main experiments for this work. We will conduct ablation experiments and qualitative analysis to further investigate the benefit of the proposed viewpoint-invariant model.



## **Part II**

# **Human Trajectory Prediction with Scene Semantics**





In this part, we focus on the human future trajectory prediction problem. We study how trajectory prediction can benefit from semantic context understanding of the scene. Since the future is uncertain, we first introduce the *Multiverse* model to tackle the multiple-future trajectory prediction problem ([chapter 5](#)). To alleviate the limited training data challenge as mentioned in previous section, we propose a machine learning algorithm called *SimAug*, to efficiently learn from 3D simulation data for trajectory prediction ([chapter 6](#)).



## Chapter 5

# Multiple-future Pedestrian Trajectory Prediction

In this chapter, we study the uncertainty of future trajectory predictions, by proposing the *Multiverse* model [109], which generates multiple-future trajectories with probability distributions. We also develop a novel multiple-future trajectory benchmark, called the *ForkingPaths* dataset, using 3D simulation. Later on in [chapter 6](#), we focus on training a robust trajectory prediction model, with multi-view video data from 3D simulation. In [chapter 8](#), we propose to work on long-term trajectory and action prediction, which could help improve traffic safety and public safety.

### 5.1 Overview

Forecasting future human behavior is a fundamental problem in video understanding. In particular, future path prediction, which aims at forecasting a pedestrian’s future trajectory in the next few seconds, has received a lot of attention in our community [3, 50, 82, 97]. This functionality is a key component in a variety of applications such as autonomous driving [9, 16], long-term object tracking [76, 152], safety monitoring [107], robotic planning [143, 144], etc.

Of course, the future is often very uncertain: Given the same historical trajectory, a person may take different paths, depending on their (latent) goals. Thus recent work has started focusing on *multi-future trajectory prediction* [16, 92, 97, 122, 172, 173].

Consider the example in [Fig. 5.1](#). We see a person moving from the bottom left towards the top right of the image, and our task is to predict where he will go next. Since there are many possible future trajectories this person might follow, we are interested in learning a model that

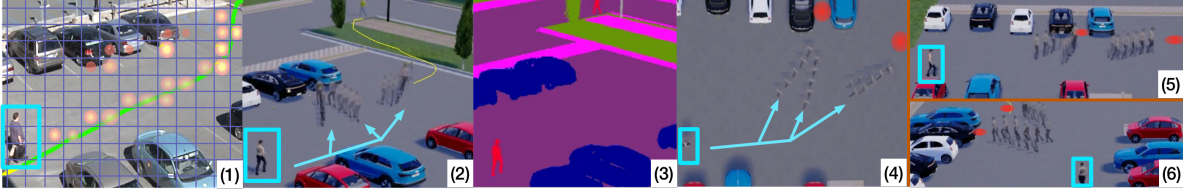


Figure 5.1: Illustration of person trajectory prediction. (1) A person walks towards a car (data from the VIRAT/ActEV dataset). The green line is the actual future trajectory and the yellow-orange heatmaps are example future predictions. Although these predictions near the cars are plausible, they would be considered errors in the real video dataset. (2) To combat this, we propose a new dataset called “Forking Paths”; here we illustrate 3 possible futures created by human annotators controlling agents in a synthetic world derived from real data. (3) Here we show semantic segmentation of the scene. (4-6) Here we show the same scene rendered from different viewing angles, where the red circles are future destinations.

can generate multiple plausible futures. However, since the ground truth data only contains one trajectory, it is difficult to evaluate such probabilistic models.

To overcome the aforementioned challenges, our first contribution is the creation of a realistic synthetic dataset that allows us to compare models in a quantitative way in terms of their ability to predict multiple plausible futures, rather than just evaluating them against a single observed trajectory as in existing studies. We create this dataset using the 3D CARLA [37] simulator, where the scenes are manually designed to be similar to those found in the challenging real-world benchmark VIRAT/ActEV [6, 131]. Once we have recreated the static scene, we automatically reconstruct trajectories by projecting real-world data to the 3D simulation world. See Fig. 5.1 and 5.3. We then semi-automatically select a set of plausible future destinations (corresponding to semantically meaningful locations in the scene), and ask human annotators to create multiple possible continuations of the real trajectories towards each such goal. In this way, our dataset is “anchored” in reality, and yet contains plausible variations in high-level human behavior, which is impossible to simulate automatically.

We call this dataset the “Forking Paths” dataset, a reference to the short story by Jorge Luis Borges.<sup>1</sup> As shown in Fig. 5.1, different human annotations have created forkings of future trajectories for the identical historical past. So far, we have collected 750 sequences, with each covering about 15 seconds, from 10 annotators, controlling 127 agents in 7 different scenes. Each agent contains 5.9 future trajectories on average. We render each sequence from 4 differ-

<sup>1</sup>[https://en.wikipedia.org/wiki/The\\_Garden\\_of\\_Forking\\_Paths](https://en.wikipedia.org/wiki/The_Garden_of_Forking_Paths)

ent views, and automatically generate dense labels, as illustrated in Fig. 5.1 and 5.3. In total, this amounts to 3.2 hours of trajectory sequences, which is comparable to the largest person trajectory benchmark VIRAT/ActEV [6, 131] (4.5 hours), or 5 times bigger than the common ETH/UCY [94, 116] benchmark. We therefore believe this will serve as a benchmark for evaluating models that can predict multiple futures.

Our second contribution is to propose a new probabilistic model, *Multiverse*, which can generate multiple plausible trajectories given the past history of locations and the scene. The model contains two novel design decisions. First, we use a multi-scale representation of locations. In the first scale, the coarse scale, we represent locations on a 2D grid, as shown in Fig. 5.1(1). This captures high level uncertainty about possible destinations and leads to a better representation of multi-modal distributions. In the second fine scale, we predict a real-valued offset for each grid cell, to get more precise localization. This two-stage approach is partially inspired by object detection methods [142]. The second novelty of our model is to design convolutional RNNs [190] over the spatial graph as a way of encoding inductive bias about the movement patterns of people.

In addition, we empirically validate our model on the challenging real-world benchmark VIRAT/ActEV [6, 131] for single-future trajectory prediction, in which our model achieves the best-published result. On the proposed simulation data for multi-future prediction, experimental results show our model compares favorably against the state-of-the-art models across different settings. To summarize, the main contributions of this chapter are as follows: (i) We introduce the first dataset and evaluation methodology that allows us to compare models in a quantitative way in terms of their ability to predict multiple plausible futures. (ii) We propose a new effective model for multi-future trajectory prediction. (iii) We establish a new state of the art result on the challenging VIRAT/ActEV benchmark, and compare various methods on our multi-future prediction dataset.

## 5.2 Related Work

This work falls under the category of sequential models that utilize both static and dynamic environmental cues in the human motion prediction literature [149]. In the following, we also review a few relevant recent approaches based on their outputs. Then we also review the trajectory prediction datasets.

**Single-future trajectory prediction.** Recent works have tried to predict a single best trajectory for pedestrians or vehicles. Early works [124, 193, 201] focused on modeling person

motions by considering them as points in the scene. These research works [83, 107, 120, 194] have attempted to predict person paths by utilizing visual features. Recently Liang et al. [107] proposed a joint future activity and trajectory prediction framework that utilized multiple visual features using focal attention [105, 106]. Many works [9, 58, 92, 154, 204] in vehicle trajectory prediction have been proposed. CAR-Net [154] proposed attention networks on top of scene semantic CNN to predict vehicle trajectories. ChauffeurNet [9] utilized imitation learning for trajectory prediction.

**Multi-future trajectory prediction.** Many works have tried to model the uncertainty of trajectory prediction. Various papers (e.g. [82, 144, 145]) use Inverse Reinforcement Learning (IRL) to forecast human trajectories. Social-LSTM [3] is a popular method using social pooling to predict future trajectories. Other works [5, 50, 97, 153] like Social-GAN [50] have utilized generative adversarial networks [46] to generate diverse person trajectories. In vehicle trajectory prediction, DESIRE [92] utilized variational auto-encoders (VAE) to predict future vehicle trajectories. Many recent works [16, 122, 172, 173] also proposed probabilistic frameworks for multi-future vehicle trajectory prediction. Different from these previous works, we present a flexible two-stage framework that combines multi-modal distribution modeling and precise location prediction.

**Trajectory Prediction Datasets.** Many vehicle trajectory datasets [14, 17] have been proposed as a result of self-driving’s surging popularity. With the recent advancement in 3D computer vision research [37, 54, 101, 146, 148, 155, 203], many research works [31, 32, 42, 136, 167, 186, 206] have looked into 3D simulated environment for its flexibility and ability to generate enormous amount of data. We are the first to propose a 3D simulation dataset that is reconstructed from real-world scenarios complemented with a variety of human trajectory continuations for multi-future person trajectory prediction.

### 5.3 The *Multiverse* Model

In this section, we describe our model for forecasting agent trajectories, which we call *Multiverse*. We focus on predicting the locations of a single agent for multiple steps into the future,  $L_{h+1:T}$ , given a sequence of past video frames,  $V_{1:h}$ , and agent locations,  $L_{1:h}$ , where  $h$  is the history length and  $T - h$  is the prediction length. Since there is inherent uncertainty in this task, our goal is to design a model that can effectively predict multiple plausible future trajectories, by computing the multimodal distribution  $p(L_{h+1:T}|L_{1:h}, V_{1:h})$ . See Fig. 5.2 for a high level summary of the model, and the sections below for more details.

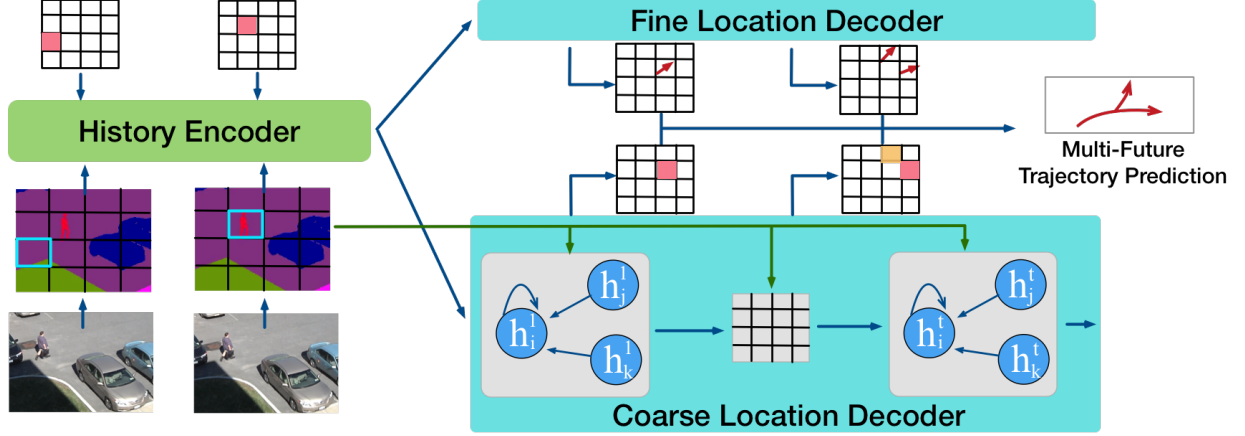


Figure 5.2: Overview of our model. The input to the model is the ground truth location history, and a set of video frames, which are preprocessed by a semantic segmentation model. This is encoded by the “History Encoder” convolutional RNN. The output of the encoder is fed to the convolutional RNN decoder for location prediction. The coarse location decoder outputs a heatmap over the 2D grid of size  $H \times W$ . The fine location decoder outputs a vector offset within each grid cell. These are combined to generate a multimodal distribution over  $\mathbb{R}^2$  for predicted locations.

### 5.3.1 History Encoder

The encoder computes a representation of the scene from the history of past locations,  $L_{1:h}$ , and frames,  $V_{1:h}$ . We encode each ground truth location  $L_t$  by an index  $Y_t \in G$  representing the nearest cell in a 2D grid  $G$  of size  $H \times W$ , indexed from 1 to  $HW$ . Inspired by [91, 113], we encode location with two different grid scales ( $36 \times 18$  and  $18 \times 9$ ); we show the benefits of this multi-scale encoding in Section 5.5.3. For simplicity of presentation, we focus on a single  $H \times W$  grid.

To make the model more invariant to low-level visual details, and thus more robust to domain shift (e.g., between different scenes, different views of the same scene, or between real and synthetic images), we preprocess each video frame  $V_t$  using a pre-trained semantic segmentation model, with  $K = 13$  possible class labels per pixel. We use the Deeplab model [22] trained on the ADE20k [205] dataset, and keep its weights frozen. Let  $S_t$  be this semantic segmentation map modeled as a tensor of size  $H \times W \times K$ .

We then pass these inputs to a convolutional RNN [182, 190] to compute a spatial-temporal feature history:

$$H_t^e = \text{ConvRNN}(\text{one-hot}(Y_t) \odot (W * S_t), H_{t-1}^e) \quad (5.1)$$

where  $\odot$  is element wise product, and  $*$  represents 2D-convolution. The function  $\text{one-hot}(\cdot)$  projects a cell index into an one-hot embedding of size  $H \times W$  according to its spatial location.

We use the final state of this encoder  $H_t^e \in \mathbb{R}^{H \times W \times d_{enc}}$ , where  $d_{enc}$  is the hidden size, to initialize the state of the decoders. We also use the temporal average of the semantic maps,  $\bar{S} = \frac{1}{h} \sum_{t=1}^h S_t$ , during each decoding step. The context is represented as  $\mathcal{H} = [H_h^e, \bar{S}]$ .

### 5.3.2 Coarse Location Decoder

After getting the context  $\mathcal{H}$ , our goal is to forecast future locations. We initially focus on predicting locations at the level of grid cells,  $Y_t \in G$ . In Section 5.3.3, we discuss how to predict a continuous offset in  $\mathbb{R}^2$ , which specifies a “delta” from the center of each grid cell, to get a fine-grained location prediction.

Let the coarse distribution over grid locations at time  $t$  (known as the “belief state”) be denoted by  $C_t(i) = p(Y_t = i | Y_{h:t-1}, \mathcal{H})$ , for  $\forall i \in G$  and  $t \in [h+1, T]$ . For brevity, we use a single index  $i$  to represent a cell in the 2D grid. Rather than assuming a Markov model, we update this using a convolutional recurrent neural network, with hidden states  $H_t^C$ . We then compute the belief state by:

$$C_t = \text{softmax}(W * H_t^C) \in \mathbb{R}^{HW} \quad (5.2)$$

Here we use 2D-convolution with one filter and flatten the spatial dimension before applying softmax. The hidden state is updated using:

$$H_t^C = \text{ConvRNN}(\text{GAT}(H_{t-1}^C), \text{embed}(C_{t-1})) \quad (5.3)$$

where  $\text{embed}(C_{t-1})$  embeds into a 3D tensor of size  $H \times W \times d_e$  and  $d_e$  is the embedding size.  $\text{GAT}(H_{t-1}^C)$  is a graph attention network [180], where the graph structure corresponds to the 2D grid in  $G$ . More precisely, let  $h_i$  be the feature vector corresponding to the  $i$ -th grid cell in  $H_{t-1}^C$ , and let  $\tilde{h}_i$  be the corresponding output in  $\tilde{H}_{t-1}^C = \text{GAT}(H_{t-1}^C) \in \mathbb{R}^{H \times W \times d_{dec}}$ , where  $d_{dec}$  is the size of the decoder hidden state. We compute these outputs of GAT using:

$$\tilde{h}_i = \frac{1}{|\mathcal{N}_i|} \sum_{j \in \mathcal{N}_i} f_e([v_i, v_j]) + h_i \quad (5.4)$$

where  $\mathcal{N}_i$  are the neighbors of node  $v_i$  in  $G$  with each node represented as  $v_i = [h_i, \bar{S}_i]$ , where  $\bar{S}_i$  collects the cell  $i$ ’s feature in  $\bar{S}$ .  $f_e$  is some edge function (implemented as an MLP in our experiments) that computes the attention weights.



The graph-structured update function for the RNN ensures that the probability mass “diffuses out” to nearby grid cells in a controlled manner, reflecting the prior knowledge that people do not suddenly jump between distant locations. This inductive bias is also encoded in the convolutional structure, but adding the graph attention network gives improved results, because the weights are input-dependent and not fixed.

### 5.3.3 Fine Location Decoder

The 2D heatmap is useful for capturing multimodal distributions, but does not give very precise location predictions. To overcome this, we train a second convolutional RNN decoder  $H_t^O$  to compute an offset vector for each possible grid cell using a regression output,  $O_t = \text{MLP}(H_t^O) \in \mathbb{R}^{H \times W \times 2}$ . This RNN is updated using

$$H_t^O = \text{ConvRNN}(\text{GAT}(H_{t-1}^O), O_{t-1}) \in \mathbb{R}^{H \times W \times d_{dec}} \quad (5.5)$$

To compute the final prediction location, we first flatten the spatial dimension of  $O_t$  into  $\tilde{O}_t \in \mathbb{R}^{HW \times 2}$ . Then we use

$$L_t = Q_i + \tilde{O}_{ti} \quad (5.6)$$

where  $i$  is the index of the selected grid cell,  $Q_i \in \mathbb{R}^2$  is the center of that cell, and  $\tilde{O}_{ti} \in \mathbb{R}^2$  is the predicted offset for that cell at time  $t$ . For single-future prediction, we use greedy search, namely  $i = \arg\max C_t$  over the belief state. For multi-future prediction, we use beam search in Section 5.3.5.

This idea of combining classification and regression is partially inspired by object detection methods (e.g., [142]). It is worth noting that in concurrent work, [16] also designed a two-stage model for trajectory forecasting. However, their classification targets are pre-defined anchor trajectories. Ours is not limited by the predefined anchors.

### 5.3.4 Training

Our model trains on the observed trajectory from time 1 to  $h$  and predicts the future trajectories (in  $xy$ -coordinates) from time  $h+1$  to  $T$ . We supervise this training by providing ground truth targets for both the heatmap (belief state),  $C_t^*$ , and regression offset map,  $O_t^*$ . In particular, for the coarse decoder, the cross-entropy loss is used:

$$\mathcal{L}_{cls} = -\frac{1}{T} \sum_{t=h+1}^T \sum_{i \in G} C_{ti}^* \log(C_{ti}) \quad (5.7)$$

For the fine decoder, we use the smoothed  $L_1$  loss used in object detection [142]:

$$\mathcal{L}_{reg} = \frac{1}{T} \sum_{t=h+1}^T \sum_{i \in G} \text{smooth}_{L_1}(O_{ti}^*, O_{ti}) \quad (5.8)$$

where  $O_{ti}^* = L_t^* - Q_i$  is the delta between the true location and the center of the grid cell at  $i$  and  $L_t^*$  is the ground truth for  $L_t$  in Eq.(5.6). We impose this loss on every cell to improve the robustness.

The final loss is then calculated using

$$\mathcal{L}(\theta) = \mathcal{L}_{cls} + \lambda_1 \mathcal{L}_{reg} + \lambda_2 \|\theta\|_2^2 \quad (5.9)$$

where  $\lambda_2$  controls the  $\ell_2$  regularization (weight decay), and  $\lambda_1 = 0.1$  is used to balance the regression and classification losses.

Note that during training, when updating the RNN, we feed in the predicted soft distribution over locations,  $C_t$ . See Eq. (5.2). An alternative would be to feed in the true values,  $C_t^*$ , i.e., use teacher forcing. However, this is known to suffer from problems [137].

### 5.3.5 Inference

To generate multiple qualitatively distinct trajectories, we use the diverse beam search strategy from [96]. To define this precisely, let  $B_{t-1}$  be the beam at time  $t - 1$ ; this set contains  $K$  trajectories (history selections)  $M_{t-1}^k = \{\hat{Y}_1^k, \dots, \hat{Y}_{t-1}^k\}$ ,  $k \in [1, K]$ , where  $\hat{Y}_t^k$  is an index in  $G$ , along with their accumulated log probabilities,  $P_{t-1}^k$ . Let  $C_t^k = f(M_{t-1}^k) \in \mathbb{R}^{HW}$  be the coarse location output probability from Eq. (5.2) and (5.3) at time  $t$  given inputs  $M_{t-1}^k$ .

The new beam is computed using

$$B_t = \text{topK}(\{P_{t-1}^k + \log(C_t^k(i)) + \gamma(i) | \forall i \in G, k \in [1, K]\}) \quad (5.10)$$

where  $\gamma(i)$  is a diversity penalty term, and we take the top  $K$  elements from the set produced by considering values with  $k = 1 : K$ . If  $K = 1$ , this reduces to greedy search.

Once we have computed the top  $K$  future predictions, we add the corresponding offset vectors to get  $K$  trajectories by  $L_t^k \in \mathbb{R}^2$ . This constitutes the final output of our model.

## 5.4 The Forking Paths Dataset

In this section, we describe our human-annotated simulation dataset, called Forking Paths, for multi-future trajectory evaluation.

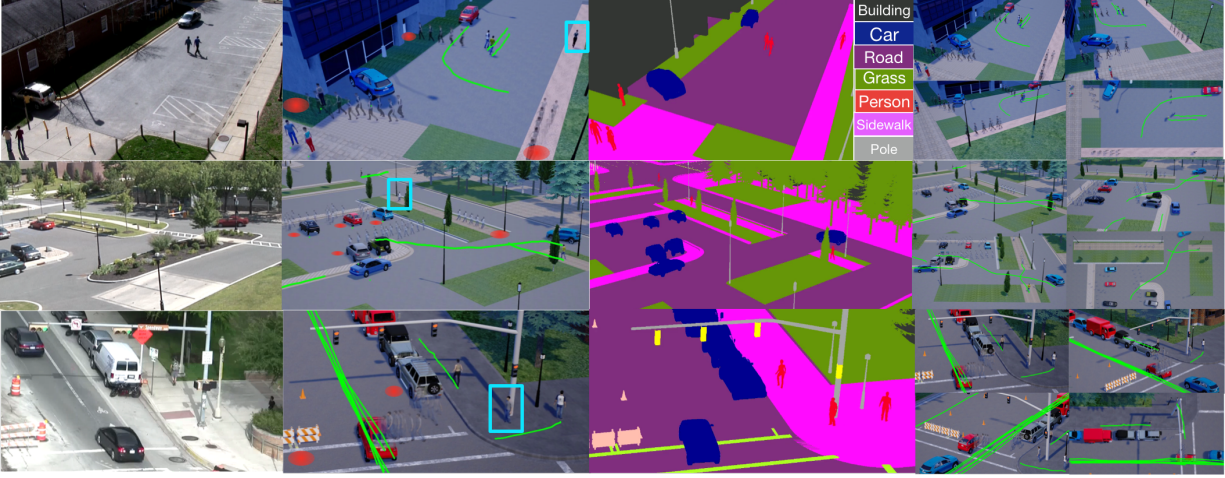


Figure 5.3: Visualization of the Forking Paths dataset. On the left is examples of the real videos and the second column shows the reconstructed scenes. The person in the blue bounding box is the controlled agent and multiple future trajectories annotated by humans are shown by overlaid person frames. The red circles are the defined destinations. The green trajectories are future trajectories of the reconstructed uncontrolled agents. The scene semantic segmentation ground truth is shown in the third column and the last column shows all four camera views including the top-down view.

**Existing datasets.** There are several real-world datasets for trajectory evaluation, such as SDD [147], ETH/UCY [94, 133], KITTI [44], nuScenes [14] and VIRAT/ActEV [6, 131]. However, they all share the fundamental problem that one can only observe one out of many possible future trajectories sampled from the underlying distribution. This is broadly acknowledged in prior works [16, 50, 122, 144, 145, 173] but has not yet been addressed.

The closest work to ours is the simulation used in [16, 122, 173]. However, these only contain artificial trajectories, not human generated ones. Also, they use a highly simplified 2D space, with pedestrians oversimplified as points and vehicles as blocks; no other scene semantics are provided.

**Reconstructing reality in simulator.** In this work, we use CARLA [37], a near-realistic open source simulator built on top of the Unreal Engine 4. Following prior simulation datasets [42, 148], we *semi-automatically* reconstruct static scenes and their dynamic elements from the real-world videos in ETH/UCY and VIRAT/ActEV. There are 4 scenes in ETH/UCY and 5 in VIRAT/ActEV. We exclude 2 cluttered scenes (UNIV & 0002) that we are not able to reconstruct in CARLA, leaving 7 static scenes in our dataset.

For dynamic movement of vehicle and pedestrian, we first convert the ground truth trajectory annotations from the real-world videos to the ground plane using the provided homography matrices. We then match the real-world trajectories’ origin to correct locations in the re-created scenes.

**Human generation of plausible futures.** We manually select sequences with more than one pedestrian. We also require that at least one pedestrian could have multiple plausible alternative destinations. We insert plausible pedestrians into the scene to increase the diversity of the scenarios. We then select one of the pedestrians to be the “controlled agent” (CA) for each sequence, and set meaningful destinations within reach, like a car or an entrance of a building. On average, each agent has about 3 destinations to move towards. In total, we have 127 CAs from 7 scenes. We call each CA and their corresponding scene a scenario.

For each scenario, there are on average 5.9 human annotators to control the agent to the defined destinations. Specifically, they are asked to watch the first 5 seconds of video, from a first-person view (with the camera slightly behind the pedestrian) and/or an overhead view (to give more context). They are then asked to control the motion of the agent so that it moves towards the specified destination in a “natural” way, e.g., without colliding with other moving objects (whose motion is derived from the real videos, and is therefore unaware of the controlled agent). The annotation is considered successful if the agent reached the destination without colliding within the time limit of 10.4 seconds. All final trajectories in our dataset are examined by humans to ensure reliability.

Note that our videos are up to 15.2 seconds long. This is slightly longer than previous works (e.g. [3, 50, 97, 107, 153, 201, 204]) that use 3.2 seconds of observation and 4.8 seconds for prediction. (We use 10.4 seconds for the future to allow us to evaluate longer term forecasts.)

**Generating the data.** Once we have collected human-generated trajectories, 750 in total after data cleaning, we render each one in four camera views (three 45-degree and one top-down view). Each camera view has 127 scenarios in total and each scenario has on average 5.9 future trajectories. With CARLA, we can also simulate different weather conditions, although we did not do so in this work. In addition to agent location, we collect ground truth for pixel-precise scene semantic segmentation from 13 classes including sidewalk, road, vehicle, pedestrian, etc. See Fig. 5.3.

## 5.5 Experimental Results

This section evaluates various methods, including our *Multiverse* model, for multi-future trajectory prediction on the proposed Forking Paths dataset. To allow comparison with previous works, we also evaluate our model on the challenging VIRAT/ActEV [6, 131] benchmark for single-future path prediction.

**Multi-Future Evaluation.** Let  $Y^{ij} = Y_{t=(h+1)\dots T}^{ij}$  be the  $j$ -th true future trajectory for the  $i$ -th test sample, for  $\forall j \in [1, J]$ , and let  $\hat{Y}^{ik}$  be the  $k$ 'th sample from the predicted distribution over trajectories, for  $k \in [1, K]$ . Since there is no agreed-upon evaluation metric for this setting, we simply extend the above metrics, as follows: i) *Minimum Average Displacement Error Given  $K$  Predictions* ( $\text{minADE}_K$ ): similar to the metric described in [16, 50, 144, 145], for each true trajectory  $j$  in test sample  $i$ , we select the closest overall prediction (from the  $K$  model predictions), and then measure its average error:

$$\text{minADE}_K = \frac{\sum_{i=1}^N \sum_{j=1}^J \min_{k=1}^K \sum_{t=h+1}^T \|Y_t^{ij} - \hat{Y}_t^{ik}\|_2}{N \times (T - h) \times J} \quad (5.11)$$

ii) *Minimum Final Displacement Error Given  $K$  Predictions* ( $\text{minFDE}_K$ ): similar to  $\text{minADE}_K$ , but we only consider the predicted points and the ground truth point at the final prediction time instant:

$$\text{minFDE}_K = \frac{\sum_{i=1}^N \sum_{j=1}^J \min_{k=1}^K \|Y_T^{ij} - \hat{Y}_T^{ik}\|_2}{N \times J} \quad (5.12)$$

iii) *Negative Log-Likelihood (NLL)*: Similar to NLL metrics used in [16, 122], we measure the fit of ground-truth samples to the predicted distribution.

### 5.5.1 Multi-Future Prediction on Forking Paths

**Dataset & Setups.** The proposed Forking Paths dataset is used for multi-future trajectory prediction evaluation. Following the setting in previous works [3, 50, 107, 122, 153], we down-sample the videos to 2.5 fps and extract person trajectories using code released in [107], and let the models observe 3.2 seconds (8 frames) of the controlled agent before outputting trajectory coordinates in the pixel space. Since the length of the ground truth future trajectories are different, each model needs to predict the maximum length at test time but we evaluate the predictions using the actual length of each true trajectory.

**Baseline methods.** We compare our method with two simple baselines, and three recent methods with released source code, including a recent model for multi-future prediction and the

Method	Input Types	minADE <sub>20</sub>		minFDE <sub>20</sub>	
		45-degree	top-down	45-degree	top-down
Linear	Traj.	213.2	197.6	403.2	372.9
LSTM	Traj.	201.0 $\pm$ 2.2	183.7 $\pm$ 2.1	381.5 $\pm$ 3.2	355.0 $\pm$ 3.6
Social-LSTM [3]	Traj.	197.5 $\pm$ 2.5	180.4 $\pm$ 1.0	377.0 $\pm$ 3.6	350.3 $\pm$ 2.3
Social-GAN (PV) [50]	Traj.	191.2 $\pm$ 5.4	176.5 $\pm$ 5.2	351.9 $\pm$ 11.4	335.0 $\pm$ 9.4
Social-GAN (V) [50]	Traj.	187.1 $\pm$ 4.7	172.7 $\pm$ 3.9	342.1 $\pm$ 10.2	326.7 $\pm$ 7.7
Next [107]	Traj.+Bbox+RGB+Seg.	186.6 $\pm$ 2.7	166.9 $\pm$ 2.2	360.0 $\pm$ 7.2	326.6 $\pm$ 5.0
Ours	Traj.+Seg.	<b>168.9</b> $\pm$ 2.1	<b>157.7</b> $\pm$ 2.5	<b>333.8</b> $\pm$ 3.7	<b>316.5</b> $\pm$ 3.4

Table 5.1: Comparison of different methods on the Forking Paths dataset. Lower numbers are better. The numbers for the column labeled “45 degrees” are averaged over 3 different 45-degree views. For the input types, “Traj.,” “RGB,” “Seg.” and “Bbox.” mean the inputs are  $xy$  coordinates, raw frames, semantic segmentations and bounding boxes of all objects in the scene, respectively. All models are trained on real VIRAT/ActEV videos and tested on synthetic (CARLA-rendered) videos.

state-of-the-art model for single-future prediction: **Linear** is a single layer model that predicts the next coordinates using a linear regressor based on the previous input point. **LSTM** is a simple LSTM [56] encoder-decoder model with coordinates input only. **Social LSTM** [3]: We use the open source implementation from (<https://github.com/agrimgupta92/sgan/>). **Next** [107] is the state-of-the-art method for single-future trajectory prediction on the VIRAT/ActEV dataset. We train the Next model without the activity labels for fair comparison using the code from (<https://github.com/google/next-prediction/>). **Social GAN** [50] is a recent multi-future trajectory prediction model trained using Minimum over N (MoN) loss. We train two model variants (called PV and V) detailed in the paper using the code from [50].

All models are trained on real videos (from VIRAT/ActEV – see Section 5.5.2 for details) and tested on our synthetic videos (with CARLA-generated pixels, and annotator-generated trajectories). Most models just use trajectory data as input, except for our model (which uses trajectory and semantic segmentation) and Next (which uses trajectory, bounding box, semantic segmentation, and RGB frames).

**Implementation Details.** We use ConvLSTM [190] cell for both the encoder and decoder. The embedding size is set to 32, and the hidden sizes for the encoder and decoder are both 256. The scene semantic segmentation features are extracted from the deeplab model [22], pretrained on



Method	$T_{pred} = 1$	$T_{pred} = 2$	$T_{pred} = 3$
(PV) [14]	10.08 $\pm 0.25$	17.28 $\pm 0.42$	23.34 $\pm 0.47$
(V) [14]	9.95 $\pm 0.35$	17.38 $\pm 0.49$	23.24 $\pm 0.54$
Next [27]	8.32 $\pm 0.10$	14.98 $\pm 0.19$	22.71 $\pm 0.11$
Ours	<b>2.22</b> $\pm 0.54$	<b>4.46</b> $\pm 1.33$	<b>8.14</b> $\pm 2.81$

Table 5.2: Negative Log-likelihood comparison of different methods on the Forking Paths dataset. For methods that output multiple trajectories, we quantize the xy-coordinates into the same grid as our method and get a normalized probability distribution prediction.

the ADE-20k [205] dataset. We use Adadelta optimizer [197] with an initial learning rate of 0.3 and weight decay of 0.001. Other hyper-parameters for the baselines are the same to the ones in [50, 107]. We evaluate the top  $K = 20$  predictions for multi-future trajectories. For the models that only output a single trajectory, including Linear, LSTM, Social-LSTM, and Next, we duplicate the output for  $K$  times before evaluating. For Social-GAN, we use  $K$  different random noise inputs to get the predictions. For our model, we use diversity beam search [96, 134] as described in Section 5.3.5.

**Quantitative Results.** Table 5.1 lists the multi-future evaluation results, where we divide the evaluation according to the viewing angle of camera, 45-degree vs. top-down view. We repeat all experiments (except “linear”) 5 times with random initialization to produce the mean and standard deviation values. As we see, our model outperforms baselines in all metrics and it performs significantly better on the minADE metric, which suggests better prediction quality over all time instants. Notably, our model outperforms Social GAN by a large margin of at least 8 points on all metrics. We also measure the standard negative log-likelihood (NLL) metric for the top methods in Table 5.2.

**Qualitative analysis.** We visualize some outputs of the top 4 methods in Fig. 5.4. In each image, the yellow trajectories are the history trajectory of each controlled agent (derived from real video data) and the green trajectories are the ground truth future trajectories from human annotators. The predicted trajectories are shown in yellow-orange heatmaps for multi-future prediction methods, and in red lines for single-future prediction methods. As we see, our model correctly generally puts probability mass where there is data, and does not “waste” probability mass where there is no data.

**Error analysis.** We show some typical errors our model makes in Fig. 5.5. The first image shows our model misses the correct direction, perhaps due to lack of diversity in our sampling

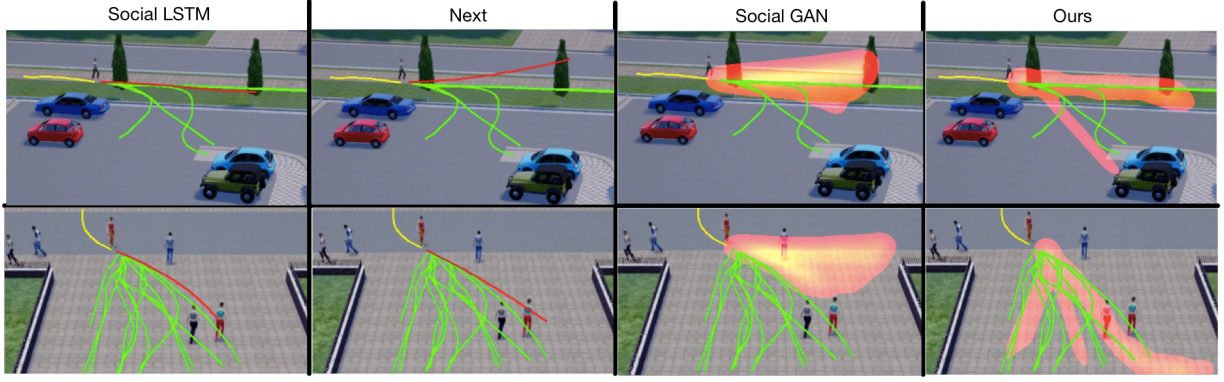


Figure 5.4: Qualitative analysis. The red trajectories are single-future method predictions and the yellow-orange heatmaps are multi-future method predictions. The yellow trajectories are observations and the green ones are ground truth multi-future trajectories. See text for details.

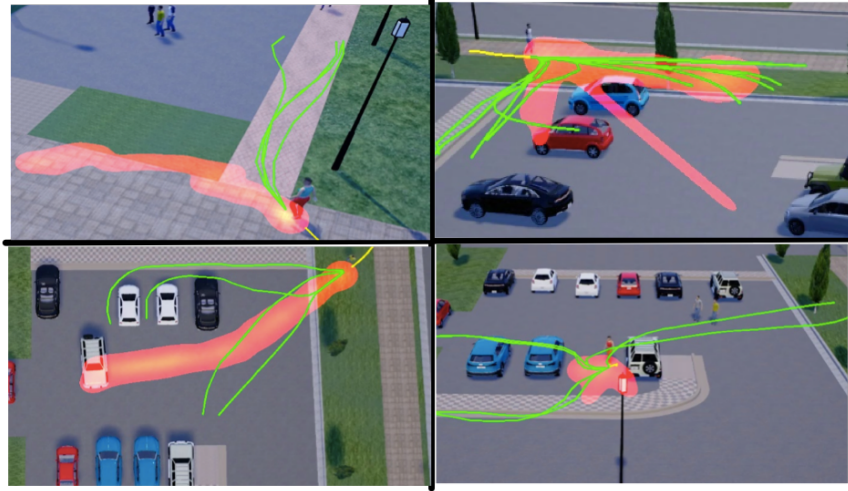


Figure 5.5: Error analysis. See text for details.

procedure. The second image shows our model sometimes predicts the person will “go through” the car (diagonal red beam) instead of going around it. This may be addressed by adding more training examples of “going around” obstacles. The third image shows our model predicts the person will go to a moving car. This is due to the lack of modeling of the dynamics of other far-away agents in the scene. The fourth image shows a hard case where the person just exits the vehicle and there is no indication of where they will go next (so our model “backs off” to a sensible “stay nearby” prediction). We leave solutions to these problems to future work.



### 5.5.2 Single-Future Prediction on VIRAT/ActEV

**Dataset & Setups.** NIST released VIRAT/ActEV [6] for activity detection research in streaming videos in 2018. This dataset is a new version of the VIRAT [131] dataset, with more videos and annotations. The length of videos with publicly available annotations is about 4.5 hours. Following [107], we use the official training set for training and the official validation set for testing. Other setups are the same as in Section 5.5.1, except we use the single-future evaluation metric.

**Quantitative Results.** Table 5.3 (first column) shows the evaluation results. As we see, our model achieves state-of-the-art performance. The improvement is especially large on Final Displacement Error (FDE) metric, attributing to the coarse location decoder that helps regulate the model prediction for long-term prediction. The gain shows that our model does well at both single future prediction (on real data) and multiple future prediction on our quasi-synthetic data.

**Generalizing from simulation to real-world.** As described in the previous section, we generate simulation data first by reconstructing from real-world videos. To verify the quality of the reconstructed data, and the efficacy of learning from simulation videos, we train all the models on the simulation videos derived from the real data. We then evaluate on the real test set of VIRAT/ActEV. As we see from the right column in Table 5.3, all models do worse in this scenario, due to the difference between synthetic and real data. We find the performance ranking of different methods are consistent between the real and our simulation training data. This suggests the errors mainly coming from the model, and substantiates the rationality of using the proposed dataset to compare the relative performance of different methods.

There are two sources of error. The synthetic trajectory data only contains about 60% of the real trajectory data, due to difficulties reconstructing all the real data in the simulator. In addition, the synthetic images are not photo realistic. Thus methods (such as Next [107]) that rely on RGB input obviously suffer the most, since they have never been trained on “real pixels”. Our method, which uses trajectories plus high level semantic segmentations (which transfers from synthetic to real more easily) suffers the least drop in performance, showing its robustness to “domain shift”. See Table 5.1 for input source comparison between methods.

### 5.5.3 Ablation Experiments

We test various ablations of our model on both the single-future and multi-future trajectory prediction to substantiate our design decisions. Results are shown in Table 5.4, where the

Method	Trained on Real.	Trained on Sim.
Linear	32.19 / 60.92	48.65 / 90.84
LSTM	23.98 / 44.97	28.45 / 53.01
Social-LSTM [3]	23.10 / 44.27	26.72 / 51.26
Social-GAN (V) [50]	30.40 / 61.93	36.74 / 73.22
Social-GAN (PV) [50]	30.42 / 60.70	36.48 / 72.72
Next [107]	19.78 / 42.43	27.38 / 62.11
Ours	<b>18.51 / 35.84</b>	<b>22.94 / 43.35</b>

Table 5.3: Comparison of different methods on the VIRAT/ActEV dataset. We report ADE/FDE metrics. First column is for models trained on real video training set and second column is for models trained on the simulated version of this dataset.

Method	Single-Future	Multi-Future
Our full model	18.51 / 35.84	166.1 / 329.5
No spatial graph	28.68 / 49.87	184.5 / 363.2
No fine location decoder	53.62 / 83.57	232.1 / 468.6
No multi-scale grid	21.09 / 38.45	171.0 / 344.4

Table 5.4: Performance on ablated versions of our model on single and multi-future trajectory prediction. Lower numbers are better.

ADE/FDE metrics are shown in the “single-future” column and  $\text{minADE}_{20}/\text{minFDE}_{20}$  metrics (averaged across all views) in the “multi-future” column. We verify three of our key designs by leaving the module out from the full model.

(1) *Spatial Graph*: Our model is built on top of a spatial 2D graph that uses graph attention to model the scene features. We train model without the spatial graph. As we see, the performance drops on both tasks. (2) *Fine location decoder*: We test our model without the fine location decoder and only use the grid center as the coordinate output. As we see, the significant performance drops on both tasks verify the efficacy of this new module proposed in our study. (3) *Multi-scale grid*: We utilize two different grid scales ( $36 \times 18$ ) and ( $18 \times 9$ ) in training. We see that performance is slightly worse if we only use the fine scale ( $36 \times 18$ ).

## Chapter 6

# Learning from 3D Simulation

In this chapter, we explore the benefit of multi-camera-view video data from 3D simulation created in [chapter 5](#) to train a robust trajectory prediction model that could perform fairly well on out-of-domain testing datasets.

### 6.1 Overview

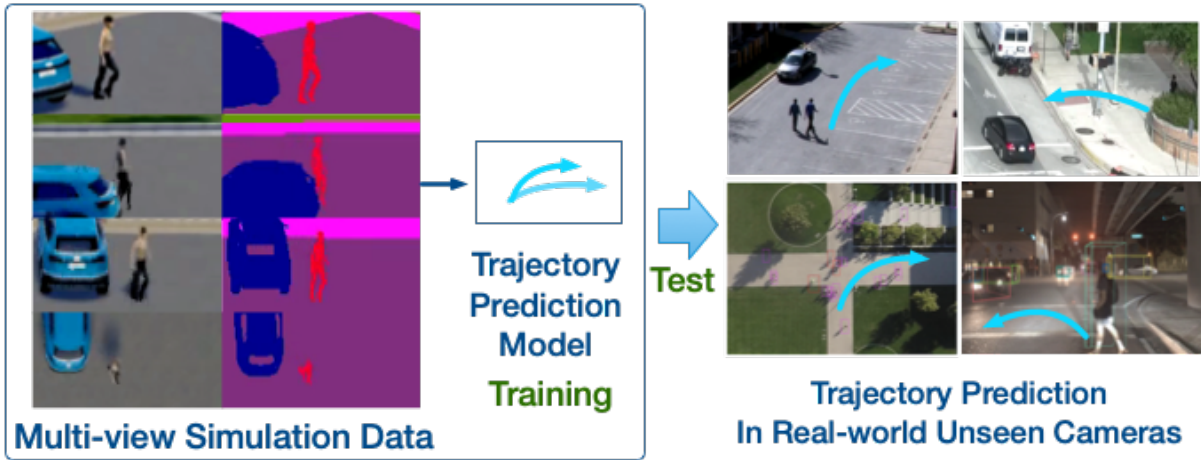


Figure 6.1: Illustration of pedestrian trajectory prediction in unseen cameras. We propose to learn robust representations only from 3D simulation data that could generalize to real-world videos captured by unseen cameras.

Future trajectory prediction [3, 50, 82, 92, 107, 109, 153] is a fundamental problem in video analytics, which aims at forecasting a pedestrian’s future path in the video in the next few

seconds. Recent advancements in future trajectory prediction have been successful in a variety of vision applications such as self-driving vehicles [9, 16, 17], safety monitoring [107], robotic planning [143, 144], among others.

A notable bottleneck for existing works is that the current model is closely coupled with the video cameras on which it is trained, and generalizes poorly on new cameras with novel views or scenes. For example, prior works have proposed various models to forecast a pedestrian’s trajectories in video cameras of different types such as stationary outdoor cameras [3, 50, 94, 106, 116, 131], drone cameras [34, 97, 153], ground-level egocentric cameras [143, 165, 194], or dash cameras [17, 123, 164]. However, existing models are all separately trained and tested within one or two datasets, and there have been no attempts at successfully generalizing the model across datasets of novel camera views. This bottleneck significantly hinders the application whenever there is a new camera because it requires annotating new data to fine-tune the model, resulting in a procedure that is not only expensive but also tardy in deploying the model.

An ideal model should be able to disentangle human behavioral dynamics from specific camera views, positions, and scenes. It should produce robust trajectory prediction despite the variances in these camera settings. Motivated by this idea, in this work, we learn a robust representation for future trajectory prediction that can generalize to unseen video cameras. Different from existing works, we study a *real-data-free* setting where a model is trained only on synthetic data but tested, out of the box, on unseen real-world videos, without further re-training or fine-tuning the model. Following the success of learning from simulation [32, 42, 146, 150, 179, 202], our synthetic data is generalized from a 3D simulator, called CARLA [37], which anchors to the static scene and dynamic elements in the VIRAT/ActEV videos [131]. By virtue of the 3D simulator, we can generate multiple views and pixel-precise semantic segmentation labels for each training trajectory, as illustrated in Figure 6.1. Meanwhile, following the previous works [109, 153], scene semantic segmentation is used instead of RGB pixels to alleviate the influence of different lighting conditions, scene textures, subtle noises produced by camera sensors, etc. At test time, we extract scene features from real videos using pretrained segmentation models. The use of segmentation features is helpful but is insufficient for learning robust representation for future trajectory prediction.

To tackle this issue, we propose a novel data augmentation method called *SimAug* to augment the features of the simulation data with the goal of learning robust representation to various semantic scenes and camera views in real videos. To be specific, first, after representing each training trajectory by high-level scene semantic segmentation features, we defend

our model from adversarial examples generated by white-box attack methods [47]. Second, to overcome the changes in camera views, we generate multiple views for the same trajectory, and encourage the model to focus on overcoming the “hardest” view to which the model has learned. Following [71, 72], the classification loss is adopted and the view with the highest loss is favored during training. Finally, the augmented trajectory is computed as a convex combination of the trajectories generated in previous steps. Our trajectory prediction backbone model is built on a recent work called Multiverse [109]. The final model is trained to minimize the empirical vicinal risk over the distribution of augmented trajectories. Our method is partially inspired by recent robust deep learning methods using adversarial training [27, 89], Mixup [200], and MentorMix [72].

We empirically validate our model, which is trained only on simulation data, on three real-world benchmarks for future trajectory prediction: VIRAT/ActEV [6, 131], Stanford Drone [147], and Argoverse [17]. These benchmarks represent three distinct camera views: 45-degree view, top-down view and dashboard camera view with ego-motions. The results show our method performs favorably against baseline methods including standard data augmentation, adversarial learning, and imitation learning. Notably, our method achieves better results compared to the state-of-the-art on the VIRAT/ActEV and Stanford Drone benchmark. Our code and models are released at <https://next.cs.cmu.edu/simaug>. To summarize, our contribution is threefold:

- We study a new setting of future trajectory prediction in which the model is trained only on synthetic data and tested, out of the box, on any unseen real video with novel views or scenes.
- We propose a novel and effective approach to augment the representation of trajectory prediction models using multi-view simulation data.
- Ours is the first work on future trajectory prediction to demonstrate the efficacy of training on 3D simulation data, and establishes new state-of-the-art results on three public benchmarks.

## 6.2 Related Work

This work studies the novel direction of robustness in trajectory prediction model [149]. We are the first to look into the generalization of trajectory prediction model and study the invariant representation for different environments and camera views. In the following, we also review

some of the trajectory prediction works based on their specific camera views. We then review more broadly of learning from simulation and robust model learning.

**Trajectory prediction.** Recently there is a large body of work on predicting person future trajectories in a variety of scenarios. Many works [3, 107, 109, 153, 193, 201] focused on modeling person motions in videos recorded with 45-degree-view stationary cameras. Datasets like VIRAT/ActEV [131], ETH/UCY [94, 116] have been used for such direction. Meanwhile, many works [9, 58, 92, 97, 122, 144, 154, 204] have been proposed for top-down view videos for trajectory prediction. Notably, the Stanford Drone Dataset (SDD) [147] is used in many works [34, 97, 153] for trajectory prediction with drone videos. Other works have also looked into pedestrian prediction in dashcam videos [83, 92, 123, 164] and first-person videos [165, 194]. Many vehicle trajectory datasets [14, 17, 196] have been proposed as a result of self-driving’s surging popularity.

**Learning from 3D simulation data.** As the increasing research focus in 3D computer vision [37, 54, 101, 146, 148, 155, 203], many research works have used 3D simulation for training and evaluating real-world tasks [8, 20, 32, 42, 78, 109, 167, 168, 186, 206]. Many works [32, 42, 136] were proposed to use data generated from 3D simulation for video object detection, tracking, and action recognition analysis. For example, Sun et al. [167] proposed a forecasting model by using a gaming simulator. AirSim [155] and CARLA [37] were proposed for robotic autonomous controls for drones and vehicles. Zeng et al. [199] proposed to use 3D simulation for adversarial attacks. RSA [202] used randomized simulation data for human action recognition. The ForkingPaths dataset [109] was proposed for evaluating multi-future trajectory prediction. Human annotators were asked to control agents in a 3D simulator to create a multi-future trajectory dataset.

**Robust Deep Learning.** Traditional domain adaptation approaches [13, 43, 77, 176] may not be applicable as our target domain is considered “unseen” during training. Methods for learning using privileged information [90, 115, 118, 177] is not applicable for a similar reason. Closest to ours is robust deep learning methods. In particular, our approach is inspired by the following methods: (i) *adversarial training* [47, 121, 188, 199] to defend the adversarial attacks generated on-the-fly during training using gradient-based methods [26, 47, 121, 175]; (ii) data augmentation methods to overcome unknown variances between training and test examples such as Mixup [200], MentorMix [72], AugMix [27], etc; (iii) example re-weighting or selection [69, 71, 100, 130, 141] to mitigate network memorization. Different from prior work, ours uses 3D simulation data as a new perspective for data augmentation and is carefully designed for future trajectory prediction.

## 6.3 The *SimAug* Model

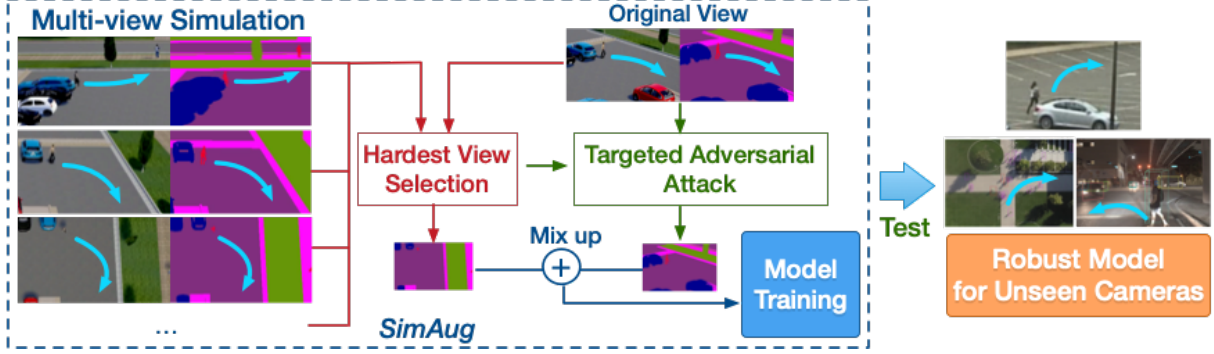


Figure 6.2: Overview of our method *SimAug* that is trained on simulation and tested on real unseen videos. Each training trajectory is represented by multi-view segmentation features extracted from the simulator. *SimAug* mixes the feature of the hardest camera view with the adversarial feature of the original view.

## 6.4 Approach

In this section, we describe our approach to learn robust representation for future trajectory prediction, which we call *SimAug*. Our goal is to train a model only on simulation training data that can effectively predict the future trajectory in the real-world test videos that are unseen during training.

### 6.4.1 Problem Formulation

We focus on predicting the locations of a single agent for multiple steps into the future. Given a sequence of historical video frames  $V_{1:h}$  of the past  $h$  steps and the past agent locations  $L_{1:h}$  in training, we learn a probabilistic model on simulation data to estimate  $P(L_{h+1:T} | L_{1:h}, V_{1:h})$  for  $T - h$  steps into the future. At test time, our model takes as input an agent’s observable past  $(V_{1:h}, L_{1:h})$  in real videos to predict the agent’s future locations  $L_{h+1:T} = \{y_{h+1}, \dots, y_T\}$ , where  $y_t$  is the location coordinates. As the test real videos are unseen during training, the model is supposed to be invariant to the variances in semantic scenes, camera views, and camera motions.





Figure 6.3: Visualization of the multi-view 3D simulation data used in *SimAug* training. Data generation process is described in Section 6.4.2. We use 4 camera views from 4 scenes defined in [109]. “0400” and “0401” scene have overlapping views. The top-left views are the original views from VIRAT/ActEV dataset.



### 6.4.2 Training Data Generation From Simulation

Our model is trained only on simulation data. To ensure high-level realism, the training trajectories are generated by CARLA [37], an open-source 3D simulator built on top of the state-of-the-art game engine *Unreal Engine 4*. We use the trajectories from the Forking Paths dataset [109] that are semi-manually recreated from the VIRAT/ActEV benchmark that projects real-world annotations to the 3D simulation world. Note that it is not our intention to build an exact replica of the real-world scene, nor it is necessary to help train a model for real-world tasks as suggested in previous works [42, 109, 148, 202].

With CARLA, we record multiple views of the same trajectory of different camera angles and positions. For a trajectory  $(V_{1:T}, L_{1:T})$  in original view, let  $\mathcal{S} = \{(V_{1:T}^{(i)}, L_{1:T}^{(i)})\}_{i=1}^{|\mathcal{S}|}$  denote a set of additional views for the same trajectory. In our experiments, we use four camera parameters pre-specified in [109], including three 45-degree views and one top-down view. We use a total of 4 scenes shown in Fig. 6.3. The ground-truth location varies under different camera views i.e.  $L_{1:T}^{(i)} \neq L_{1:T}^{(j)}$  for  $i \neq j$ . Note that these camera positions and angles are defined in [109] specifically for VIRAT/ActEV dataset. The top-down view cameras in Stanford Drone dataset [147] are still considered unseen to the model since the scenes and camera positions are quite different.

In simulation, we also collect the ground-truth scene semantic segmentation for  $K = 13$  classes including sidewalk, road, vehicle, pedestrian, etc. At test time, we extract the semantic segmentation feature from real videos using a pre-trained model with the same number of class labels per pixel. To be specific, we use the Deeplab model [22] trained on the ADE20k [205] dataset and keep its weights frozen. To bridge the gap between real and simulated video frames, we represent all trajectory  $V_{1:T}$  as a sequence of scene semantic segmentation features, following previous works [34, 107, 109, 153]. As we show in our experiments, the use of segmentation features is helpful but is still insufficient for learning the robust representation.

### 6.4.3 Multi-view Simulation Augmentation (*SimAug*)

In this subsection, we first describe *SimAug* for learning robust representations. Our trajectory prediction backbone model is built on the Multiverse model [109] and will be discussed in Section 6.4.4.

Given a trajectory in its original view  $(V_{1:T}, L_{1:T})$ , we generate a set of additional views in  $\mathcal{S} = \{(V_{1:T}^{(i)}, L_{1:T}^{(i)})\}_{i=1}^{|\mathcal{S}|}$  as described in the previous section, where  $V_t^{(i)}$  represents the scene

semantic feature of view  $i$  at time  $t$ .  $L_{1:T}^{(i)}$  is a sequence of ground-truth locations for the  $i$ -th view.

Each time given a camera view, we use it as an anchor to search for the “hardest” view that is most inconsistent with what the model has learned. Inspired by [71], we use the classification loss as the criteria and compute:

$$j^* = \operatorname{argmax}_{j \in [1, |\mathcal{S}|]} \{\mathcal{L}_{\text{cls}}(V_{1:h} + \delta, L_{h+1:T}^{(j)})\}, \quad (6.1)$$

where  $\delta$  is the  $\ell_\infty$ -bounded random perturbation applied to the input features.  $\mathcal{L}_{\text{cls}}$  is the location classification loss used in our backbone Multiverse model and will be discussed in the next subsection.

Then for the original view, we generate an adversarial trajectory by the targeted-FGSM attack [89]:

$$V_{1:h}^{\text{adv}} = V_{1:h} - \epsilon \cdot \operatorname{sign}(\nabla_{V_{1:h}} \mathcal{L}_{\text{cls}}(V_{1:h} + \delta, L_{h+1:T}^{(j^*)})), \quad (6.2)$$

where  $\epsilon$  is the hyper-parameter. The attack tries to make the model predict the future locations in the selected “hardest” camera view rather than the original view. In essence, the resulting adversarial feature is “warped” to the “hardest” camera view by a small perturbation. By defending against such adversarial trajectory, our model learns representations that are robust against variances in camera views.

Finally, we mix up the trajectory locations of the selected view and the adversarial trajectory locations by a convex combination function [200] over their features and one-hot location labels.

$$\begin{aligned} V_{1:h}^{\text{aug}} &= \lambda \cdot V_{1:h}^{\text{adv}} + (1 - \lambda) \cdot V_{1:h}^{(j^*)} \\ y_t^{\text{aug}} &= \lambda \cdot \operatorname{one-hot}(y_t) + (1 - \lambda) \cdot \operatorname{one-hot}(y_t^{(j^*)}) \quad \forall t \in [h + 1, T] \\ L_{h+1:T}^{\text{aug}} &= [y_{h+1}^{\text{aug}}, \dots, y_T^{\text{aug}}] \end{aligned} \quad (6.3)$$

where  $[y_{h+1}, \dots, y_T] = L_{h+1:T}$  are the ground-truth locations of the original view. The  $\operatorname{one-hot}(\cdot)$  function projects the location in  $xy$  coordinates into an one-hot embedding over the predefined grid used in our backbone trajectory prediction model. Please find the details in [109]. Following [200],  $\lambda$  is drawn from a Beta distribution  $\operatorname{Beta}(\alpha, \alpha)$  controlled by the hyper-parameter  $\alpha$ .

The algorithm for training with one training step is listed in Algorithm 2. To train robust models to various camera views and semantic scenes, we learn representations over augmented

training trajectories to overcome (i) feature perturbations (Step 3 and 5) (ii) targeted adversarial attack (Step 5), and (iii) the “hardest” feature from other views (Step 4). By the mix-up operation in Eq. (6.3), our model is trained to minimize the empirical vicinal risk over a new distribution constituted by the generated augmented trajectories, which is proved to be useful in improving model robustness to real-world distributions under various settings [72].

---

**Algorithm 2** Multi-view Simulation Adversarial Augmentation (*SimAug*)

---

**Input** : Mini-batch of trajectories; hyper-parameters  $\alpha$  and  $\epsilon$

**Output**: Classification loss  $\mathcal{L}_{\text{cls}}$  computed over augmented trajectories

---

```

1 for each trajectory  $(V_{1:T}, L_{1:T})$  in the mini-batch do
2   Generate trajectories from additional views  $\mathcal{S} = \{(V_{1:T}^{(i)}, L_{1:T}^{(i)})\}$ 
3   Compute the loss for each camera view  $\mathcal{L}_{\text{cls}}(V_{1:h} + \delta, L_{h+1:T}^{(j)})$ 
4   Select the view with the largest loss  $j^*$  by Eq. (6.1)
5   Generate an adversarial trajectory  $V_{1:h}^{adv}$  by Eq. (6.2)
6   Mix up  $(V_{1:h}^{adv}, L_{h+1:T})$  and  $(V_{1:h}^{(j^*)}, L_{h+1:T}^{(j^*)})$  by Eq. (6.3)
7   Compute  $\mathcal{L}_{\text{cls}}$  over the augmented trajectory  $(V_{1:h}^{aug}, L_{h+1:T}^{aug})$  from Step 6
8 end
9 return averaged  $\mathcal{L}_{\text{cls}}$  over the augmented trajectories

```

---

#### 6.4.4 Backbone Model for Trajectory Prediction

We employ Multiverse [109] as our backbone network, a state-of-the-art multi-future trajectory prediction model. Although we showcase the use of *SimAug* to improve the robustness of Multiverse, *SimAug* is a general approach that can be applied to other trajectory prediction models.

**Input Features.** The model is given the past locations,  $L_{1:h}$ , and the scene,  $V_{1:h}$ . Each ground-truth location  $L_t$  is encoded by an one-hot vector  $y_t \in \mathbb{R}^{HW}$  representing the nearest cell in a 2D grid of size  $H \times W$ . In our experiment, we use a grid scale of  $36 \times 18$ . Each video frame  $V_t$  is encoded as semantic segmentation feature of size  $H \times W \times K$  where  $K = 13$  is the total number of class labels as in [107, 109]. As discussed in the previous section, we use *SimAug* to generate augmented trajectories  $(V_{1:h}^{aug}, L_{1:h}^{aug})$  as our training features.

**History Encoder.** A convolutional RNN [182, 190] is used to get the final spatial-temporal feature state  $H_t \in \mathbb{R}^{H \times W \times d_{\text{enc}}}$ , where  $d_{\text{enc}}$  is the hidden size. The context is a concatenation of the last hidden state and the historical video frames,  $\mathcal{H} = [H_h, V_{1:h}]$ .

**Location Decoder.** After getting the context  $\mathcal{H}$ , a coarse location decoder is used to predict locations at the level of grid cells at each time-instant by:

$$\hat{y}_t = \text{softmax}(f_c(\mathcal{H}, H_{t-1}^c)) \in \mathbb{R}^{HW} \quad (6.4)$$

where  $f_c$  is the convolutional recurrent neural network (ConvRNN) with graph attention proposed in [109] and  $H_t^c$  is the hidden state of the ConvRNN. Then a fine location decoder is used to predict a continuous offset in  $\mathbb{R}^2$ , which specifies a “delta” from the center of each grid cell, to get a fine-grained location prediction:

$$\hat{O}_t = \text{MLP}(f_o(\mathcal{H}, H_{t-1}^o)) \in \mathbb{R}^{HW \times 2}, \quad (6.5)$$

where  $f_o$  is a separate ConvRNN and  $H_t^o$  is its hidden state. To compute the final prediction location, we use

$$\hat{L}_t = Q_g + \hat{O}_{tg} \quad (6.6)$$

where  $g = \text{argmax } \hat{y}_t$  is the index of the selected grid cell,  $Q_g \in \mathbb{R}^2$  is the center of that cell, and  $\hat{O}_{tg} \in \mathbb{R}^2$  is the predicted offset for that cell at time  $t$ .

**Training.** We use *SimAug* (see Section 6.4.3) to generate  $L_{h+1:T}^{aug} = \{y_{h+1}^{aug}, \dots, y_T^{aug}\}$  as labels for training. For the coarse decoder, the cross-entropy loss is used:

$$\mathcal{L}_{\text{cls}} = -\frac{1}{T} \sum_{t=h+1}^T \sum_{c=1}^{HW} y_{tc}^{aug} \log(\hat{y}_{tc}) \quad (6.7)$$

For the fine decoder, we use the original ground-truth location label  $L_{h+1:T}$ :

$$\mathcal{L}_{\text{reg}} = \frac{1}{T} \sum_{t=h+1}^T \sum_{c=1}^{HW} \text{smooth}_{l_1}(O_{tc}, \hat{O}_{tc}) \quad (6.8)$$

where  $O_{tc} = L_t - Q_c$  is the delta between the ground true location and the center of the  $c$ -th grid cell. The final loss is then calculated using

$$\mathcal{L}(\theta) = \mathcal{L}_{\text{cls}} + \lambda_1 \mathcal{L}_{\text{reg}} + \lambda_2 \|\theta\|_2^2 \quad (6.9)$$

where  $\lambda_2$  controls the  $\ell_2$  regularization (weight decay), and  $\lambda_1 = 0.5$  is used to balance the regression and classification losses.

## 6.5 Experiments

In this section, we evaluate various methods, including our *SimAug* method, on three public video benchmarks of real-world videos captured under different camera views and scenes: the VIRAT/ActEV [6, 131] dataset, the Stanford Drone Dataset (SDD) [147], and the autonomous driving dataset Argoverse [17]. We demonstrate the efficacy of our method for unseen cameras in Section 6.5.2 and how our method can also improve state-of-the-art when fine-tuned on the real training data in Section 6.5.3 and Section 6.5.4.

### 6.5.1 Evaluation Metrics

Following prior works [3, 109], we utilize two common metrics for trajectory prediction evaluation. Let  $L^i = L_{t=(h+1)\dots T}^i$  be the true future trajectory for the  $i^{th}$  test sample, and  $\hat{L}^{ik}$  be the corresponding  $k^{th}$  prediction sample, for  $k \in [1, K]$ .

i) *Minimum Average Displacement Error Given K Predictions* ( $\text{minADE}_K$ ): for each true trajectory sample  $i$ , we select the closest  $K$  predictions, and then measure its average error:

$$\text{minADE}_K = \frac{\sum_{i=1}^N \min_{k=1}^K \sum_{t=h+1}^T \|L_t^i - \hat{L}_t^{ik}\|_2}{N \times (T - h)} \quad (6.10)$$

ii) *Minimum Final Displacement Error Given K Predictions* ( $\text{minFDE}_K$ ): similar to  $\text{minADE}_K$ , but we only consider the predicted points and the ground truth point at the final prediction time instant:

$$\text{minFDE}_K = \frac{\sum_{i=1}^N \min_{k=1}^K \|L_T^i - \hat{L}_T^{ik}\|_2}{N} \quad (6.11)$$

iii) *Grid Prediction Accuracy* ( $\text{Grid\_Acc}$ ): As our base model also predicts coarse grid locations as described in Section 6.4.4, we also evaluate the accuracy between the predicted grid  $\hat{y}_t$  and the ground truth grid  $y_t$ . This is an intermediate metric and hence is less indicative than the  $\text{minADE}_K$  and  $\text{minFDE}_K$ .

### 6.5.2 Main Results

**Dataset & Setups.** We compare *SimAug* with classical data augmentation methods as well as adversarial learning methods to train robust representations. All methods are trained using the same backbone on the same *simulation training data* described in Section 6.4.2, and tested on the same benchmarks. Real videos are not allowed to be used during training except in our finetuning experiments. For VIRAT/ActEV and SDD, we use the standard test split as in

[107, 109] and [34, 153], respectively. For Argoverse, we use the official validation set from the 3D tracking task, and the videos from the “ring\_front\_center” camera are used.

These datasets have different levels of difficulties. VIRAT/ActEV is the easiest one because its training trajectories have been projected in the simulation training data. SDD is more difficult as its camera positions and scenes are different from the training data. Argoverse is the most challenging one with distinct scenes, camera views, and ego-motions.

Following the setting in previous works [3, 3, 34, 50, 50, 107, 109, 122, 153], the models observe 3.2 seconds (8 frames) of every pedestrian and predict the future 4.8 seconds (12 frames) of the person trajectory. We use the pixel values for the trajectory coordinates as it is done in [9, 16, 34, 58, 92, 97, 107, 122, 194]. By default, we evaluate the top  $K = 1$  future trajectory prediction of all models.

**Baseline methods.** We compare *SimAug* with the following baseline methods for learning robust representations. All methods are built on the same backbone network and trained using the same simulation training data. *Base Model* is the trajectory prediction model proposed in [109]. *Standard Aug* is the base model trained with standard data augmentation techniques including horizontal flipping and random input jittering. *Fast Gradient Sign Method (FGSM)* is the base model trained with adversarial examples generated by the targeted-FGSM attack method [47]. Random labels are used for the targeted-FGSM attack. *Projected Gradient Descent (PGD)* is learned with an iterative adversarial learning method [121, 188]. The number of iterations is set to 10 and other hyper-parameters following [188].

**Implementation Details.** We use  $\alpha = 0.2$  for the Beta distribution in Eq (6.3) and we use  $\epsilon = \delta = 0.1$  in Eq (6.2). As the random perturbation is small, we do not normalize the perturbed features and the normalized features yield comparable results. All models are trained using Adadelata optimizer [197] with an initial learning rate of 0.3 and a weight decay of 0.001. Other hyper-parameters for the baselines are the same as the ones in [109].

**Quantitative Results.** Table 6.1 shows the evaluation results. Our method performs favorably against other baseline methods across all evaluation metrics on all three benchmarks. In particular, “Standard Aug” seems to be not generalizing well to unseen cameras. FGSM improves significantly on the “Grid\_Acc” metric but fails to translate the improvement to final location predictions. *SimAug* is able to improve the model overall stemming from the effective use of multi-view simulation data. All other methods are unable to improve trajectory prediction on Argoverse, whose data characteristics include ego-motions and distinct dashboard-view cameras. The results substantiate the efficacy of *SimAug* for future trajectory prediction in unseen cameras. Note as the baseline methods use the same features as ours, the results indicate the

Table 6.1: Comparison to the standard data augmentation method and recent adversarial learning methods on three datasets. We report three metrics: Grid\_Acc( $\uparrow$ )/minADE<sub>1</sub>( $\downarrow$ )/minFDE<sub>1</sub>( $\downarrow$ ). The units of ADE/FDE are pixels. All methods are built on the same backbone model in [109] and trained using the same multi-view simulation data described in Section 6.4.2.

Method	VIRAT/ActEV	Stanford Drone	Argoverse
Base Model [109]	44.2%/26.2/49.7	31.4%/21.9/42.8	26.6%/69.1/183.9
Standard Aug	45.5%/25.8/48.3	21.3%/23.7/47.6	28.9%/70.9/183.4
PGD [121, 188]	47.5%/25.1/48.4	28.5%/21.0/42.2	25.9%/72.8/184.0
FGSM [47]	48.6%/25.4/49.3	42.3%/19.3/39.9	29.2%/71.1/185.4
SimAug	<b>51.1%/21.7/42.2</b>	<b>45.4%/15.7/30.2</b>	<b>30.9%/67.9/175.6</b>

use of segmentation features is insufficient for learning robust representations.

**Qualitative Analysis.** We visualize outputs of the base model with and without *SimAug* in Fig. 6.4. We show visualizations on all three datasets. In each image, the yellow trajectories denote historical trajectories and the green ones are ground truth future trajectories. Outputs of the base model without *SimAug* are colored with blue heatmaps and the yellow-orange heatmaps are from the same model with *SimAug*. As we see, the base model with *SimAug* augmentation yields more accurate trajectories for turnings (Fig. 6.4 1a., 3a.) while without it the model sometimes predicts the wrong turns (Fig. 6.4 1b., 1c., 2a., 3a., 3b.). In addition, the length of *SimAug* predictions is more accurate (Fig. 6.4 1d., 2b., 2c., 2d.).

### 6.5.3 State-of-the-Art Comparison on Stanford Drone Dataset

In this section, we compare our *SimAug* model with the state-of-the-art generative models, including Social-LSTM [3], Social-GAN [50], DESIRE [92], and SoPhie [153]. We also compare with the imitation learning model, IDL [97], and the inverse reinforcement learning model, P2T<sub>IRL</sub> [34] for trajectory prediction on the Stanford Drone Dataset. Following previous works, we evaluate the minimal errors over  $K = 20$  predictions.

**Results & Analysis.** The results are shown in Table 6.3, where *SimAug* is built on top of the *Multiverse* model. As it shows, *SimAug* model trained only on the simulation data (second to the last row) achieves comparable or even better performance than other state-of-the-art models that are trained on in-domain real videos. By further fine-tuning on the learned representations of *SimAug*, we achieve the state-of-the-art performance on the Stanford Drone Dataset. The

Table 6.2: State-of-the-art comparison on the VIRAT/ActEV dataset. Numbers are minimal errors over 1 predictions and lower the better.

Method	minADE <sub>1</sub> (↓)	minFDE <sub>1</sub> (↓)
Social-LSTM [3]	23.10	44.27
Social-GAN [50]	30.42	60.70
Next [107]	19.78	42.43
Multiverse [109]	18.51	35.84
Multiverse (Trained on Sim.) [109]	22.94	43.35
SimAug	21.73	42.22
SimAug + finetune	<b>17.96</b>	<b>34.68</b>

promising results demonstrate the efficacy of *SimAug* for future trajectory prediction in unseen cameras.

#### 6.5.4 State-of-the-Art Comparison on VIRAT/ActEV

In this section, we compare our *SimAug* model with state-of-the-art models on VIRAT/ActEV. Following the previous work [109], we compute the errors for the top  $K = 1$  prediction. Experimental results are shown in Table 6.2 (b), where all models in the top four rows are trained on the real-world training videos in VIRAT/ActEV. Our model trained on simulation data achieves competitive performance and outperforms *Multiverse* [109] model that is trained on the same data. With fine-tuning, which means using exactly the same training data without any extra annotation of real trajectories compared to [3, 50, 107, 109], we achieve the best performance on the VIRAT/ActEV benchmark.

#### 6.5.5 Ablation Experiments

We test various ablations of our approach to validate our design decisions. Results are shown in Table 6.4, where the top-1 prediction is used in the evaluation. We verify four key design choices by removing each, at a time, from the full model. The results show that by introducing viewpoint selection (Eq. (6.1)) and adversarial perturbation (Eq. (6.2)), our method improves model generalization.

- (1) *Multi-view data*: Our method is trained on multi-view simulation data and we use 4



Table 6.3: State-of-the-art comparison on the Stanford Drone Dataset (SDD). Numbers are minimal errors over 20 predictions and lower the better. Baseline numbers are taken from [34, 153]. “SimAug” is trained without using SDD training data and “SimAug + finetune” is further fine-tuned on SDD training data.

Method	minADE <sub>20</sub> (↓)	minFDE <sub>20</sub> (↓)
Social-LSTM [3]	31.19	56.97
Social-GAN [50]	27.25	41.44
DESIRE [92]	19.25	34.05
SoPhie [153]	16.27	29.38
Multiverse [109]	14.78	27.09
IDL [97]	13.93	24.40
P2T <sub>IRL</sub> [34]	12.58	22.07
SimAug	12.03	23.98
SimAug + finetune	<b>10.27</b>	<b>19.71</b>

camera views in our experiments. We test our method without the top-down view because it is similar to the ones in the SDD dataset. As we see, the performance drops due to the fewer number of data and less diverse views, suggesting that we should use more views in augmentation (which is effortless to do in 3D simulators).

(2) *Random perturbation*: We test our model without random perturbation on the original view trajectory samples by setting  $\delta = 0$  in Eq. (6.1). This leads to the performance drop on all three datasets and particularly on the more difficult Argoverse dataset.

(3) *Adversarial attack*: We test our model without adversarial attack by replacing Eq. (6.2) with  $V_{1:h}^{adv} = V_{1:h}$ . This is similar to applying the Mixup method [200] to two views in the feature space. The performance drops across all three benchmarks.

(4) *View selection*: We replace Eq. (6.1) with random search to see the effect of view selection. As we see, the significant performance drops, especially on the Stanford Drone dataset, verifying the effectiveness of this design.

Table 6.4: Performance on ablated versions of our method on three benchmarks. We report the  $\text{minADE}_1(\downarrow)/\text{minFDE}_1(\downarrow)$  metrics.

Method	VIRAT/ActEV	Stanford Drone	Argoverse
SimAug full model	21.7 / 42.2	15.7 / 30.2	67.9 / 175.6
- top-down view data	22.8 / 43.6	18.4 / 35.6	68.4 / 178.3
- random perturbation	23.6 / 43.8	18.7 / 35.6	69.1 / 180.2
- adversarial attack	23.1 / 43.8	17.4 / 32.9	68.0 / 177.5
- view selection	23.0 / 42.9	19.6 / 38.2	68.6 / 177.0

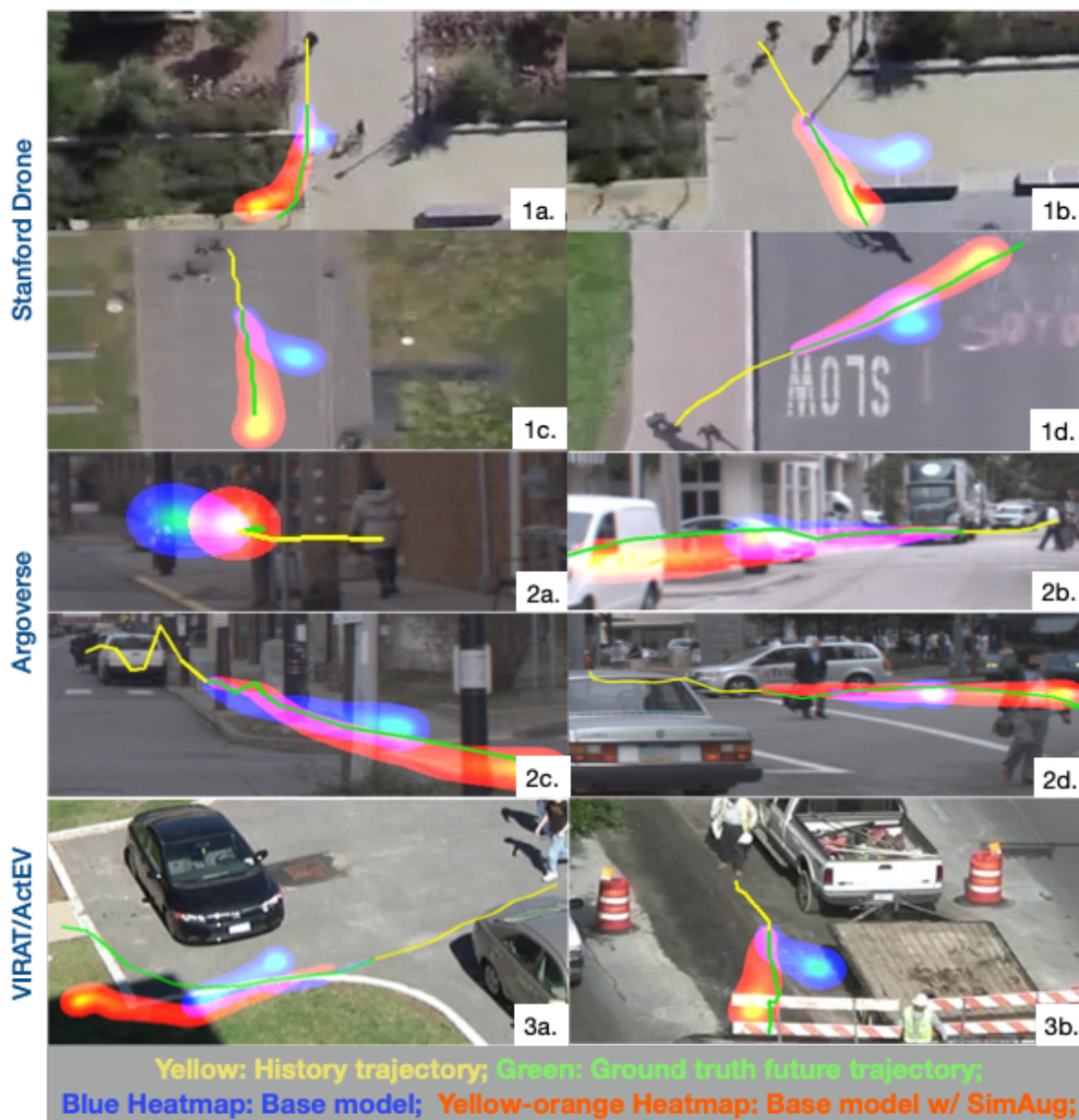


Figure 6.4: Qualitative analysis. Trajectory predictions from different models are colored and overlaid in the same image. See text for details.



## **Part III**

# **Joint Analysis and Prediction of Human Actions and Paths**



In the final part, we aim to build joint end-to-end systems with multi-task learning and utilizing enhanced contextual cues in the scene. We first study jointly predicting pedestrian trajectories and activities ([chapter 7](#)). Since short-term future prediction is not enough to ensure safe operations in autonomous driving applications, we introduce the long-term trajectory and action prediction benchmark and propose a model that takes into account intention forecasting ([chapter 8](#)). Finally in [chapter 9](#), we propose the work to jointly model action detection, action prediction and trajectory prediction to achieve optimal performance.





## Chapter 7

# Joint Pedestrian Trajectory and Action Prediction

In this chapter, we explore joint trajectory and action prediction in extended videos. We propose the *Next* model [107] for pedestrian prediction which utilizes rich visual features and multi-task learning. Then in [chapter 9](#), we jointly model action detection with action and trajectory prediction to achieve optimal performance.

### 7.1 Overview

With the advancement in deep learning, systems now are able to analyze an unprecedented amount of rich visual information from videos. An important analysis is forecasting the future path of pedestrians, called future person trajectory prediction. This problem has received increasing attention in the computer vision community [3, 50, 82]. It is regarded as an essential building block in video understanding because looking at the visual information from the past to predict the future is useful in many applications like self-driving cars, socially-aware robots [116], etc.

Humans navigate through public spaces often with specific purposes in mind, ranging from simple ones like entering a room to more complicated ones like putting things into a car. Such intention, however, is mostly neglected in existing work. Consider the example in [Fig. 7.1](#), the person (at the top-right corner) might take different paths depending on their intention, e.g., they might take the green path to *transfer object* or the yellow path to *load object into the car*. Inspired by this, this work is interested in modeling the future path jointly with such intention in videos. We model the intention in terms of a predefined set of 29 activities provided by the

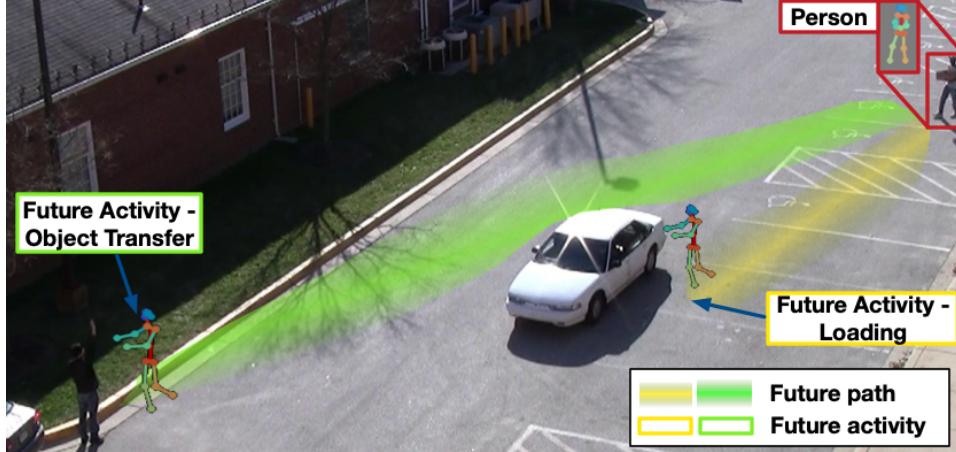


Figure 7.1: Our goal is to jointly predict a person’s future path and activity. The green and yellow line show two possible future trajectories and two possible activities are shown in the green and yellow boxes. Depending on the future activity, the person (top right) may take different paths, e.g., the yellow path for “loading” and the green path for “object transfer”.

NIST such as “loading”, “object transfer”, etc. See supplementary material for the full list.

The joint prediction model can have two benefits. First, learning the activity together with the path may benefit the future path prediction. Intuitively, humans are able to read from others’ body language to anticipate whether they are going to cross the street or continue walking along the sidewalk. In the example of Fig. 7.1, the person is carrying a box, and the man at the bottom left corner is waving at the person. Based on common sense, we may agree that the person will take the green path instead of the yellow path. Second, the joint model advances the capability of understanding not only the future path but also the future activity by taking into account the rich semantic context in videos. This increases the capabilities of automated video analytics for social good, such as safety applications like anticipating pedestrian movement at traffic intersections or a road robot helping humans transport goods to a car. Note that our techniques focus on predicting a few seconds into the future, and should not be useful for non-routine activities.

To this end, we propose a multi-task learning model called *Next* which has prediction modules for learning future paths and future activities simultaneously. As predicting future activity is challenging, we introduce two new techniques to address the issue. First, unlike most of the existing work [3, 50, 82, 124, 153, 189] which oversimplifies a person as a point in space, we encode a person through rich semantic features about visual appearance, body movement and interaction with the surroundings, motivated by the fact that humans derive such predictions

by relying on similar visual cues. Second, to facilitate the training, we introduce an auxiliary task for future activity prediction, i.e., activity location prediction. In the auxiliary task, we design a discretized grid which we call the Manhattan Grid as location prediction target for the system.

To the best of our knowledge, our work is the first on joint future path and activity prediction in streaming videos, and more importantly the first to demonstrate such joint modeling can considerably improve the future path prediction. We empirically validate our model on two benchmarks: ETH & UCY [94, 133], and ActEV/VIRAT [6, 131]. Experimental results show that our method outperforms state-of-the-art baselines, achieving the best-published result on two common benchmarks and producing additional prediction about the future activity. To summarize, the contributions of this work are threefold: **(i)** We conduct a pilot study on joint future path and activity prediction in videos. We are the first to empirically demonstrate the benefit of such joint learning. **(ii)** We propose a multi-task learning framework with new techniques to tackle the challenge of joint future path and activity prediction. **(iii)** Our model achieves the best-published performance on two public benchmarks. Ablation studies are conducted to verify the contribution of the proposed sub-modules.

## 7.2 Related Work

This work falls under the category of sequential models that utilize both static and dynamic environmental cues in the human motion prediction literature [149]. We utilize multiple contextual visual cues from both the target agent and the environment. We are the first work to jointly optimize activity and trajectory prediction with a unified framework. In the following, we review a few relevant recent approaches based on their use of these contextual cues. Then we also review some activity prediction works.

**Person-person models for trajectory prediction.** Person trajectory prediction models try to predict the future path of people, mostly pedestrians. A large body of work learns to predict person path by considering human social interactions and behaviors in crowded scene [192, 195]. Zou et al. in [207] learned human behaviors in crowds by imitating a decision-making process. Social-LSTM [3] added social pooling to model nearby pedestrian trajectory patterns. Social-GAN [50] added adversarial training on Social-LSTM to improve performance. Different from these previous work, we represent a person by rich visual features instead of simply considering a person as points in the scene. Meanwhile we use *geometric relation* to explicitly model the person-person relations in the scene, which has not been used in previous work.

**Person-scene models for trajectory prediction.** A number of works focused on learning the effects of the physical scene, e.g., people tend to walk on the sidewalk instead of grass. Kitani et al. in [82] used Inverse Reinforcement Learning to forecast human trajectory. Xie et al. in [189] considered pedestrian as “particles” whose motion dynamics are modeled within the framework of Lagrangian Mechanics. Scene-LSTM [124] divided the static scene into Manhattan Grid and predict pedestrian’s location using LSTM. CAR-Net [66] proposed an attention network on top of scene semantic CNN to predict person trajectory. SoPhie [153] combined deep neural network features from scene semantic segmentation model and generative adversarial network (GAN) using attention to model person trajectory. A disparity to [153] is that we explicitly pool scene semantic features around each person at each time instant so that the model can directly learn from such interactions.

**Person visual features for trajectory prediction.** Some recent works have attempted to predict person path by utilizing individual’s visual features instead of considering them as points in the scene. Kooij et al. in [83] looked at pedestrian’s faces to model their awareness to predict whether they will cross the road using a Dynamic Bayesian Network in dash-cam videos. Yagi et al. in [194] used person keypoint features with a convolutional neural network to predict future path in first-person videos. Different from these works, we consider rich visual semantics for future prediction that includes both the person behavior and their interactions with soundings .

**Activity prediction/early recognition & Tracking.** Many works have been proposed to anticipate future human actions using Recurrent Neural Network (RNN). [119] and [4] proposed different losses to encourage LSTM to recognize actions early in internet videos. Srivastava et al. in [163] utilized unsupervised learning with LSTM to reconstruct and predict video representations. Another line of works is anticipating human activities in robotic vision [64, 84]. There are previous works that take into account multiple cues in videos for tracking [65, 152] and group activity recognition [28, 156, 157]. Our work differs in that rich visual features and focal attention are used for joint person path and activity prediction. Meanwhile, our work utilizes novel activity location prediction to bridge the two tasks.

### 7.3 The Next Model

Humans navigate through spaces often with specific purposes in mind. Such purposes may considerably orient the future trajectory/path. This motivates us to study the future path prediction jointly with the intention. In this work, we model the intention in terms of a predefined

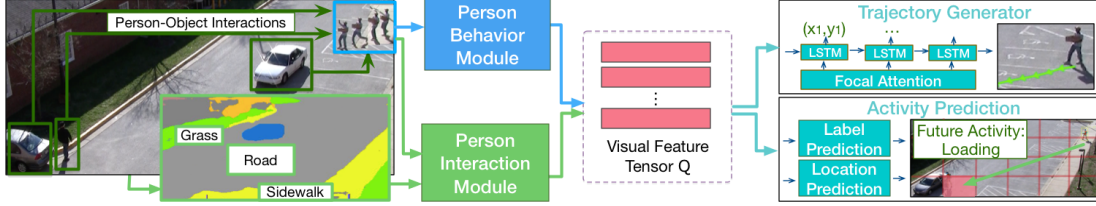


Figure 7.2: Overview of our model. Given a sequence of frames containing the person for prediction, our model utilizes person behavior module and person interaction module to encode rich visual semantics into a feature tensor.

set of future activities such as “walk”, “open\_door”, “talk”, etc.

**Problem Formulation:** Following [3, 50, 153], we assume each scene is first processed to obtain the spatial coordinates of all people at different time instants. Based on the coordinates, we can automatically extract their bounding boxes. Our system observes the bounding box of all the people from time 1 to  $T_{obs}$ , and objects if there are any, and predicts their positions (in terms of  $xy$ -coordinates) for time  $T_{obs+1}$  to  $T_{pred}$ , meanwhile estimating the possibilities of future activity labels at time  $T_{pred}$ .

### 7.3.1 Network Architecture

Fig. 7.2 shows the overall network architecture of our *Next* model. Unlike most of the existing work [3, 50, 82, 124, 153, 189] which oversimplifies a person as a point in space, our model employs two modules to encode rich visual information about each person’s behavior and interaction with the surroundings. *Next* has the following key components:

**Person behavior module** extracts visual information from the behavioral sequence of the person.

**Person interaction module** looks at the interaction between a person and their surroundings.

**Trajectory generator** summarizes the encoded visual features and predicts the future trajectory by the LSTM decoder with focal attention [105].

**Activity prediction** utilizes rich visual semantics to predict the future activity label for the person. In addition, we divide the scene into a discretized grid of multiple scales, which we call the Manhattan Grid, to compute classification and regression for robust activity location prediction.

In the rest of this section, we will introduce the above modules and the learning objective in details.

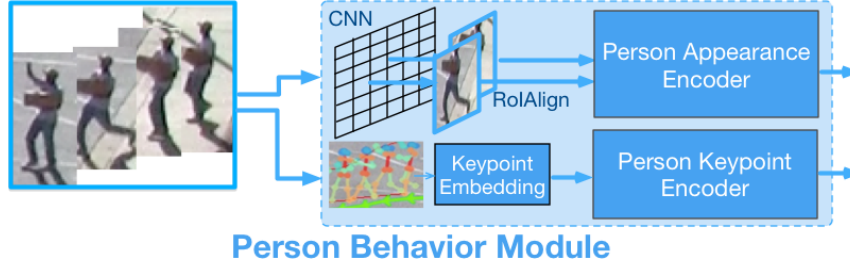


Figure 7.3: Person behavior module given a sequence of person frames.

### 7.3.2 Person Behavior Module

This module encodes the visual information about every individual in a scene. As opposed to oversimplifying a person as a point in space, we model the person’s appearance and body movement. To model appearance changes of a person, we utilize a pre-trained object detection model with “RoIAlign” [53] to extract fixed size CNN features for each person bounding box. See Fig. 7.3. We average the features along the spatial dimensions for each person and feed them into an LSTM encoder. Finally, we obtain a feature representation of  $T_{obs} \times d$ , where  $d$  is the hidden size of the LSTM. To capture the body movement, we utilize a person keypoint detection model trained on MSCOCO dataset [40] to extract person keypoint information. We apply the linear transformation to embed the keypoint coordinates before feeding into the LSTM encoder. The shape of the encoded feature has the shape of  $T_{obs} \times d$ . These appearance and movement features are commonly used in a wide variety of studies and thus do not introduce new concern on machine learning fairness.

### 7.3.3 Person Interaction Module

This module looks at the interaction between a person and their surroundings, i.e. person-scene and person-objects interactions.

**Person-scene.** To encode the nearby scene of a person, we first use a pre-trained scene segmentation model [23] to extract pixel-level scene semantic classes for each frame. We use totally  $N_s = 10$  common scene classes, such as roads, sidewalks, etc. The scene semantic features are integers (class indexes) of the size  $T_{obs} \times h \times w$ , where  $h, w$  are the spatial resolution. We first transform the integer tensor into  $N_s$  binary masks (one mask for each class), and average along the temporal dimension. This results in  $N_s$  real-valued masks, each of the size of  $h \times w$ . We apply two convolutional layers on the mask feature with a stride of 2 to get the *scene CNN*



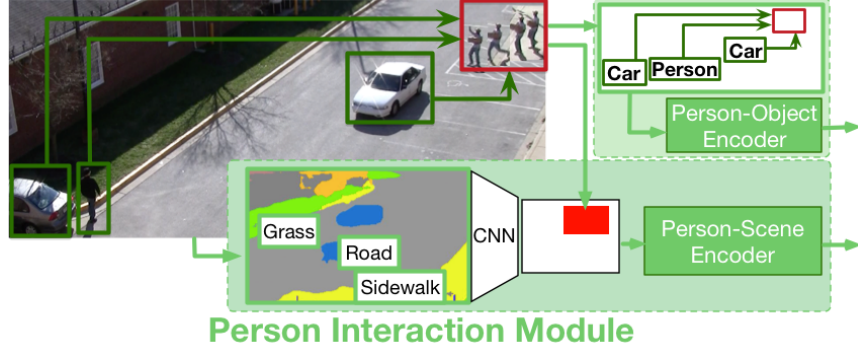


Figure 7.4: The person interaction module includes person-scene and person-objects modeling.

features in two scales.

Given a person’s  $xy$ -coordinate, we pool the scene features at the person’s current location from the convolution feature map. As the example shown at the bottom of Fig. 7.4, the red part of the convolution feature is the discretized location of the person at the current time instant. The receptive field of the feature at each time instant, i.e. the size of the spatial window around the person which the model looks at, depends on which scale is being pooled from and the convolution kernel size. In our experiments, we set the scale to 1 and the kernel size to 3, which means our model looks at the 3-by-3 surrounding area of the person at each time instant. The person-scene representation for a person is in  $\mathbb{R}^{T_{obs} \times C}$ , where  $C$  is the number of channels in the convolution layer. We feed this into a LSTM encoder in order to capture the temporal information and get the final person-scene features in  $\mathbb{R}^{T_{obs} \times d}$ .

**Person-objects.** Unlike previous work [3, 50] which relies on LSTM hidden states to model nearby people, our module explicitly models the *geometric relation* and the *object type* of all the objects/persons in the scene. At any time instant, given the observed box of a person  $(x_b, y_b, w_b, h_b)$  and  $K$  other objects/persons in the scene  $\{(x_k, y_k, w_k, h_k) | k \in [1, K]\}$ , we encode the geometric relation into  $\mathcal{G} \in \mathbb{R}^{K \times 4}$ , the  $k$ -th row of which equals to:

$$\mathcal{G}_k = [\log(\frac{|x_b - x_k|}{w_b}), \log(\frac{|y_b - y_k|}{h_b}), \log(\frac{w_k}{w_b}), \log(\frac{h_k}{h_b})] \quad (7.1)$$

This encoding computes the geometric relation in terms of the geometric distance and the fraction box size. We use a logarithmic function to reflect our observation that human trajectories are more likely to be affected by close-by objects or people. This encoding has been proven effective in object detection [60]. For the object type, we simply use one-hot encoding to get the feature in  $\mathbb{R}^{K \times N_o}$ , where  $N_o$  is the total number of object classes. We then embed the geometric features and the object type features at the current time into  $d_e$ -dimensional vectors and feed

the embedded features into an LSTM encoder to obtain the final feature in  $\mathbb{R}^{T_{obs} \times d}$ .

As shown in the example from Fig. 7.4, the person-objects feature can capture how far away the person is to the other person and the cars. The person-scene feature can capture whether the person is near the sidewalk or grass. We design this information to the model with the hope of learning things like a person walks more often on the sidewalk than the grass and tends to avoid bumping into cars.

### 7.3.4 Trajectory Generation with Focal Attention

As discussed, the above four types of visual features, i.e. appearance, body movement, person-scene, and person-objects, are encoded by separate LSTM encoders into the same dimension. Besides, given a person’s trajectory output from the last time instant, we extract the trajectory embedding by

$$e_{t-1} = \tanh\{W_e[x_{t-1}, y_{t-1}]\} + b_e \in \mathbb{R}^d, \quad (7.2)$$

where  $[x_{t-1}, y_{t-1}]$  is the trajectory prediction of time  $t - 1$  and  $W_e, b_e$  are learnable parameters. We then feed the embedding  $e_{t-1}$  into another LSTM encoder for the trajectory. The hidden states of all encoders are packed into a tensor named  $Q \in \mathbb{R}^{M \times T_{obs} \times d}$ , where  $M = 5$  denotes the total number of features and  $d$  is the hidden size of the LSTM.

Following [50], we use an LSTM decoder to directly predict the future trajectory in the  $xy$ -coordinate. The hidden state of this decoder is initialized using the last state of the person’s trajectory LSTM encoder. At each time instant, the  $xy$ -coordinate will be computed from the decoder state  $h_t = \text{LSTM}(h_{t-1}, [e_{t-1}, \tilde{q}_t])$  and by a fully connected layer.  $\tilde{q}_t$  is an important attended feature vector which summarizes salient cues in the input features  $Q$ . We employ an effective focal attention [105] to this end. It was originally proposed to carry out multimodal inference over a sequence of images for visual question answering. The key idea is to project multiple features into a space of correlation, where discriminative features can be easier to capture by the attention mechanism. To do so, we compute a correlation matrix  $S^t \in \mathbb{R}^{M \times T_{obs}}$  at every time instant  $t$ , where each entry  $S_{ij}^t = h_{t-1}^\top \cdot Q_{ij:}$  is measured using the dot product similarity and  $:$  is a slicing operator that extracts all elements from that dimension. Then we compute two attention matrices:

$$A^t = \text{softmax}(\max_{i=1}^M S_{i,:}^t) \in \mathbb{R}^M \quad (7.3)$$

$$B^t = [\text{softmax}(S_{1,:}^t), \dots, \text{softmax}(S_{M,:}^t)] \in \mathbb{R}^{M \times T_{obs}} \quad (7.4)$$



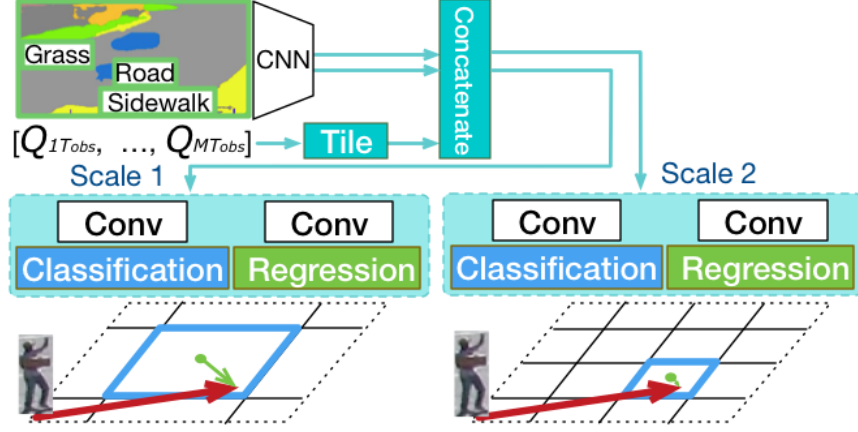


Figure 7.5: Activity location prediction with classification and regression on the multi-scale Manhattan Grid.

Then the attended feature vector is given by:

$$\tilde{q}_t = \sum_{j=1}^M A_j^t \sum_{k=1}^{T_{obs}} B_{jk}^t Q_{jk} \in \mathbb{R}^d \quad (7.5)$$

As shown, the focal attention models the correlation among different features and summarizes them into a low-dimensional attended vector.

### 7.3.5 Activity Prediction

Since the trajectory generation module outputs one location at a time, errors may accumulate across time and the final destination would deviate from the actual location. Using the wrong location for activity prediction may lead to bad accuracy. To counter this disadvantage, we introduce an auxiliary task, i.e. activity location prediction, in addition to predicting the future activity label of the person. We describe the two prediction modules in the following.

**Activity location prediction with the Manhattan Grid.** To bridge the gap between trajectory generation and activity label prediction, we propose an activity location prediction module to predict the final location of where the person will engage in the future activity. The activity location prediction includes two tasks, *location classification* and *location regression*. As illustrated in Fig. 7.5, we first divide a video frame into a discretized  $h \times w$  grid, namely *Manhattan Grid*, and learn to classify the correct grid block and at the same time to regress from the center of that grid block to the actual location. Specifically, the aim for the classification task is to predict the correct grid block in which the final location coordinates reside. After classifying

the grid block, the aim for the regression task is to predict the deviation of the grid block center (green dots in the figure) to the final location coordinate (the end of green arrows). The reason for adding the regression task are: (i) it will provide more precise locations than just a grid block area; (ii) it is complementary to the trajectory prediction which requires  $xy$ -coordinates localization. We repeat this process on the Manhattan Grid of different scales and use separate prediction heads to model them. These prediction heads are trained end-to-end with the rest of the model. Our idea is partially inspired by the region proposal network [142] and our intuition is that similar to object detection problem, we need accurate localization using multi-scale features in a cost-efficient way.

As shown in Fig. 7.5, we first concatenate the scene CNN features (see Section 7.3.3) with the last hidden state of the encoders (see Section 7.3.4). For compatibility, we tile the hidden state  $Q_{:T_{obs}}$  along the height and width dimension resulting in a tensor of the size  $M \times d \times w \cdot h$ , where  $w \cdot h$  is the total number of the grid blocks. The hidden state contains rich information from all encoders and allow gradients flow smoothly through from prediction to feature encoders.

The concatenated features are fed into two separate convolution layers for classification and regression. The convolution output for grid classification  $\text{cls}_{grid} \in \mathbb{R}^{w \cdot h \times 1}$  indicates the probability of each grid block being the correct destination. In comparison, the convolution output for grid regression  $\text{rg}_{grid} \in \mathbb{R}^{w \cdot h \times 2}$  denotes the deviation, in the  $xy$ -coordinates, between the final destination and every grid block center. A row of  $\text{rg}_{grid}$  represents the difference to a grid block, calculated from  $[x_t - x_{ci}, y_t - y_{ci}]$  where  $(x_t, y_t)$  denotes the predicted location and  $(x_{ci}, y_{ci})$  is the center of the  $i$ -th grid block. The ground truth for the grid regression can be computed in a similar way. During training, only the correct grid block receives gradients for regression. Recent work [124] also incorporates the grid for location prediction. Our model differs in that we link grid locations to scene semantics, and use a classification layer and a regression layer together to make more robust predictions.

**Activity label prediction.** Given the encoded visual observation sequence, the activity label prediction module predicts the future activity at time instant  $T_{pred}$ . We compute the future  $N_a$  activity probabilities using the concatenated last hidden states of the encoders:

$$\text{cls}_{act} = \text{softmax}(W_a \cdot [Q_{1T_{obs}}, \dots, Q_{MT_{obs}}]) \quad (7.6)$$

where  $W_a$  is a learnable weight. The future activity of a person could be multi-class, e.g. a person could be “walking” and “carrying” at the same time.

### 7.3.6 Training

The entire network is trained end-to-end by minimizing a multi-task objective. The primary loss is the common  $L_2$  loss between the predicted future trajectories and the ground-truth trajectories [50, 124, 153]. The loss is summed into  $L_{xy}$  over all persons from  $T_{obs+1}$  to  $T_{pred}$ .

The second category of loss is the activity location classification and regression loss. We have  $L_{grid\_cls} = \sum_{i=1}^N \text{ce}(\text{cls}_{grid}^i, \text{cls}_{grid}^{*i})$ , where  $\text{cls}_{grid}^{*i}$  is the ground-truth final location grid block ID for the  $i^{th}$  training trajectory. Likewise  $L_{grid\_reg} = \sum_{i=1}^N \text{smooth}_{L_1}(\text{rg}_{grid}^i, \text{rg}_{grid}^{*i})$  and  $\text{rg}_{grid}^{*i}$  is the ground-truth difference to the correct grid block center. This loss is designed to bridge the gap between the trajectory generation task and activity label prediction task.

The third loss is for activity label prediction. We employ the cross-entropy loss:  $L_{act} = \sum_{i=1}^N \text{ce}(\text{cls}_{act}^i, \text{cls}_{act}^{*i})$ . The final loss is then calculated from:

$$L = L_{xy} + \lambda(L_{grid\_cls} + L_{grid\_reg}) + L_{act} \quad (7.7)$$

We use a balance controller  $\lambda = 0.1$  for location destination prediction to offset their higher loss values during training.

## 7.4 Experimental Results

We evaluate the proposed *Next* model on two common benchmarks for future path prediction: ETH [133] and UCY [94], and ActEV/VIRAT [6, 131].

### 7.4.1 ActEV/VIRAT

**Dataset & Setups.** ActEV/VIRAT [6] is a public dataset released by NIST in 2018 for activity detection research in streaming video (<https://actev.nist.gov/>). This dataset is an improved version of VIRAT [131], with more videos and annotations. It includes 455 videos at 30 fps from 12 scenes, more than 12 hours of recordings. Most of the videos have a high resolution of 1920x1080. We use the official training set for training and the official validation set for testing. Following [3, 50, 153], the models observe 3.2 seconds (8 frames) of every person and predict the future 4.8 seconds (12 frames) of person trajectory. We downsample the videos to 2.5 fps and extract person trajectories using the code released in [50]. Since we do not have the homographic matrix, we use the pixel values for the trajectory coordinates as it is done in [194].

**Evaluation Metrics.** Following prior work [3, 50, 153], we use two error metrics for person trajectory prediction:

i) *Average Displacement Error (ADE)*: The average Euclidean distance between the ground truth coordinates and the prediction coordinates over all time instants,

$$\text{ADE} = \frac{\sum_{i=1}^N \sum_{t=1}^{T_{pred}} \|\tilde{Y}_t^i - Y_t^i\|_2}{N * T_{pred}} \quad (7.8)$$

ii) *Final Displacement Error (FDE)*: The euclidean distance between the predicted points and the ground truth point at the final prediction time instant  $T_{pred}$ ,

$$\text{FDE} = \frac{\sum_{i=1}^N \|\tilde{Y}_{T_{pred}}^i - Y_{T_{pred}}^i\|_2}{N} \quad (7.9)$$

The errors are measured in the pixel space on ActEV/VIRAT whereas in meters on ETH and UCY. For future activity prediction, we use mean average precision (mAP).

**Baseline methods.** We compare our method with the two simple baselines and two recent methods: **Linear** is a single layer model that predicts the next coordinates using a linear regressor based on the previous input point. **LSTM** is a simple LSTM encoder-decoder model with coordinates input only. **Social LSTM** [3]: We train the social LSTM model to directly predict trajectory coordinates instead of Gaussian parameters. **SGAN** [50]: We train two model variants (PV & V) detailed in this work using the released code from Social-GAN [50] (<https://github.com/agrimgupta92/sgan/>).

Aside from using a single model at test time, Gupta et al. [50] also used 20 model outputs per frame and selected the best prediction to count towards the final performance. Following the practice, we train 20 identical models using random initializations and report the same evaluation results, which are marked “20 outputs” in Table 7.1.

**Implementation Details.** We use LSTM cell for both the encoder and decoder. The embedding size  $d_e$  is set to 128, and the hidden sizes  $d$  of encoder and decoder are both 256. Ground truth bounding boxes of persons and objects are used during the observation period (from time 1 to  $T_{obs}$ ). For person keypoint features, we utilize the pre-trained pose estimator from [40] to extract 17 joints for each ground truth person box. For person appearance feature, we utilize the pre-trained object detection model FPN [113] to extract appearance features from person bounding boxes. The scene semantic segmentation features are resized to (64, 36) and the scene convolution layers are set to have a kernel size of 3, a stride of 2 and the channel dimension is 64. We resize all videos to 1920x1080 and utilize two grid scales, 32x18 and 16x9. The activation function is  $\tanh$  if not stated otherwise and we do not use any normalization. For training, we use Adadelata optimizer [197] with an initial learning rate of 0.1 and the dropout value is 0.3. We use gradient clipping of 10 and weight decay of 0.0001. For Social LSTM, the neighbor

	Method	ADE	FDE	move_ADE	move_FDE
Single Model	Linear	32.19	60.92	42.82	80.18
	LSTM	23.98	44.97	30.55	56.25
	Social LSTM	23.10	44.27	28.59	53.75
	SGAN-PV	30.51	60.90	37.65	73.01
	SGAN-V	30.48	62.17	35.41	68.77
	Ours	<b>17.99</b>	<b>37.24</b>	<b>20.34</b>	<b>42.54</b>
	Ours-Noisy	34.32	57.04	40.33	66.73
20 Outputs	SGAN-PV-20	23.11	41.81	29.80	53.04
	SGAN-V-20	21.16	38.05	26.97	47.57
	Ours-20	<b>16.00</b>	<b>32.99</b>	<b>17.97</b>	<b>37.28</b>

Table 7.1: Comparison to baseline methods on the ActEV/VIRAT validation set. Top uses the single model output. Bottom uses 20 outputs. Numbers denote errors thus lower are better.

is set to 256 pixels as in [194]. All baselines use the same embedding size and hidden size as our model, therefore all encoder-decoder models have about the same numbers of parameters. Other hyper-parameters we use for the baselines follow the ones in [50].

**Main Results.** Table 7.1 lists the testing error, where the top part is the error of a single model output and the bottom shows the best result of 20 model outputs. The “ADE” and “FDE” columns summarize the error over all trajectories, and the last two columns further detail the subset trajectories of moving activities (“walk”, “run”, and “ride\_bike”). We report the mean performance of 20 runs of our single model at Row 7. The standard deviation on “ADE” metric is 0.043. Full numbers can be found in supplemental material. As we see, our method performs favorably against other methods, especially in predicting the trajectories of moving activities. For example, our model outperforms Social-LSTM and Social-GAN by a large margin of 10 points in terms of the “move\_FDE” metric. The results demonstrate the efficacy of the proposed model and its state-of-the-art performance on future trajectory prediction. Additionally, as a step towards real-world application, we train our model with noisy outputs from object detection and tracking during the observation period. For evaluation, following common practise in tracking [185], for each trajectory, we assume the person bounding box location at time 1 is close to the ground truth location, and we evaluate the model prediction using tracking inputs and other visual features from time 1 to  $T_{obs}$  as shown in Table 7.1 “Ours-Noisy”.

**Qualitative analysis.** We visualize and compare our model outputs and the baselines in



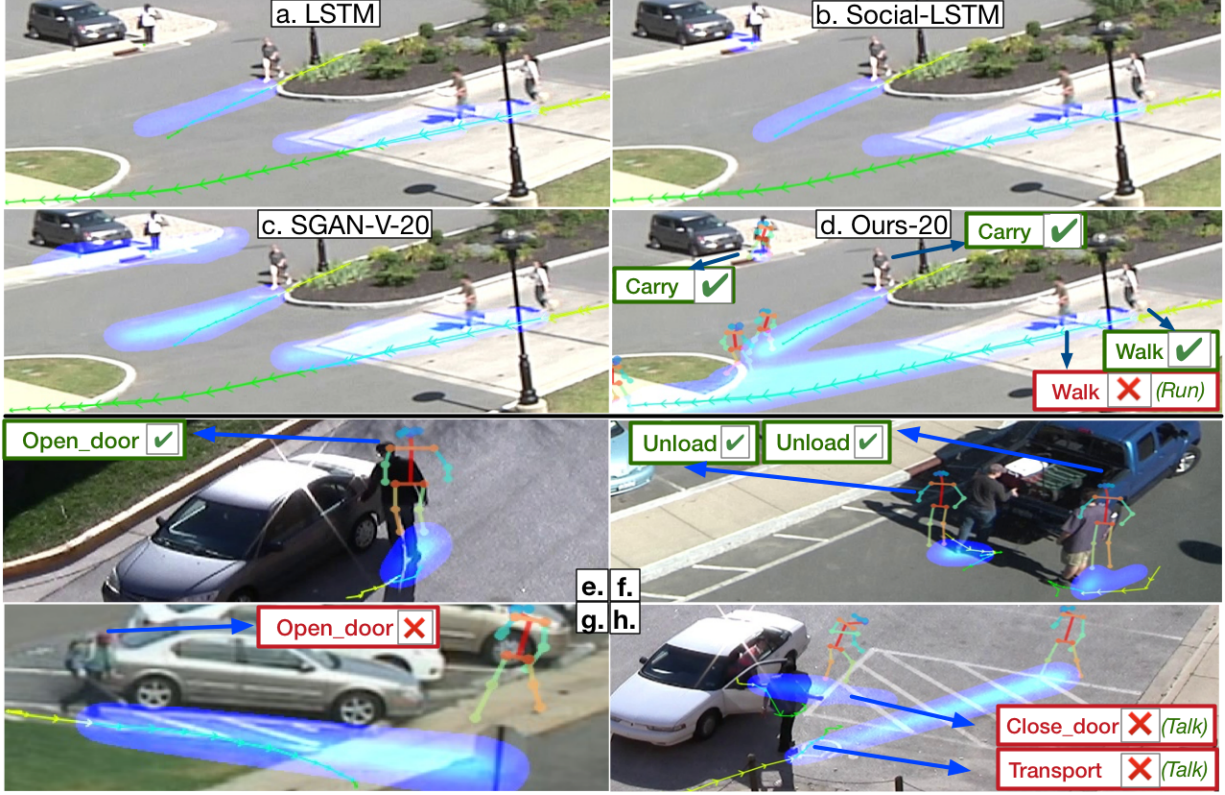


Figure 7.6: (Better viewed in color.) Qualitative comparison between our method and the baselines. Yellow path is the observable trajectory and green path is the ground truth trajectory during the prediction period. Predictions are shown as blue heatmaps. Our model also predicts the future activity, which is shown in the text and with the person pose template.

Fig. 7.6. As we see, our method outputs more accurate trajectories for each person, especially for the two persons on the right that were about to accelerate their movement. Our method is also able to predict most of the activities correct except one (walk versus run). Our model successfully predicts the activity “carry” and the static trajectory of the person near the car, while in Fig 7.6(c), SGAN predicts several moving trajectories in different directions. We further provide a qualitative analysis of our model predictions. (i) Successful cases: In Fig 7.6(e) and 7.6(f), both the trajectory prediction and future activity prediction are correct. (ii) Imperfect case: In Fig 7.6(g), although the trajectory prediction is mostly correct, our model predicts that the person is going to open the door of the car, given the observation that he is walking towards the side of the car. (iii) Failed case: In Fig 7.6(h), our model fails to capture the subtle interactions between the two persons and predicts that they will go separate ways, while in fact they are going to stop and talk to each other.

Method	ADE ↓	FDE ↓	Act mAP ↑
Our full model	17.91	37.11	0.192
No p-behavior	18.99	39.82	0.139
No p-interaction	18.83	39.35	0.163
No focal attention	19.93	42.08	0.144
No act label loss	19.48	41.45	-
No act location loss	19.07	39.91	0.152
No multi-task	20.37	42.79	-

Table 7.2: Multi-task performance &amp; ablation experiments.

### 7.4.2 Ablation Model

In Table 7.2, we systematically evaluate our method through a series of ablation experiments, where “ADE” and “FDE” denotes the errors thus lower are better. “Act” is the mean Average Precision (mAP) of the activity label prediction over 29 activities and higher are better.

**Efficacy of rich visual features.** We investigate the feature contribution of person behavior and person interactions. As shown in the first three rows in Table 7.2, both features are important to trajectory prediction while person behavior features are more essential for activity prediction. Individual feature ablations are in the supplementary material.

**Effect of focal attention.** In the fourth row of Table 7.2, we replace focal attention in Eq. (7.5) with a simple average of the last hidden states from all encoders. Both trajectory and activity prediction hurt as a result.

**Impact of multi-task learning.** In the last three rows of Table 7.2, we remove the additional tasks of predicting the activity label or the activity location or both to see the impact of multi-task learning. Results show the benefit of our multi-task learning method.

### 7.4.3 ETH & UCY

**Dataset.** ETH [133] and UCY [94] are common datasets for person trajectory prediction benchmark [3, 50, 124, 153]. Same as previous works, we report performance by averaging over both datasets. We use the same data processing method and settings detailed in [50]. This benchmark includes videos from five scenes: ETH, HOTEL, UNIV, ZARA1 and ZARA2. Leave-one-scene-out data split is used and we evaluate our model on 5 sets of data. We follow the same testing scenario and baselines as in the previous section. We have also cited the latest state-of-the-art

	Method	ETH	HOTEL	UNIV *	ZARA1	ZARA2	AVG
Single Model	Linear	1.33 / 2.94	0.39 / 0.72	0.82 / 1.59	0.62 / 1.21	0.77 / 1.48	0.79 / 1.59
	LSTM	1.09 / 2.41	0.86 / 1.91	<b>0.61 / 1.31</b>	<b>0.41 / 0.88</b>	0.52 / 1.11	0.70 / 1.52
	Alahi et al. [3]	1.09 / 2.35	0.79 / 1.76	0.67 / 1.40	0.47 / 1.00	0.56 / 1.17	0.72 / 1.54
	Ours-single	<b>0.88 / 1.98</b>	<b>0.36 / 0.74</b>	0.62 / 1.32	0.42 / 0.90	<b>0.34 / 0.75</b>	<b>0.52 / 1.14</b>
20 Outputs	[50](V)	0.81 / 1.52	0.72 / 1.61	0.60 / 1.26	0.34 / 0.69	0.42 / 0.84	0.58 / 1.18
	[50](PV)	0.87 / 1.62	0.67 / 1.37	0.76 / 1.52	0.35 / 0.68	0.42 / 0.84	0.61 / 1.21
	[153]	<b>0.70 / 1.43</b>	0.76 / 1.67	<b>0.54 / 1.24</b>	<b>0.30 / 0.63</b>	0.38 / 0.78	0.54 / 1.15
	Ours-20	0.73 / 1.65	<b>0.30 / 0.59</b>	0.60 / 1.27	0.38 / 0.81	<b>0.31 / 0.68</b>	<b>0.46 / 1.00</b>

Table 7.3: Comparison of different methods on ETH (Column 3 and 4) and UCY datasets (Column 5-7). \* We use a smaller test set on UNIV since 1 video is unable to download.

results from [153]. Due to 1 video cannot be downloaded, we use a smaller test set for UNIV and a smaller training set across all splits. The other 4 test sub-datasets are the same as in [50] so the numbers are comparable.

Since there is no activity annotation, we do not use activity label prediction module in our model. Since the annotation is only a point for each person and the human scale in each video doesn't change much, we apply a fixed size expansion from points for each video to get the person bounding box annotation for feature pooling. We do not use any other bounding box. We don't use any additional annotation compared to baselines to ensure a fair comparison.

**Implementation Details.** We do not use person keypoint feature. Final location loss and trajectory L2 loss are used. Unlike [153], we don't utilize any data augmentation. We train our model for 40 epochs with the adadelata optimizer. Other hyper-parameters are the same as in Section 7.4.1.

**Results & Analysis.** Experiments are shown in Table 7.3. Our model outperforms other methods in both evaluations, where we obtain the best-published single model on ETH and best average performance on the ETH & UCY benchmark. As shown in the table, our model performs much better on HOTEL and ZARA2. The average movement at each time-instant in these two scenes are 0.18 and 0.22, respectively, much lower than others: 0.389 (ZARA1), 0.460 (ETH), 0.258 (UNIV). Recall that the leave-one-scene-out data split is used in training. The results suggest other methods are more likely to overfit to the trajectories of large movements, e.g. Social-GAN [50] often "over-shoot" when predicting the future trajectories. In comparison, our method uses attention to find the "right" visual signal and show better performance



for trajectories of small movements on HOTEL and ZARA2 while still being competitive for trajectories of large movements.

#### **7.4.4 Real-time Prediction**

In this section we briefly discuss the possibilities of achieving real-time prediction during test time. As shown in [chapter 2](#), our object detection and tracking system can achieve real-time speed if we process about 5 video frames per second (Table [2.4](#)) given a relatively new 4-GPU machine listed in Table [2.3](#). Recall that in this work we only need 2.5 frame-per-second observation features to achieve the good results we have shown in the previous section. The prediction inference time is about 10x faster than real-time, which means the bottleneck for real-time prediction lies in the feature extraction process of scene semantic segmentation and person pose detection.



## Chapter 8

# Long-term Joint Trajectory and Action Prediction with Intention Recognition

In this chapter, we explore the problem of long-term trajectory and action prediction, which aims to expand the prediction horizon two-fold to three-fold compared to most previous works.

### 8.1 Overview

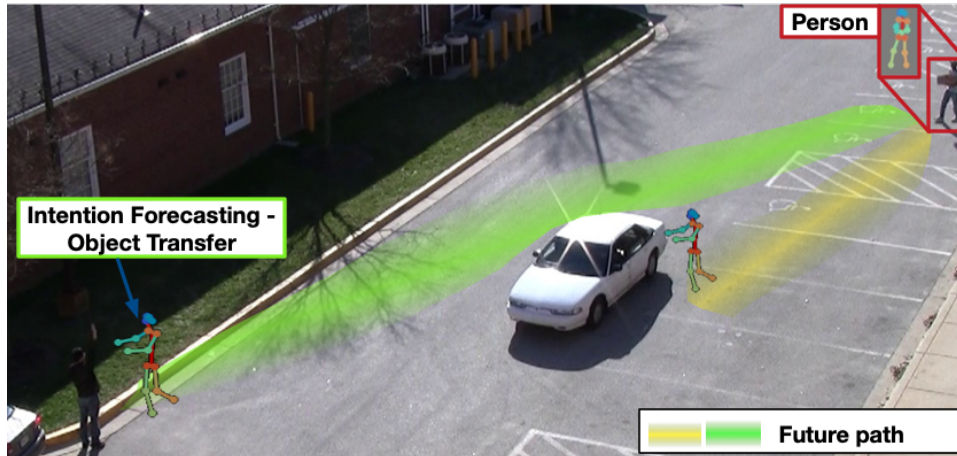


Figure 8.1: Our goal is to jointly predict a person’s long-term future path and activity. The green and yellow line show two possible future trajectories. By forecasting the intention based on scene constraints and social interactions (the person at the bottom left is waving at the target person), the model chooses the correct future path predictions.

With the advancement in deep learning, systems now are able to analyze an unprecedented amount of rich visual information from videos to enable many AI applications. An important analysis is forecasting the future path of pedestrians, called future person path/trajectory prediction, which aims at forecasting a pedestrian’s future trajectory in the next few seconds, has received a lot of attention in our community [3, 50, 82, 107]. It is regarded as an fundamental building block in video understanding because forecasting human behaviors is useful in many applications like self-driving cars, socially-aware robots [116], etc.

However, most previous works [50, 107] only focus on predicting pedestrian trajectories in the near future (within 5 seconds). In applications like autonomous systems, safe operation and collision avoidance are crucial for the systems to be co-mingling with humans. This requires predicting human motion beyond a short time-horizon. While near-future prediction can be informed by recent observed trajectory history, long-term prediction depends on inferring human intents or goals, which requires the model to make use of scene constraints, social interactions and even common sense reasoning.

Long-term prediction has the following challenges. First, it is highly uncertain compared to short-term forecasting. Using only the trajectory history is not enough to achieve accurate long-term prediction, and semantic reasoning with scene constraints is crucial. Second, the target person might be traveling out-of-frame and hence require the models to infer the final intended destination without actually seeing it. Third, long-term prediction may require more observation inputs that result in greater computation demand while it is critical to have an efficient system that could output prediction in a timely fashion.

Humans navigate through public spaces often with specific purposes in mind, ranging from simple ones like entering a room to more complicated ones like putting things into a car. Such intention, however, is mostly neglected in existing works. Consider the example in Fig. 8.1, the person (at the top-right corner) might take different paths depending on their intention, e.g., they might take the green path to *transfer object* or the yellow path to *load object into the car*. Inspired by this, this work is interested in modeling the future path by conditioning on forecasting such intentions in videos. We model the intention in terms of a predefined set of 29 activities provided by NIST such as “loading”, “object transfer”.

The intention modeling can have two benefits. First, learning human intentions may benefit long-term future path prediction. Intuitively, humans are able to read from others’ body language to anticipate whether they are going to cross the street or continue walking along the sidewalk. After understanding these behaviors, humans can make better and further predictions. In the example of Fig. 8.1, the person is carrying a box, and the man at the bottom left

corner is waving at the person. Based on common sense, we may agree that the person will take the green path instead of the yellow path. Second, human intention prediction could be beneficial to many other tasks. This increases the capabilities of automated video analytics for social good such as real-time accident alerting, self-driving cars, and smart robot assistance. It may also have safety applications such as anticipating pedestrian movement at traffic intersections or a road robot helping humans transport goods to the trunk of a car by interpreting whether they have something in their hands.

## 8.2 Related Work

**Intention Prediction for Trajectory Prediction.** Some previous works have tried to predict intention for trajectory forecasting in self-driving scenarios where both RGB and LIDAR sensor data are available. [79] tried to predict long-term pedestrian motions using intent as a policy in the Markov Decision Process framework with an autonomous driving dataset. [15] utilized raw sensor data from self-driving cars with deep networks to predict vehicle trajectories and driver intentions. Xie et al. in [189] considered pedestrian as “particles” whose motion dynamics and human intentions are modeled within the framework of Lagrangian Mechanics. Recently, Liang et al. [107] proposed a joint future activity and trajectory prediction framework that utilized multiple visual features using focal attention [105, 106].

## 8.3 Future Plan

**Baseline Method and Tentative Proposed Method.** We will start with the *Social-GAN* [50] model for long-term trajectory prediction. *Social-GAN* utilizes an encoder-decoder framework with LSTMs to generate multiple future trajectories. Another stronger baseline is the the *Next* [107] model. *Next* model takes rich visual features as inputs and an LSTM to generate future trajectories. We will establish a new long-term trajectory prediction evaluation protocol as opposed to the previous commonly used short-term benchmarks. To tackle the aforementioned challenges in long-term trajectory/activity prediction, we plan to propose a model called *IntentNet*, which takes into account scene graph constraints and social interactions to forecast intentions, and then predict the conditioned trajectories. Our model will utilize action recognition results during the observation period to better understand the social interactions of the scenarios. Meanwhile, we will also look into using common sense modeling (in our case, the action sequence knowledge that could be mined from the training dataset).

**Datasets & Experiments.** In this work, we will develop a novel long-term pedestrian trajectory forecasting benchmark based on the VIRAT [131] dataset and the MEVA dataset [93]. In addition, we may also utilize pedestrian intention datasets including the JAAD dataset [138] and the PIE dataset [139]. Previous works have focused on predicting future trajectories within the next 5 seconds. We plan to extend this to 10-15 seconds as well as adding an unlimited time scenario. We will measure model performance on trajectory prediction as well as action prediction. For trajectory prediction, we plan to use both geometric metrics like ADE and FDE, and probabilistic metrics like Negative Log-Likelihood (NLL). We plan to conduct **robustness experiments** by evaluating prediction accuracy as a function of various influences including the length of observation period, the size of training dataset, number of agents in the scene, the amount of noise in the object detection and tracking results during inference, different classes of actions, and the length of prediction horizon.

## Chapter 9

# Joint Modeling of Action Detection, Action Prediction and Path Prediction

In the previous chapters, we have laid the foundation of standalone perception models and future prediction models. In this chapter, we propose to leverage these models and explore the best end-to-end learning scheme that achieves optimal performance in future trajectory and action prediction.

### 9.1 Overview

Traditional autonomous systems [9, 16, 36] decompose the problem into three subtasks: object detection, object tracking, and trajectory prediction. These independent components perform these subtasks sequentially. As they are developed separately, it may lead to sub-optimal performance. The disconnected design would also prevent downstream tasks from correcting the mistakes made by upstream ones.

To tackle the aforementioned challenge, recently, models that solve the detection and prediction tasks jointly with a single neural network have been proposed [110, 117, 183], resulting in more efficient computation and improved accuracy. This end-to-end design has been extended to predict driver intention [15] and motion planning [198]. However, these previous works have not considered solving action analysis jointly with future prediction. Recognition of one's actions at the current moment is crucial to semantic reasoning of what the person is going to do, especially for long-term prediction. In this chapter, we propose to look into jointly optimizing action recognition with future trajectory/action prediction to tackle the aforementioned challenges.

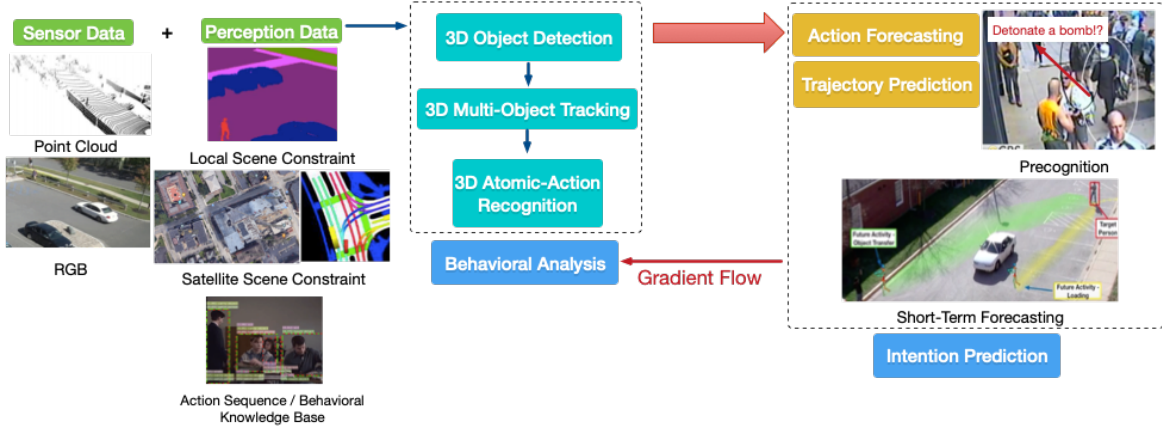


Figure 9.1: We aim to develop a robust joint detection and prediction model for future (intention) prediction with video inputs.

## 9.2 Future Plan

**Method.** An action recognition branch can be added to the *Next* [107] model as a strong baseline. We plan to incorporate the viewpoint-invariant action recognition model proposed in chapter 4 and propose a joint model that takes into account scene constraints and social interactions. We also plan to design multi-agent forecasting method like Social-LSTM [3] and DESIRE [92], which allows the prediction model to consider optimal paths for multiple agents in the scene at the same time.

**Datasets & Experiments.** In this work, we plan to utilize extended video action datasets like VIRAT [131] dataset and the MEVA dataset [93], for joint action detection and future prediction. For trajectory prediction, we plan to use both geometric metrics like ADE and FDE, and probabilistic metrics like Negative Log-Likelihood (NLL). We plan to conduct **robustness experiments** as in chapter 8. In addition, we may utilize CARLA [37] simulator and our reconstructed VIRAT dataset [108], to **augment the agent behaviors** and scene complexity in a controlled setting for the evaluation. Such evaluation allows us to see whether the models have truly captured important behavioral cues of the target agents and environmental cues. For example, adding a “wave hand” action to the target agent should clearly indicate that its goal is to meet another person in the scene, and adding a parked vehicle in the scene should alter the prediction models output even though the destination of the agent remains the same. We plan to reconstruct simple indicative actions like “wave hand” and “turn head”. We’ll focus on using scene semantic segmentation features to address the domain gap problem. To explore how well



our models perform compare to humans, we will also conduct **user studies**, which includes **perceptual validation** and **human performance**. Similar to that of the GAN research community (pix2pix [62], etc.), we will set up trials where human annotators are asked whether a machine generated future trajectories are real (perceptual validation). For human performance, we will set up an interface for human annotators to predict future trajectories given the same observations as the models.



## Chapter 10

# Conclusion

This thesis explores the problems of human behavioral analysis (perception) and future prediction. This thesis' goal is promote human safety in applications such as robotics or autonomous driving. We experiment on the public benchmark datasets, the primary driver of which is to support public safety and traffic monitoring and management by automatic activity detection in streaming video. Future research into activity and path prediction may implicate ethical issues around privacy, safety and fairness and ought to be considered carefully before being used in real-world applications. Our method for predicting trajectory and activity has not been tested for different populations of people. As such, it is important to further evaluate these issues before employing the model in situations that may differentially impact people.



# Bibliography

- [1] Martín Abadi, Ashish Agarwal, Paul Barham, Eugene Brevdo, Zhifeng Chen, Craig Citro, Greg S. Corrado, Andy Davis, Jeffrey Dean, Matthieu Devin, Sanjay Ghemawat, Ian Goodfellow, Andrew Harp, Geoffrey Irving, Michael Isard, Yangqing Jia, Rafal Jozefowicz, Lukasz Kaiser, Manjunath Kudlur, Josh Levenberg, Dandelion Mané, Rajat Monga, Sherry Moore, Derek Murray, Chris Olah, Mike Schuster, Jonathon Shlens, Benoit Steiner, Ilya Sutskever, Kunal Talwar, Paul Tucker, Vincent Vanhoucke, Vijay Vasudevan, Fernanda Viégas, Oriol Vinyals, Pete Warden, Martin Wattenberg, Martin Wicke, Yuan Yu, and Xiaoqiang Zheng. TensorFlow: Large-scale machine learning on heterogeneous systems, 2015. Software available from [tensorflow.org](https://www.tensorflow.org). [2](#)
- [2] Sami Abu-El-Haija, Nisarg Kothari, Joonseok Lee, Paul Natsev, George Toderici, Balakrishnan Varadarajan, and Sudheendra Vijayanarasimhan. Youtube-8m: A large-scale video classification benchmark. *arXiv preprint arXiv:1609.08675*, 2016. [3.1](#)
- [3] Alexandre Alahi, Kratarth Goel, Vignesh Ramanathan, Alexandre Robicquet, Li Fei-Fei, and Silvio Savarese. Social lstm: Human trajectory prediction in crowded spaces. In *CVPR*, 2016. [1.1](#), [5.1](#), [5.2](#), [5.4](#), [5.5.1](#), [??](#), [??](#), [6.1](#), [6.2](#), [6.5.1](#), [6.5.2](#), [6.5.3](#), [6.2](#), [6.5.4](#), [6.3](#), [7.1](#), [7.1](#), [7.2](#), [7.3](#), [7.3.1](#), [7.3.3](#), [7.4.1](#), [7.4.1](#), [7.4.3](#), [??](#), [8.1](#), [9.2](#)
- [4] Mohammad Sadegh Aliakbarian, Fatemehsadat Saleh, Mathieu Salzmann, Basura Fernando, Lars Petersson, and Lars Andersson. Encouraging lstms to anticipate actions very early. 2017. [7.2](#)
- [5] Javad Amirian, Jean-Bernard Hayet, and Julien Pettré. Social ways: Learning multi-modal distributions of pedestrian trajectories with gans. In *CVPRW*, 2019. [5.2](#)
- [6] George Awad, Asad Butt, Keith Curtis, Jonathan Fiscus, Afzal Godil, Alan F. Smeaton, Yvette Graham, Wessel Kraaij, Georges Quénot, Joao Magalhaes, David Semedo, and Saverio Blasi. Trecvid 2018: Benchmarking video activity detection, video captioning and matching, video storytelling linking and video search. In *TRECVID*, 2018. [5.1](#), [5.4](#),

[5.5](#), [5.5.2](#), [6.1](#), [6.5](#), [7.1](#), [7.4](#), [7.4.1](#)

- [7] George Awad, Asad A Butt, Keith Curtis, Yooyoung Lee, Jonathan Fiscus, Afzal Godil, Andrew Delgado, Jesse Zhang, Eliot Godard, Lukas Diduch, et al. Trecvid 2019: An evaluation campaign to benchmark video activity detection, video captioning and matching, and video search & retrieval. *arXiv preprint arXiv:2009.09984*, 2020. [1.6](#), [2](#), [2.1](#)
- [8] Slawomir Bak, Peter Carr, and Jean-Francois Lalonde. Domain adaptation through synthesis for unsupervised person re-identification. In *ECCV*, 2018. [6.2](#)
- [9] Mayank Bansal, Alex Krizhevsky, and Abhijit Ogale. Chauffeurnet: Learning to drive by imitating the best and synthesizing the worst. *arXiv preprint arXiv:1812.03079*, 2018. [1.1](#), [5.1](#), [5.2](#), [6.1](#), [6.2](#), [6.5.2](#), [9.1](#)
- [10] Mokhtar S Bazaraa, Hanif D Sherali, and Chitharanjan M Shetty. *Nonlinear programming: theory and algorithms*. John Wiley & Sons, 2013. [3.3.3](#)
- [11] Yoshua Bengio, Jérôme Louradour, Ronan Collobert, and Jason Weston. Curriculum learning. In *ICML*, 2009. [3.1](#), [3.2](#)
- [12] David M Blei, Andrew Y Ng, and Michael I Jordan. Latent dirichlet allocation. *the Journal of machine Learning research*, 3:993–1022, 2003. [3.3.2](#)
- [13] Konstantinos Bousmalis, Nathan Silberman, David Dohan, Dumitru Erhan, and Dilip Krishnan. Unsupervised pixel-level domain adaptation with generative adversarial networks. In *CVPR*, 2017. [6.2](#)
- [14] Holger Caesar, Varun Bankiti, Alex H Lang, Sourabh Vora, Venice Erin Liong, Qiang Xu, Anush Krishnan, Yu Pan, Giancarlo Baldan, and Oscar Beijbom. nuscenes: A multimodal dataset for autonomous driving. *arXiv preprint arXiv:1903.11027*, 2019. [5.2](#), [5.4](#), [6.2](#)
- [15] Sergio Casas, Wenjie Luo, and Raquel Urtasun. Intentnet: Learning to predict intention from raw sensor data. In *CoRL*, 2018. [8.2](#), [9.1](#)
- [16] Yuning Chai, Benjamin Sapp, Mayank Bansal, and Dragomir Anguelov. Multipath: Multiple probabilistic anchor trajectory hypotheses for behavior prediction. *arXiv preprint arXiv:1910.05449*, 2019. [1.1](#), [5.1](#), [5.2](#), [5.3.3](#), [5.4](#), [5.5](#), [5.5](#), [6.1](#), [6.5.2](#), [9.1](#)
- [17] Ming-Fang Chang, John Lambert, Patsorn Sangkloy, Jagjeet Singh, Slawomir Bak, Andrew Hartnett, De Wang, Peter Carr, Simon Lucey, Deva Ramanan, et al. Argoverse: 3d tracking and forecasting with rich maps. In *CVPR*, 2019. [5.2](#), [6.1](#), [6.2](#), [6.5](#)
- [18] Xiaojun Chang, Wenhe Liu, Po-Yao Huang, Changlin Li, Fengda Zhu, Mingfei Han,

Mingjie Li, Mengyuan Ma, Siyi Hu, Guoliang Kang, Junwei Liang, et al. Mmvg-inf-etrol@ trecvid 2019: Activities in extended video. 2019. [1.6](#)

- [19] Ken Chatfield, Karen Simonyan, Andrea Vedaldi, and Andrew Zisserman. Return of the devil in the details: Delving deep into convolutional nets. In *BMVC*, 2014. [3.3.1](#)
- [20] Hanting Chen, Yunhe Wang, Chang Xu, Zhaohui Yang, Chuanjian Liu, Boxin Shi, Chun-jing Xu, Chao Xu, and Qi Tian. Data-free learning of student networks. In *ICCV*, 2019. [6.2](#)
- [21] Jia Chen, Junwei Liang, Jiang Liu, Shizhe Chen, Chenqiang Gao, Qin Jin, and Alexander Hauptmann. Informedia@ trecvid 2017. 2017. [1.6](#)
- [22] Liang-Chieh Chen, George Papandreou, Iasonas Kokkinos, Kevin Murphy, and Alan L Yuille. Deeplab: Semantic image segmentation with deep convolutional nets, atrous convolution, and fully connected crfs. *IEEE transactions on pattern analysis and machine intelligence*, 40(4):834–848, 2017. [5.3.1](#), [5.5.1](#), [6.4.2](#)
- [23] Liang-Chieh Chen, Yukun Zhu, George Papandreou, Florian Schroff, and Hartwig Adam. Encoder-decoder with atrous separable convolution for semantic image segmentation. In *ECCV*, 2018. [1.1](#), [7.3.3](#)
- [24] Xinlei Chen and Abhinav Gupta. Webly supervised learning of convolutional networks. In *ICCV*, 2015. [3.1](#), [3.2](#)
- [25] Xinlei Chen, Abhinav Shrivastava, and Abhinav Gupta. Neil: Extracting visual knowledge from web data. In *Proceedings of the IEEE International Conference on Computer Vision*, 2013. [3.2](#)
- [26] Yong Cheng, Lu Jiang, and Wolfgang Macherey. Robust neural machine translation with doubly adversarial inputs. *ACL*, 2019. [6.2](#)
- [27] Yong Cheng, Lu Jiang, Wolfgang Macherey, and Jacob Eisenstein. Advaug: Robust data augmentation for neural machine translation. In *ACL*, 2020. [6.1](#), [6.2](#)
- [28] Wongun Choi and Silvio Savarese. Understanding collective activities of people from videos. *IEEE transactions on pattern analysis and machine intelligence*, 36(6):1242–1257, 2014. [7.2](#)
- [29] Jifeng Dai, Yi Li, Kaiming He, and Jian Sun. R-fcn: Object detection via region-based fully convolutional networks. In *NeurIPS*, 2016. [2](#)
- [30] Xiyang Dai, Bharat Singh, Guyue Zhang, Larry S Davis, and Yan Qiu Chen. Temporal

- context network for activity localization in videos. In *ICCV*, 2017. 2.1
- [31] Abhishek Das, Samyak Datta, Georgia Gkioxari, Stefan Lee, Devi Parikh, and Dhruv Batra. Embodied question answering. In *CVPRW*, 2018. 5.2
- [32] César Roberto de Souza, Adrien Gaidon, Yohann Cabon, and Antonio Manuel López. Procedural generation of videos to train deep action recognition networks. In *CVPR*, 2017. 5.2, 6.1, 6.2
- [33] Jia Deng, Wei Dong, Richard Socher, Li-Jia Li, Kai Li, and Li Fei-Fei. Imagenet: A large-scale hierarchical image database. In *CVPR*, 2009. 3.1
- [34] Nachiket Deo and Mohan M Trivedi. Trajectory forecasts in unknown environments conditioned on grid-based plans. *arXiv preprint arXiv:2001.00735*, 2020. 6.1, 6.2, 6.4.2, 6.5.2, 6.5.3, 6.3
- [35] Santosh K Divvala, Alireza Farhadi, and Carlos Guestrin. Learning everything about anything: Webly-supervised visual concept learning. In *CVPR*, 2014. 3.2
- [36] Nemanja Djuric, Vladan Radosavljevic, Henggang Cui, Thi Nguyen, Fang-Chieh Chou, Tsung-Han Lin, Nitin Singh, and Jeff Schneider. Uncertainty-aware short-term motion prediction of traffic actors for autonomous driving. In *WACV*, 2020. 9.1
- [37] Alexey Dosovitskiy, German Ros, Felipe Codevilla, Antonio Lopez, and Vladlen Koltun. Carla: An open urban driving simulator. *arXiv preprint arXiv:1711.03938*, 2017. 5.1, 5.2, 5.4, 6.1, 6.2, 6.4.2, 9.2
- [38] Lixin Duan, Dong Xu, IW-H Tsang, and Jiebo Luo. Visual event recognition in videos by learning from web data. *Pattern Analysis and Machine Intelligence, IEEE Transactions on*, 34(9):1667–1680, 2012. 3.2
- [39] Mark Everingham, Luc Van Gool, Christopher KI Williams, John Winn, and Andrew Zisserman. The pascal visual object classes (voc) challenge. *International journal of computer vision*, 88(2):303–338, 2010. 2
- [40] Hao-Shu Fang, Shuqin Xie, Yu-Wing Tai, and Cewu Lu. RMPE: Regional multi-person pose estimation. In *ICCV*, 2017. 7.3.2, 7.4.1
- [41] Christoph Feichtenhofer, Haoqi Fan, Jitendra Malik, and Kaiming He. Slowfast networks for video recognition. In *Proceedings of the IEEE international conference on computer vision*, pages 6202–6211, 2019. 4.1, ??, ??, 4.2, ??, 4.2, ??
- [42] Adrien Gaidon, Qiao Wang, Yohann Cabon, and Eleonora Vig. Virtual worlds as proxy



- for multi-object tracking analysis. In *CVPR*, 2016. [5.2](#), [5.4](#), [6.1](#), [6.2](#), [6.4.2](#)
- [43] Yaroslav Ganin, Evgeniya Ustinova, Hana Ajakan, Pascal Germain, Hugo Larochelle, François Laviolette, Mario Marchand, and Victor Lempitsky. Domain-adversarial training of neural networks. *The Journal of Machine Learning Research*, 17(1):2096–2030, 2016. [6.2](#)
- [44] Andreas Geiger, Philip Lenz, Christoph Stiller, and Raquel Urtasun. Vision meets robotics: The kitti dataset. *The International Journal of Robotics Research*, 32(11):1231–1237, 2013. [5.4](#)
- [45] Joshua Gleason, Rajeev Ranjan, Steven Schwarcz, Carlos Castillo, Jun-Cheng Chen, and Rama Chellappa. A proposal-based solution to spatio-temporal action detection in untrimmed videos. In *WACV*, 2019. [2.1](#)
- [46] Ian Goodfellow, Jean Pouget-Abadie, Mehdi Mirza, Bing Xu, David Warde-Farley, Sherjil Ozair, Aaron Courville, and Yoshua Bengio. Generative adversarial nets. In *NeurIPS*, 2014. [5.2](#)
- [47] Ian J Goodfellow, Jonathon Shlens, and Christian Szegedy. Explaining and harnessing adversarial examples. *arXiv preprint arXiv:1412.6572*, 2014. [6.1](#), [6.2](#), [6.5.2](#), [6.1](#)
- [48] Jochen Gorski, Frank Pfeuffer, and Kathrin Klamroth. Biconvex sets and optimization with biconvex functions: a survey and extensions. *Mathematical Methods of Operations Research*, 66(3):373–407, 2007. [3.3.3](#)
- [49] Chunhui Gu, Chen Sun, David A Ross, Carl Vondrick, Caroline Pantofaru, Yeqing Li, Sudheendra Vijayanarasimhan, George Toderici, Susanna Ricco, Rahul Sukthankar, et al. Ava: A video dataset of spatio-temporally localized atomic visual actions. In *CVPR*, 2018. [4.2](#), [4.2](#)
- [50] Agrim Gupta, Justin Johnson, Silvio Savarese, Li Fei-Fei, and Alexandre Alahi. Social gan: Socially acceptable trajectories with generative adversarial networks. In *CVPR*, 2018. [1.1](#), [5.1](#), [5.2](#), [5.4](#), [5.5](#), [5.5.1](#), [??](#), [??](#), [??](#), [??](#), [6.1](#), [6.5.2](#), [6.5.3](#), [6.2](#), [6.5.4](#), [6.3](#), [7.1](#), [7.1](#), [7.2](#), [7.3](#), [7.3.1](#), [7.3.3](#), [7.3.4](#), [7.3.6](#), [7.4.1](#), [7.4.1](#), [7.4.1](#), [7.4.3](#), [??](#), [??](#), [7.4.3](#), [8.1](#), [8.3](#)
- [51] Xintong Han, Bharat Singh, Vlad I Morariu, and Larry S Davis. Fast automatic video retrieval using web images. *arXiv preprint arXiv:1512.03384*, 2015. [3.2](#), [3.4.1](#), [3.2](#)
- [52] Kaiming He, Xiangyu Zhang, Shaoqing Ren, and Jian Sun. Deep residual learning for image recognition. In *CVPR*, 2016. [1.1](#), [2.2.1](#)

- [53] Kaiming He, Georgia Gkioxari, Piotr Dollár, and Ross Girshick. Mask r-cnn. In *ICCV*, 2017. [1.1](#), [2](#), [2.2.1](#), [7.3.2](#)
- [54] Nicolas Heess, Srinivasan Sriram, Jay Lemmon, Josh Merel, Greg Wayne, Yuval Tassa, Tom Erez, Ziyu Wang, SM Eslami, Martin Riedmiller, et al. Emergence of locomotion behaviours in rich environments. *arXiv preprint arXiv:1707.02286*, 2017. [5.2](#), [6.2](#)
- [55] João F Henriques, Rui Caseiro, Pedro Martins, and Jorge Batista. High-speed tracking with kernelized correlation filters. *IEEE transactions on pattern analysis and machine intelligence*, 37(3):583–596, 2014. [2.2.2](#)
- [56] Sepp Hochreiter and Jürgen Schmidhuber. Long short-term memory. *Neural computation*, 9(8):1735–1780, 1997. [5.5.1](#)
- [57] Matthew Hoffman, Francis R Bach, and David M Blei. Online learning for latent dirichlet allocation. In *advances in neural information processing systems*, pages 856–864, 2010. [3.3.2](#)
- [58] Joey Hong, Benjamin Sapp, and James Philbin. Rules of the road: Predicting driving behavior with a convolutional model of semantic interactions. In *CVPR*, 2019. [5.2](#), [6.2](#), [6.5.2](#)
- [59] Rui Hou, Chen Chen, and Mubarak Shah. Tube convolutional neural network (t-cnn) for action detection in videos. In *ICCV*, 2017. [2.1](#)
- [60] Han Hu, Jiayuan Gu, Zheng Zhang, Jifeng Dai, and Yichen Wei. Relation networks for object detection. In *CVPR*, 2018. [7.3.3](#)
- [61] Po-Yao Huang, Junwei Liang, Vaibhav Vaibhav, Xiaojun Chang, and Alexander Hauptmann. Informedia@ trecvid 2018: Ad-hoc video search with discrete and continuous representations. 2018. [1.6](#)
- [62] Phillip Isola, Jun-Yan Zhu, Tinghui Zhou, and Alexei A Efros. Image-to-image translation with conditional adversarial networks. In *CVPR*, 2017. [9.2](#)
- [63] Max Jaderberg, Karen Simonyan, Andrew Zisserman, et al. Spatial transformer networks. In *Advances in neural information processing systems*, pages 2017–2025, 2015. [4.1](#)
- [64] Ashesh Jain, Hema S Koppula, Bharad Raghavan, Shane Soh, and Ashutosh Saxena. Car that knows before you do: Anticipating maneuvers via learning temporal driving models. In *CVPR*, 2015. [7.2](#)
- [65] Ashesh Jain, Amir R Zamir, Silvio Savarese, and Ashutosh Saxena. Structural-rnn: Deep

- learning on spatio-temporal graphs. In *CVPR*, 2016. [7.2](#)
- [66] Nikita Jaipuria, Golnaz Habibi, and Jonathan P How. A transferable pedestrian motion prediction model for intersections with different geometries. *arXiv preprint arXiv:1806.09444*, 2018. [7.2](#)
- [67] Lu Jiang, Deyu Meng, Teruko Mitamura, and Alexander G Hauptmann. Easy samples first: Self-paced reranking for zero-example multimedia search. In *MM*, 2014. [3.2](#)
- [68] Lu Jiang, Deyu Meng, Shou-I Yu, Zhenzhong Lan, Shiguang Shan, and Alexander Hauptmann. Self-paced learning with diversity. In *NIPS*, 2014. [3.2](#)
- [69] Lu Jiang, Deyu Meng, Qian Zhao, Shiguang Shan, and Alexander G Hauptmann. Self-paced curriculum learning. In *AAAI*, 2015. [1.5](#), [3.1](#), [3.3.2](#), [3.3.2](#), [3.3.3](#), [6.2](#)
- [70] Lu Jiang, Shou-I Yu, Deyu Meng, Yi Yang, Teruko Mitamura, and Alexander G Hauptmann. Fast and accurate content-based semantic search in 100m internet videos. In *Proceedings of the 23rd ACM international conference on Multimedia*, 2015. [3.1](#)
- [71] Lu Jiang, Zhengyuan Zhou, Thomas Leung, Li-Jia Li, and Li Fei-Fei. Mentornet: Learning data-driven curriculum for very deep neural networks on corrupted labels. *ICML*, 2018. [6.1](#), [6.2](#), [6.4.3](#)
- [72] Lu Jiang, Di Huang, Mason Liu, and Weilong Yang. Beyond synthetic noise: Deep learning on controlled noisy labels. In *ICML*, 2020. [6.1](#), [6.2](#), [6.4.3](#)
- [73] Yu-Gang Jiang, Zuxuan Wu, Jun Wang, Xiangyang Xue, and Shih-Fu Chang. Exploiting feature and class relationships in video categorization with regularized deep neural networks. *arXiv preprint arXiv:1502.07209*, 2015. [3.1](#), [3.4](#), [3.4.1](#), [3.4](#)
- [74] Qin Jin and Junwei Liang. Video description generation using audio and visual cues. In *ICMR*, 2016. [1.6](#)
- [75] Qin Jin, Junwei Liang, and Xiaozhu Lin. Generating natural video descriptions via multimodal processing. In *Interspeech*, 2016. [1.6](#)
- [76] RE Kalman. A new approach to linear filtering and prediction problems. *Trans. ASME, D*, 82:35–44, 1960. [5.1](#)
- [77] Guoliang Kang, Lu Jiang, Yi Yang, and Alexander G Hauptmann. Contrastive adaptation network for unsupervised domain adaptation. In *CVPR*, 2019. [6.2](#)
- [78] Amlan Kar, Aayush Prakash, Ming-Yu Liu, Eric Cameracci, Justin Yuan, Matt Rusiniak, David Acuna, Antonio Torralba, and Sanja Fidler. Meta-sim: Learning to generate syn-

- thetic datasets. In *ICCV*, 2019. 6.2
- [79] Vasiliy Karasev, Alper Ayvaci, Bernd Heisele, and Stefano Soatto. Intent-aware long-term prediction of pedestrian motion. In *ICRA*, 2016. 1.2.1, 8.2
- [80] Andrej Karpathy, George Toderici, Sachin Shetty, Tommy Leung, Rahul Sukthankar, and Li Fei-Fei. Large-scale video classification with convolutional neural networks. In *CVPR*, 2014. 3.1
- [81] Will Kay, Joao Carreira, Karen Simonyan, Brian Zhang, Chloe Hillier, Sudheendra Vijayanarasimhan, Fabio Viola, Tim Green, Trevor Back, Paul Natsev, et al. The kinetics human action video dataset. *arXiv preprint arXiv:1705.06950*, 2017. 1.3, 4.2
- [82] Kris M Kitani, Brian D Ziebart, James Andrew Bagnell, and Martial Hebert. Activity forecasting. In *ECCV*, 2012. 1.1, 5.1, 5.2, 6.1, 7.1, 7.1, 7.2, 7.3.1, 8.1
- [83] Julian Francisco Pieter Kooij, Nicolas Schneider, Fabian Flohr, and Darius M Gavrila. Context-based pedestrian path prediction. In *ECCV*, 2014. 5.2, 6.2, 7.2
- [84] Hema S Koppula and Ashutosh Saxena. Anticipating human activities using object affordances for reactive robotic response. *IEEE transactions on pattern analysis and machine intelligence*, 38(1):14–29, 2016. 7.2
- [85] Adam Kosioerek, Sara Sabour, Yee Whye Teh, and Geoffrey E Hinton. Stacked capsule autoencoders. In *Advances in Neural Information Processing Systems*, pages 15512–15522, 2019. 4.1
- [86] Alex Krizhevsky, Ilya Sutskever, and Geoffrey E Hinton. Imagenet classification with deep convolutional neural networks. In *Advances in neural information processing systems*, pages 1097–1105, 2012. 3.4.1
- [87] M Pawan Kumar, Benjamin Packer, and Daphne Koller. Self-paced learning for latent variable models. In *NIPS*, 2010. 3.1, 3.2, 3.3.3, 3.4.1
- [88] M Pawan Kumar, Haithem Turki, Dan Preston, and Daphne Koller. Learning specific-class segmentation from diverse data. In *ICCV*, 2011. 3.2, 3.2, 3.4, 3.6
- [89] Alexey Kurakin, Ian Goodfellow, and Samy Bengio. Adversarial examples in the physical world. *ICLR*, 2017. 6.1, 6.4.3
- [90] John Lambert, Ozan Sener, and Silvio Savarese. Deep learning under privileged information using heteroscedastic dropout. In *CVPR*, 2018. 6.2
- [91] Svetlana Lazebnik, Cordelia Schmid, and Jean Ponce. Beyond bags of features: Spatial

- pyramid matching for recognizing natural scene categories. In *CVPR*, 2006. [5.3.1](#)
- [92] Namhoon Lee, Wongun Choi, Paul Vernaza, Christopher B Choy, Philip HS Torr, and Manmohan Chandraker. Desire: Distant future prediction in dynamic scenes with interacting agents. In *CVPR*, 2017. [1.1](#), [5.1](#), [5.2](#), [6.1](#), [6.2](#), [6.5.2](#), [6.5.3](#), [6.3](#), [9.2](#)
- [93] Yooyoung Lee, Jon Fiscus, Afzal Godil, Andrew Delgado, Jim Golden, Lukas Diduch, and Maxime Hubert. Summary of the 2019 activity detection in extended videos prize challenge. In *WACVW*, 2020. [8.3](#), [9.2](#)
- [94] Alon Lerner, Yiorgos Chrysanthou, and Dani Lischinski. Crowds by example. In *Computer Graphics Forum*, pages 655–664. Wiley Online Library, 2007. [5.1](#), [5.4](#), [6.1](#), [6.2](#), [7.1](#), [7.4](#), [7.4.3](#)
- [95] Ang Li, Meghana Thotakuri, David A Ross, João Carreira, Alexander Vostroikov, and Andrew Zisserman. The ava-kinetics localized human actions video dataset. *arXiv preprint arXiv:2005.00214*, 2020. [2.2.1](#), [4.2](#), [4.2](#), [??](#)
- [96] Jiwei Li, Will Monroe, and Dan Jurafsky. A simple, fast diverse decoding algorithm for neural generation. *arXiv preprint arXiv:1611.08562*, 2016. [5.3.5](#), [5.5.1](#)
- [97] Yuke Li. Which way are you going? imitative decision learning for path forecasting in dynamic scenes. In *CVPR*, 2019. [1.1](#), [5.1](#), [5.2](#), [5.4](#), [6.1](#), [6.2](#), [6.5.2](#), [6.5.3](#), [6.3](#)
- [98] Junwei Liang, Jia Chen, Poyao Huang, Xuanchong Li, Lu Jiang, Zhenzhong Lan, Pingbo Pan, Hehe Fan, Qin Jin, Jiande Sun, et al. Informedia@ trecvid 2016. [1.6](#)
- [99] Junwei Liang, Qin Jin, Xixi He, Gang Yang, Jieping Xu, and Xirong Li. Semantic concept annotation of consumer videos at frame-level using audio. In *Pacific Rim Conference on Multimedia*, pages 113–122. Springer, 2014. [3.1](#)
- [100] Junwei Liang, Lu Jiang, Deyu Meng, and Alexander G Hauptmann. Learning to detect concepts from webly-labeled video data. In *IJCAI*, 2016. [1.6](#), [3](#), [3.1](#), [3.3.2](#), [3.3.2](#), [6.2](#)
- [101] Junwei Liang, Desai Fan, Han Lu, Poyao Huang, Jia Chen, Lu Jiang, and Alexander Hauptmann. An event reconstruction tool for conflict monitoring using social media. In *AAAI*, 2017. [5.2](#), [6.2](#)
- [102] Junwei Liang, Lu Jiang, and Alexander Hauptmann. Temporal localization of audio events for conflict monitoring in social media. In *ICASSP*, 2017. [1.6](#)
- [103] Junwei Liang, Lu Jiang, and Alexander Hauptmann. Webly-supervised learning of multimodal video detectors. In *AAAI*, 2017. [1.6](#), [3](#)

- [104] Junwei Liang, Lu Jiang, Deyu Meng, and Alexander Hauptmann. Leveraging multi-modal prior knowledge for large-scale concept learning in noisy web data. In *ICMR*, 2017. [1.6](#), [3](#)
- [105] Junwei Liang, Lu Jiang, Liangliang Cao, Li-Jia Li, and Alexander G Hauptmann. Focal visual-text attention for visual question answering. In *CVPR*, 2018. [1.6](#), [5.2](#), [7.3.1](#), [7.3.4](#), [8.2](#)
- [106] Junwei Liang, Lu Jiang, Liangliang Cao, Yannis Kalantidis, Li-Jia Li, and Alexander G Hauptmann. Focal visual-text attention for memex question answering. *IEEE transactions on pattern analysis and machine intelligence*, 41(8):1893–1908, 2019. [1.6](#), [5.2](#), [6.1](#), [8.2](#)
- [107] Junwei Liang, Lu Jiang, Juan Carlos Niebles, Alexander G Hauptmann, and Li Fei-Fei. Peeking into the future: Predicting future person activities and locations in videos. In *CVPR*, 2019. [1.1](#), [1.2.1](#), [1.6](#), [5.1](#), [5.2](#), [5.4](#), [5.5.1](#), [??](#), [5.5.2](#), [??](#), [6.1](#), [6.2](#), [6.4.2](#), [6.4.4](#), [6.5.2](#), [6.2](#), [6.5.4](#), [7](#), [8.1](#), [8.2](#), [8.3](#), [9.2](#)
- [108] Junwei Liang, Lu Jiang, and Alexander Hauptmann. Simaug: Learning robust representations from simulation for trajectory prediction. 2020. [1.6](#), [9.2](#)
- [109] Junwei Liang, Lu Jiang, Kevin Murphy, Ting Yu, and Alexander Hauptmann. The garden of forking paths: Towards multi-future trajectory prediction. In *CVPR*, 2020. [1.6](#), [5](#), [6.1](#), [6.2](#), [6.3](#), [6.4.2](#), [6.4.3](#), [6.4.3](#), [6.4.4](#), [6.4.4](#), [6.5.1](#), [6.5.2](#), [6.1](#), [6.2](#), [6.5.4](#), [6.3](#)
- [110] Ming Liang, Bin Yang, Wenyuan Zeng, Yun Chen, Rui Hu, Sergio Casas, and Raquel Urtasun. Pnpnet: End-to-end perception and prediction with tracking in the loop. In *Proceedings of the IEEE/CVF Conference on Computer Vision and Pattern Recognition*, pages 11553–11562, 2020. [9.1](#)
- [111] Xiaodan Liang, Si Liu, Yunchao Wei, Luoqi Liu, Liang Lin, and Shuicheng Yan. Towards computational baby learning: A weakly-supervised approach for object detection. In *ICCV*, 2015. [3.1](#), [3.2](#), [3.4.1](#), [3.2](#), [3.4](#), [3.6](#)
- [112] Tsung-Yi Lin, Michael Maire, Serge Belongie, James Hays, Pietro Perona, Deva Ramanan, Piotr Dollár, and C Lawrence Zitnick. Microsoft coco: Common objects in context. In *European conference on computer vision*, pages 740–755. Springer, 2014. [1.5](#), [2](#), [2.2.1](#)
- [113] Tsung-Yi Lin, Piotr Dollár, Ross Girshick, Kaiming He, Bharath Hariharan, and Serge Belongie. Feature pyramid networks for object detection. In *CVPR*, 2017. [2.2.1](#), [5.3.1](#), [7.4.1](#)
- [114] Wenhe Liu, Guoliang Kang, Po-Yao Huang, Xiaojun Chang, Yijun Qian, Junwei Liang,

- Liangke Gui, Jing Wen, and Peng Chen. Argus: Efficient activity detection system for extended video analysis. In *WACVW*, 2020. [1.6](#), [2](#)
- [115] David Lopez-Paz, Léon Bottou, Bernhard Schölkopf, and Vladimir Vapnik. Unifying distillation and privileged information. *arXiv preprint arXiv:1511.03643*, 2015. [6.2](#)
- [116] Matthias Luber, Johannes A Stork, Gian Diego Tipaldi, and Kai O Arras. People tracking with human motion predictions from social forces. In *ICRA*, 2010. [1.1](#), [5.1](#), [6.1](#), [6.2](#), [7.1](#), [8.1](#)
- [117] Wenjie Luo, Bin Yang, and Raquel Urtasun. Fast and furious: Real time end-to-end 3d detection, tracking and motion forecasting with a single convolutional net. In *Proceedings of the IEEE conference on Computer Vision and Pattern Recognition*, pages 3569–3577, 2018. [9.1](#)
- [118] Zelun Luo, Jun-Ting Hsieh, Lu Jiang, Juan Carlos Niebles, and Li Fei-Fei. Graph distillation for action detection with privileged modalities. In *ECCV*, 2018. [6.2](#)
- [119] Shugao Ma, Leonid Sigal, and Stan Sclaroff. Learning activity progression in lstms for activity detection and early detection. In *CVPR*, 2016. [7.2](#)
- [120] Wei-Chiu Ma, De-An Huang, Namhoon Lee, and Kris M Kitani. Forecasting interactive dynamics of pedestrians with fictitious play. In *CVPR*, 2017. [5.2](#)
- [121] Aleksander Madry, Aleksandar Makelov, Ludwig Schmidt, Dimitris Tsipras, and Adrian Vladu. Towards deep learning models resistant to adversarial attacks. *arXiv preprint arXiv:1706.06083*, 2017. [6.2](#), [6.5.2](#), [6.1](#)
- [122] Osama Makansi, Eddy Ilg, Ozgun Cicek, and Thomas Brox. Overcoming limitations of mixture density networks: A sampling and fitting framework for multimodal future prediction. In *CVPR*, 2019. [1.1](#), [5.1](#), [5.2](#), [5.4](#), [5.5](#), [5.5.1](#), [6.2](#), [6.5.2](#)
- [123] Karttikeya Mangalam, Ehsan Adeli, Kuan-Hui Lee, Adrien Gaidon, and Juan Carlos Niebles. Disentangling human dynamics for pedestrian locomotion forecasting with noisy supervision. *arXiv preprint arXiv:1911.01138*, 2019. [6.1](#), [6.2](#)
- [124] Huynh Manh and Gita Alaghband. Scene-lstm: A model for human trajectory prediction. *arXiv preprint arXiv:1808.04018*, 2018. [5.2](#), [7.1](#), [7.2](#), [7.3.1](#), [7.3.5](#), [7.3.6](#), [7.4.3](#)
- [125] Christopher D Manning, Prabhakar Raghavan, et al. *Introduction to information retrieval*, volume 1. [3.3.2](#)
- [126] Michael McCandless, Erik Hatcher, and Otis Gospodnetic. *Lucene in Action: Covers*



*Apache Lucene 3.0*. Manning Publications Co., 2010. [3.3.2](#)

- [127] Deyu Meng and Qian Zhao. What objective does self-paced learning indeed optimize? *arXiv preprint arXiv:1511.06049*, 2015. [3.3.2](#), [3.3.3](#)
- [128] Tomas Mikolov, Ilya Sutskever, Kai Chen, Greg S Corrado, and Jeff Dean. Distributed representations of words and phrases and their compositionality. In *Advances in neural information processing systems*, pages 3111–3119, 2013. [3.3.2](#)
- [129] T Mitchell, W Cohen, E Hruschka, P Talukdar, J Betteridge, A Carlson, B Dalvi, M Gardner, B Kisiel, J Krishnamurthy, et al. Never-ending learning. In *AAAI*, 2015. [3.2](#)
- [130] Curtis G Northcutt, Lu Jiang, and Isaac L Chuang. Confident learning: Estimating uncertainty in dataset labels. *arXiv preprint arXiv:1911.00068*, 2019. [6.2](#)
- [131] Sangmin Oh, Anthony Hoogs, Amitha Perera, Naresh Cuntoor, Chia-Chih Chen, Jong Taek Lee, Saurajit Mukherjee, JK Aggarwal, Hyungtae Lee, Larry Davis, et al. A large-scale benchmark dataset for event recognition in surveillance video. In *CVPR*, 2011. [1.3](#), [2](#), [2.1](#), [2.2.1](#), [5.1](#), [5.4](#), [5.5](#), [5.5.2](#), [6.1](#), [6.2](#), [6.5](#), [7.1](#), [7.4](#), [7.4.1](#), [8.3](#), [9.2](#)
- [132] Paul Over, Jon Fiscus, Greg Sanders, David Joy, Martial Michel, George Awad, Alan Smeaton, Wessel Kraaij, and Georges Quénot. Trecvid 2014—an overview of the goals, tasks, data, evaluation mechanisms and metrics. In *Proceedings of TRECVID*, page 52, 2014. [3.1](#), [3.4.1](#)
- [133] Stefano Pellegrini, Andreas Ess, and Luc Van Gool. Improving data association by joint modeling of pedestrian trajectories and groupings. In *ECCV*, 2012. [5.4](#), [7.1](#), [7.4](#), [7.4.3](#)
- [134] Tobias Plötz and Stefan Roth. Neural nearest neighbors networks. In *NeurIPS*, 2018. [5.5.1](#)
- [135] Daniel Povey, Arnab Ghoshal, Gilles Boulianne, Lukáš Burget, Ondřej Glembek, Nandini Goel, Mirko Hannemann, Petr Motlíček, Yanmin Qian, Petr Schwarz, et al. The kaldi speech recognition toolkit. 2011. [3.3.1](#), [3.3.2](#)
- [136] Weichao Qiu, Fangwei Zhong, Yi Zhang, Siyuan Qiao, Zihao Xiao, Tae Soo Kim, and Yizhou Wang. Unrealcv: Virtual worlds for computer vision. In *ACM Multimedia*, 2017. [5.2](#), [6.2](#)
- [137] Marc’Aurelio Ranzato, Sumit Chopra, Michael Auli, and Wojciech Zaremba. Sequence level training with recurrent neural networks. *arXiv preprint arXiv:1511.06732*, 2015. [5.3.4](#)
- [138] Amir Rasouli, Iuliia Kotseruba, and John K Tsotsos. Are they going to cross? a benchmark dataset and baseline for pedestrian crosswalk behavior. In *ICCVW*, 2017. [8.3](#)



- [139] Amir Rasouli, Iuliia Kotseruba, Toni Kunic, and John K Tsotsos. Pie: A large-scale dataset and models for pedestrian intention estimation and trajectory prediction. In *ICCV*, 2019. [8.3](#)
- [140] Esteban Real, Jonathon Shlens, Stefano Mazzocchi, Xin Pan, and Vincent Vanhoucke. Youtube-boundingboxes: A large high-precision human-annotated data set for object detection in video. In *CVPR*, 2017. [2](#)
- [141] Mengye Ren, Wenyuan Zeng, Bin Yang, and Raquel Urtasun. Learning to reweight examples for robust deep learning. In *ICML*, 2018. [6.2](#)
- [142] Shaoqing Ren, Kaiming He, Ross Girshick, and Jian Sun. Faster r-cnn: Towards real-time object detection with region proposal networks. In *NeurIPS*, 2015. [2.1](#), [5.1](#), [5.3.3](#), [5.3.4](#), [7.3.5](#)
- [143] Nicholas Rhinehart and Kris M Kitani. First-person activity forecasting with online inverse reinforcement learning. In *ICCV*, 2017. [1.1](#), [5.1](#), [6.1](#)
- [144] Nicholas Rhinehart, Kris M Kitani, and Paul Vernaza. R2p2: A reparameterized pushforward policy for diverse, precise generative path forecasting. In *ECCV*, 2018. [5.1](#), [5.2](#), [5.4](#), [5.5](#), [6.1](#), [6.2](#)
- [145] Nicholas Rhinehart, Rowan McAllister, Kris Kitani, and Sergey Levine. Precog: Prediction conditioned on goals in visual multi-agent settings. *arXiv preprint arXiv:1905.01296*, 2019. [5.2](#), [5.4](#), [5.5](#)
- [146] Stephan R Richter, Vibhav Vineet, Stefan Roth, and Vladlen Koltun. Playing for data: Ground truth from computer games. In *ECCV*, 2016. [5.2](#), [6.1](#), [6.2](#)
- [147] Alexandre Robicquet, Amir Sadeghian, Alexandre Alahi, and Silvio Savarese. Learning social etiquette: Human trajectory understanding in crowded scenes. In *ECCV*, 2016. [5.4](#), [6.1](#), [6.2](#), [6.4.2](#), [6.5](#)
- [148] German Ros, Laura Sellart, Joanna Materzynska, David Vazquez, and Antonio M Lopez. The synthia dataset: A large collection of synthetic images for semantic segmentation of urban scenes. In *CVPR*, 2016. [5.2](#), [5.4](#), [6.2](#), [6.4.2](#)
- [149] Andrey Rudenko, Luigi Palmieri, Michael Herman, Kris M Kitani, Dariu M Gavrilă, and Kai O Arras. Human motion trajectory prediction: A survey. *The International Journal of Robotics Research*, 39(8):895–935, 2020. [1.1](#), [1.1](#), [1.5](#), [5.2](#), [6.2](#), [7.2](#)
- [150] Nataniel Ruiz, Samuel Schuster, and Manmohan Chandraker. Learning to simulate. *ICLR*,

2018. [1.1](#), [6.1](#)

- [151] Olga Russakovsky, Jia Deng, Hao Su, Jonathan Krause, Sanjeev Satheesh, Sean Ma, Zhiheng Huang, Andrej Karpathy, Aditya Khosla, Michael Bernstein, Alexander C. Berg, and Li Fei-Fei. ImageNet Large Scale Visual Recognition Challenge. *International Journal of Computer Vision (IJCV)*, 115(3):211–252, 2015. [3.3.2](#)
- [152] Amir Sadeghian, Alexandre Alahi, and Silvio Savarese. Tracking the untrackable: Learning to track multiple cues with long-term dependencies. In *ICCV*, 2017. [1.1](#), [5.1](#), [7.2](#)
- [153] Amir Sadeghian, Vineet Kosaraju, Ali Sadeghian, Noriaki Hirose, and Silvio Savarese. Sophie: An attentive gan for predicting paths compliant to social and physical constraints. *arXiv preprint arXiv:1806.01482*, 2018. [5.2](#), [5.4](#), [5.5.1](#), [6.1](#), [6.2](#), [6.4.2](#), [6.5.2](#), [6.5.3](#), [6.3](#), [7.1](#), [7.2](#), [7.3](#), [7.3.1](#), [7.3.6](#), [7.4.1](#), [7.4.3](#), [??](#), [7.4.3](#)
- [154] Amir Sadeghian, Ferdinand Legros, Maxime Voisin, Ricky Vesel, Alexandre Alahi, and Silvio Savarese. Car-net: Clairvoyant attentive recurrent network. In *ECCV*, 2018. [5.2](#), [6.2](#)
- [155] Shital Shah, Debadeepta Dey, Chris Lovett, and Ashish Kapoor. Airsim: High-fidelity visual and physical simulation for autonomous vehicles. In *Field and service robotics*, pages 621–635. Springer, 2018. [5.2](#), [6.2](#)
- [156] Tianmin Shu, Dan Xie, Brandon Rothrock, Sinisa Todorovic, and Song Chun Zhu. Joint inference of groups, events and human roles in aerial videos. In *CVPR*, 2015. [7.2](#)
- [157] Tianmin Shu, Sinisa Todorovic, and Song-Chun Zhu. Cern: confidence-energy recurrent network for group activity recognition. In *CVPR*, 2017. [7.2](#)
- [158] Gunnar A Sigurdsson, Gül Varol, Xiaolong Wang, Ali Farhadi, Ivan Laptev, and Abhinav Gupta. Hollywood in homes: Crowdsourcing data collection for activity understanding. In *ECCV*, 2016. [4.2](#)
- [159] Gunnar A Sigurdsson, Abhinav Gupta, Cordelia Schmid, Ali Farhadi, and Karteek Alahari. Charades-ego: A large-scale dataset of paired third and first person videos. *arXiv preprint arXiv:1804.09626*, 2018. [4.2](#), [??](#)
- [160] Karen Simonyan and Andrew Zisserman. Very deep convolutional networks for large-scale image recognition. *arXiv preprint arXiv:1409.1556*, 2014. [3.3.2](#), [3.4.1](#)
- [161] Ray Smith. An overview of the tesseract ocr engine. In *icdar*, pages 629–633. IEEE, 2007. [3.3.1](#), [3.3.2](#)

- [162] Valentin I Spitkovsky, Hiyan Alshawi, and Daniel Jurafsky. Baby steps: How “less is more” in unsupervised dependency parsing. *NIPS GRLL*, 2009. [3.2](#)
- [163] Nitish Srivastava, Elman Mansimov, and Ruslan Salakhudinov. Unsupervised learning of video representations using lstms. In *ICML*, 2015. [7.2](#)
- [164] Oily Styles, Arun Ross, and Victor Sanchez. Forecasting pedestrian trajectory with machine-annotated training data. In *2019 IEEE Intelligent Vehicles Symposium (IV)*, pages 716–721. IEEE, 2019. [6.1](#), [6.2](#)
- [165] Olly Styles, Tanaya Guha, and Victor Sanchez. Multiple object forecasting: Predicting future object locations in diverse environments. *arXiv preprint arXiv:1909.11944*, 2019. [6.1](#), [6.2](#)
- [166] Sainbayar Sukhbaatar, Joan Bruna, Manohar Paluri, Lubomir Bourdev, and Rob Fergus. Training convolutional networks with noisy labels. *arXiv preprint arXiv:1406.2080*, 2014. [3.4.1](#), [3.4.3](#), [3.5](#)
- [167] Chen Sun, Per Karlsson, Jiajun Wu, Joshua B Tenenbaum, and Kevin Murphy. Stochastic prediction of multi-agent interactions from partial observations. *arXiv preprint arXiv:1902.09641*, 2019. [5.2](#), [6.2](#)
- [168] Shao-Hua Sun, Minyoung Huh, Yuan-Hong Liao, Ning Zhang, and Joseph J Lim. Multi-view to novel view: Synthesizing novel views with self-learned confidence. In *ECCV*, 2018. [6.2](#)
- [169] James Steven Supancic and Deva Ramanan. Self-paced learning for long-term tracking. In *CVPR*, 2013. [3.2](#)
- [170] Mingxing Tan, Ruoming Pang, and Quoc V Le. Efficientdet: Scalable and efficient object detection. In *CVPR*, 2020. [2](#), [2.2.1](#)
- [171] Kevin Tang, Vignesh Ramanathan, Li Fei-Fei, and Daphne Koller. Shifting weights: Adapting object detectors from image to video. In *NIPS*, 2012. [3.2](#)
- [172] Yichuan Charlie Tang and Ruslan Salakhutdinov. Multiple futures prediction. *arXiv preprint arXiv:1911.00997*, 2019. [1.1](#), [5.1](#), [5.2](#)
- [173] Luca Anthony Thiede and Pratik Prabhanjan Brahma. Analyzing the variety loss in the context of probabilistic trajectory prediction. *arXiv preprint arXiv:1907.10178*, 2019. [1.1](#), [5.1](#), [5.2](#), [5.4](#)
- [174] Bart Thomee, David A. Shamma, Gerald Friedland, Benjamin Elizalde, Karl Ni, Douglas

- Poland, Damian Borth, and Li-Jia Li. The new data and new challenges in multimedia research. *arXiv preprint arXiv:1503.01817*, 2015. [3.4](#), [3.4.1](#)
- [175] Florian Tramèr, Alexey Kurakin, Nicolas Papernot, Ian Goodfellow, Dan Boneh, and Patrick McDaniel. Ensemble adversarial training: Attacks and defenses. *arXiv preprint arXiv:1705.07204*, 2017. [1.1](#), [4.1](#), [6.2](#)
- [176] Eric Tzeng, Judy Hoffman, Kate Saenko, and Trevor Darrell. Adversarial discriminative domain adaptation. In *CVPR*, 2017. [6.2](#)
- [177] Vladimir Vapnik and Rauf Izmailov. Learning using privileged information: similarity control and knowledge transfer. *Journal of machine learning research*, 16(2023-2049):2, 2015. [6.2](#)
- [178] Balakrishnan Varadarajan, George Toderici, Sudheendra Vijayanarasimhan, and Apostol Natsev. Efficient large scale video classification. *arXiv preprint arXiv:1505.06250*, 2015. [3.2](#), [3.3.1](#), [3.3.2](#), [3.4.1](#), [3.2](#), [3.4](#), [3.6](#)
- [179] Gül Varol, Ivan Laptev, Cordelia Schmid, and Andrew Zisserman. Synthetic humans for action recognition from unseen viewpoints. *arXiv preprint arXiv:1912.04070*, 2019. [6.1](#)
- [180] Petar Veličković, Guillem Cucurull, Arantxa Casanova, Adriana Romero, Pietro Lio, and Yoshua Bengio. Graph attention networks. *arXiv preprint arXiv:1710.10903*, 2017. [1.1](#), [5.3.2](#)
- [181] Xiaolong Wang, Ross Girshick, Abhinav Gupta, and Kaiming He. Non-local neural networks. In *Proceedings of the IEEE conference on computer vision and pattern recognition*, pages 7794–7803, 2018. [4.1](#), [??](#)
- [182] Yunbo Wang, Lu Jiang, Ming-Hsuan Yang, Li-Jia Li, Mingsheng Long, and Li Fei-Fei. Eidetic 3d lstm: A model for video prediction and beyond. In *ICLR*, 2019. [5.3.1](#), [6.4.4](#)
- [183] Xinshuo Weng, Ye Yuan, and Kris Kitani. End-to-end 3d multi-object tracking and trajectory forecasting. *arXiv preprint arXiv:2008.11598*, 2020. [9.1](#)
- [184] Nicolai Wojke, Alex Bewley, and Dietrich Paulus. Simple online and realtime tracking with a deep association metric. In *ICIP*, 2017. [2.2.2](#)
- [185] Yi Wu, Jongwoo Lim, and Ming-Hsuan Yang. Object tracking benchmark. *IEEE Transactions on Pattern Analysis and Machine Intelligence*, 37(9):1834–1848, 2015. [1.1](#), [7.4.1](#)
- [186] Yu Wu, Lu Jiang, and Yi Yang. Revisiting embodiedqa: A simple baseline and beyond. *arXiv preprint arXiv:1904.04166*, 2019. [5.2](#), [6.2](#)

- [187] Tong Xiao, Tian Xia, Yi Yang, Chang Huang, and Xiaogang Wang. Learning from massive noisy labeled data for image classification. In *Proceedings of the IEEE Conference on Computer Vision and Pattern Recognition*, 2015. [3.2](#), [3.4.1](#), [3.4.3](#), [3.5](#)
- [188] Cihang Xie, Yuxin Wu, Laurens van der Maaten, Alan L Yuille, and Kaiming He. Feature denoising for improving adversarial robustness. In *CVPR*, 2019. [6.2](#), [6.5.2](#), [6.1](#)
- [189] Dan Xie, Tianmin Shu, Sinisa Todorovic, and Song-Chun Zhu. Learning and inferring “dark matter” and predicting human intents and trajectories in videos. *IEEE transactions on pattern analysis and machine intelligence*, 40(7):1639–1652, 2018. [7.1](#), [7.2](#), [7.3.1](#), [8.2](#)
- [190] SHI Xingjian, Zhourong Chen, Hao Wang, Dit-Yan Yeung, Wai-Kin Wong, and Wang-chun Woo. Convolutional lstm network: A machine learning approach for precipitation nowcasting. In *NeurIPS*, 2015. [5.1](#), [5.3.1](#), [5.5.1](#), [6.4.4](#)
- [191] Huijuan Xu, Abir Das, and Kate Saenko. R-c3d: Region convolutional 3d network for temporal activity detection. In *ICCV*, 2017. [2.1](#)
- [192] Yanyu Xu, Zhixin Piao, and Shenghua Gao. Encoding crowd interaction with deep neural network for pedestrian trajectory prediction. In *CVPR*, 2018. [7.2](#)
- [193] Hao Xue, Du Q Huynh, and Mark Reynolds. Ss-lstm: A hierarchical lstm model for pedestrian trajectory prediction. In *WACV*, 2018. [5.2](#), [6.2](#)
- [194] Takuma Yagi, Karttikeya Mangalam, Ryo Yonetani, and Yoichi Sato. Future person localization in first-person videos. In *CVPR*, 2018. [1.1](#), [5.2](#), [6.1](#), [6.2](#), [6.5.2](#), [7.2](#), [7.4.1](#), [7.4.1](#)
- [195] Shuai Yi, Hongsheng Li, and Xiaogang Wang. Pedestrian behavior understanding and prediction with deep neural networks. In *ECCV*, 2016. [7.2](#)
- [196] Fisher Yu, Wenqi Xian, Yingying Chen, Fangchen Liu, Mike Liao, Vashisht Madhavan, and Trevor Darrell. Bdd100k: A diverse driving video database with scalable annotation tooling. *arXiv preprint arXiv:1805.04687*, 2018. [6.2](#)
- [197] Matthew D Zeiler. Adadelata: an adaptive learning rate method. *arXiv preprint arXiv:1212.5701*, 2012. [5.5.1](#), [6.5.2](#), [7.4.1](#)
- [198] Wenyan Zeng, Wenjie Luo, Simon Suo, Abbas Sadat, Bin Yang, Sergio Casas, and Raquel Urtasun. End-to-end interpretable neural motion planner. In *Proceedings of the IEEE Conference on Computer Vision and Pattern Recognition*, pages 8660–8669, 2019. [9.1](#)
- [199] Xiaohui Zeng, Chenxi Liu, Yu-Siang Wang, Weichao Qiu, Lingxi Xie, Yu-Wing Tai, Chi-Keung Tang, and Alan L Yuille. Adversarial attacks beyond the image space. In *CVPR*,

2019. [6.2](#)

- [200] Hongyi Zhang, Moustapha Cisse, Yann N Dauphin, and David Lopez-Paz. mixup: Beyond empirical risk minimization. In *ICLR*, 2018. [6.1](#), [6.2](#), [6.4.3](#), [6.4.3](#), [6.5.5](#)
- [201] Pu Zhang, Wanli Ouyang, Pengfei Zhang, Jianru Xue, and Nanning Zheng. Sr-lstm: State refinement for lstm towards pedestrian trajectory prediction. In *CVPR*, 2019. [5.2](#), [5.4](#), [6.2](#)
- [202] Yi Zhang, Xinyue Wei, Weichao Qiu, Zihao Xiao, Gregory D Hager, and Alan Yuille. Rsa: Randomized simulation as augmentation for robust human action recognition. *arXiv preprint arXiv:1912.01180*, 2019. [6.1](#), [6.2](#), [6.4.2](#)
- [203] Yiwei Zhang, Graham M Gibson, Rebecca Hay, Richard W Bowman, Miles J Padgett, and Matthew P Edgar. A fast 3d reconstruction system with a low-cost camera accessory. *Scientific reports*, 5:10909, 2015. [5.2](#), [6.2](#)
- [204] Tianyang Zhao, Yifei Xu, Mathew Monfort, Wongun Choi, Chris Baker, Yibiao Zhao, Yizhou Wang, and Ying Nian Wu. Multi-agent tensor fusion for contextual trajectory prediction. In *CVPR*, 2019. [5.2](#), [5.4](#), [6.2](#)
- [205] Bolei Zhou, Hang Zhao, Xavier Puig, Sanja Fidler, Adela Barriuso, and Antonio Torralba. Scene parsing through ade20k dataset. In *CVPR*, 2017. [5.3.1](#), [5.5.1](#), [6.4.2](#)
- [206] Yuke Zhu, Roozbeh Mottaghi, Eric Kolve, Joseph J Lim, Abhinav Gupta, Li Fei-Fei, and Ali Farhadi. Target-driven visual navigation in indoor scenes using deep reinforcement learning. In *ICRA*, 2017. [5.2](#), [6.2](#)
- [207] Haosheng Zou, Hang Su, Shihong Song, and Jun Zhu. Understanding human behaviors in crowds by imitating the decision-making process. *arXiv preprint arXiv:1801.08391*, 2018. [7.2](#)